Functional Anatomy of the Macaque Face Processing System

Dissertation zur Erlangung des Grades eines
Doktors der Naturwissenschaften

Betreut durch:
D.Y. Tsao (PhD)

Begutachtet durch
D.Y. Tsao (PhD)
Prof. Dr. Manfred Fahle

Sebastian Moeller
Institut für Hirnforschung
Abteilung Theoretische Neurobiologie

Universitaet Bremen
Fachbereich 2
Bremen, 12. November 2008

Authorship and Copyright

Three components of this thesis have shared authorship and thereby copyright:

"Patches with links: A unified system for processing faces in the macaque temporal lobe" by Moeller, Freiwald, and Tsao (Science 320: 1355-1359)

"Comparing face patch systems in macaques and humans" by Tsao, Moeller & Freiwald (PNAS, 2008, in press)

"Patches of face-selective cortex in the macaque frontal lobe" by Tsao, Schweers, Moeller, and Freiwald (Nature Neuroscience 11: 877-879

The authors of these papers declare by signature that they do agree to grant Sebastian Moeller the non-exclusive right to republish the results of their cooperation, namely the three published papers, for this doctoral thesis.

Bremen, November 12th, 2008

Doris Y. Tsao

Winrich A. Freiwald

Nicole Schweers

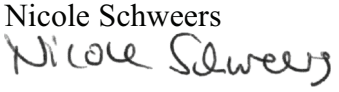

Table of contents

Acknowledgements

I would like to thank everybody involved in the projects leading up to this thesis. This includes those that helped in my scientific endeavors as well as those that helped me to get to where I am now in life.

I would like to thank my supervisor Doris Tsao, for all the things I learned from her, the excellent supervision, and the positive spirit in our common project. I would also like to thank Winrich Freiwald for all the help and support he gave as senior scientific advisor, not least for getting me introduced to Doris Tsao and the project that culminated in the current manuscript.

Many thanks also to Nicole Schweers for all the help and support in getting the project started as well as the excellent monkey training and lab management. All members of the greater group that turned into friends, especially Mikhail Borisov, Bevil Conway, and Tim Blanche, thank you..

Katrin Thoss and Ramazani Hakizimana, I thank for the expert animal care taking.

I would like to thank the people of the Institut fuer Hirnforschung that supported me in any imaginable way; I am especially grateful to fellow graduate students and friends Heiko Stemmann and Aurel Wanning for help, support and hiking trips; also to Maria De la O Olmedo, Katja Taylor, and Wolf Zinke.

I would like to thank the members of the thesis committee, Prof. Dr. Manfred Fahle, Doris Tsao, Prof. Dr. Michael Koch, Thorsten Becker, and Nicole Schweers for spending their time on preparing and performing the thesis defense.

Without my family none of this would have happened. Therefore I thank my parents, Beatrix and Peter Moeller, my siblings Sirkka Moeller, Julia Abbate and Philip Moeller.

Finally I would like to thank my wife Sandra for love and moral support.

Introduction to the visual system

1. Organization of the visual system: dorsal and ventral stream

All vertebrate vision starts at the photoreceptors in the retinae of the eyes. The retinal ganglion cells are the only input source to the five visual pathways (known to date). The two main pathways are the retinotecal pathway, connecting the retinae with the superior colliculus (the optic tectum in birds) in the visual midbrain, and the retinogeniculate pathway, connecting the retinae with the primary visual cortex by relay through the lateral geniculate nucleus. The retinopretectal pathway connects the retinae with the pretectal area; it is involved in the pupillary light reflex via the Edinger-Westphal nuclei and the 3rd brain nerve. The retinothalamic pathway connects the retinae with the nucleus suprachiasmaticus in the hypothalamus; it is involved in the generation of circadian rhythms and the control of sleep. And finally the accessory optic system connects the retinae with the three terminal nuclei and the nucleus of the optic tract; it is involved in the processing of self-motion. Interestingly, all vertebrates also posses centrifugal pathways; fibers starting in subcortical areas (often hypthalamic) and terminating in the retinae; for primates the precise function of these sparse pathways is not well understood, for a review see Repérant et al. (2006).

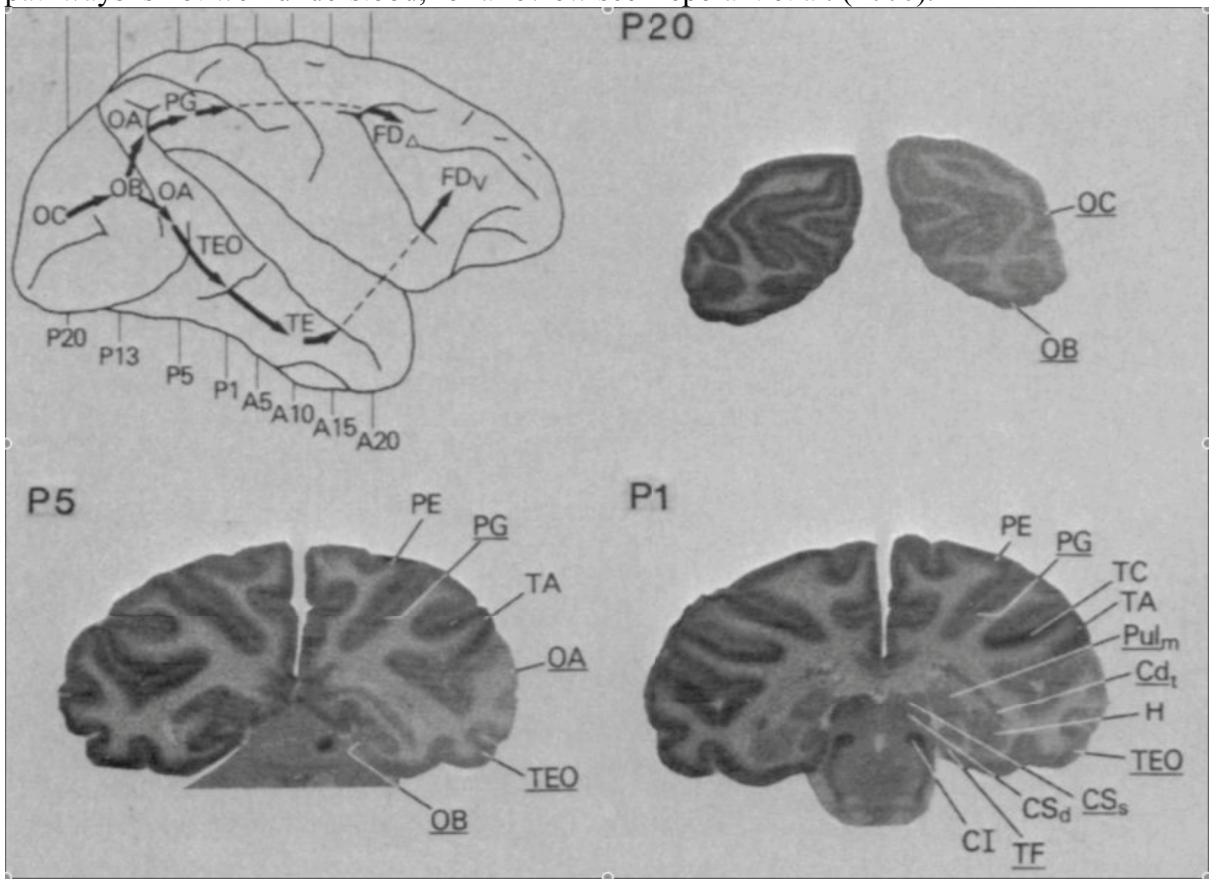

Figure 1: Overview of the macaque's visual system (from Macko et al. (1982)). Top left: lateral view of the right hemisphere, schematic display of all areas detected as visual. Top right to bottom right: three coronal slices, taken 20 mm, 5 mm, and 1 mm posterior of the interaural line, deafferented right hemisphere. Areas darker on the left than the right side are visually driven. Abbreviations: OC refers to striate cortex (V1), OB to posterior prestriate cortex, OA to anterior prestriate cortex, PG to posterior inferior parietal cortex, TEO to posterior inferior temporal cortex, TE to anterior inferior temporal cortex, TF to fusiform cortex, and FD to posterior prefrontal cortex; non-

visual cortical areas: PE refers to superior parietal cortex, TA to superior temporal cortex, TC to the supratemporal plane of the superior temporal cortex; subcortical visual areas: Pul_m refers to the medial pulvinar, Cd to the caudate nucleus, CS_S to the superficial layers of the superior colliculus; subcortical non-visual areas: H refers to the hippocampal formation, CS_d to the deep layers of the superior colliculus, and CI to the inferior colliculus.

Lower vertebrates and birds, mainly process their visual surround using the retinotectal pathway, while higher mammals shift more to the retinogeniculate pathway (summarized in Glickstein, M. (1969)). In primates, the main 'conscious visual processing' occurs via the retinogeniculate pathway, while the retinotectal system is mainly concerned with visuo-motor processes including saccade generation and control.

Primates are mainly visual animals and therefore a large fraction of their cortical surface area is dedicated for visual processing. Macko et al. (1982) used [2-^{14}C]Deoxyglucose injections in rhesus monkey to map the extent of visually responsive cortex. Monkeys received unilateral sections of the optic tract (and anterior commissure and corpus callosum), and then fixated a high contrast rotating visual stimulus while radioactive glucose was injected in their blood stream. Autoradiography was used to measure the amount of glucose uptake in both hemispheres; comparison of radiation strength in the afferented versus the deafferentated hemisphere revealed the ratio to which each area was activated by visual input. Since deafferented neurons did not receive the visual stimulation they were less active (and less dark in the autoradiographs) than the corresponding neurons in the intact hemisphere. The results of this mapping experiment demonstrated that visual input is processed in the occipital, the inferior temporal, and the posterior parietal, as well as in parts of prefrontal cortex (Figure 1).

Mishkin, Ungerleider and Macko (1983) performed targeted lesion studies to further differentiate extrastriate visual areas. Lesions in inferior temporal cortex impair the animals' object recognition abilities, while lesions in the posterior parietal cortex impair the ability to choose based on proximity to landmarks. The first task, object recognition, requires the interpretation of an object's qualities, while the landmark discrimination task requires the interpretation of spatial relations. Strikingly, each lesion impaired one discrimination ability only, while leaving the other intact.

Receptive fields of inferior temporal neurons, tend to be very large in size and offer therefore only little information about stimulus position. These large receptive fields qualify these neurons well to act as position independent object detectors. In addition, their selectivity for features as color, shape, and complex shapes qualify them for object identification.

Cells in posterior parietal cortex, unlike the purely visual driven cells in inferior temporal cortex, are polysensory, that is, they respond to both visual as well as tactual stimuli. These cells are mainly responsive to stimuli in the contralateral hemisphere (a crossing of hemispheres also typical for somatosensory and motor systems). The visual features these cells prefer are spatial in nature, like motion, direction of motion, velocity, rotation, and depth (see Orban (2008) and Maunsell & Newsome (1987) for reviews of neuronal selectivity in both pathways).

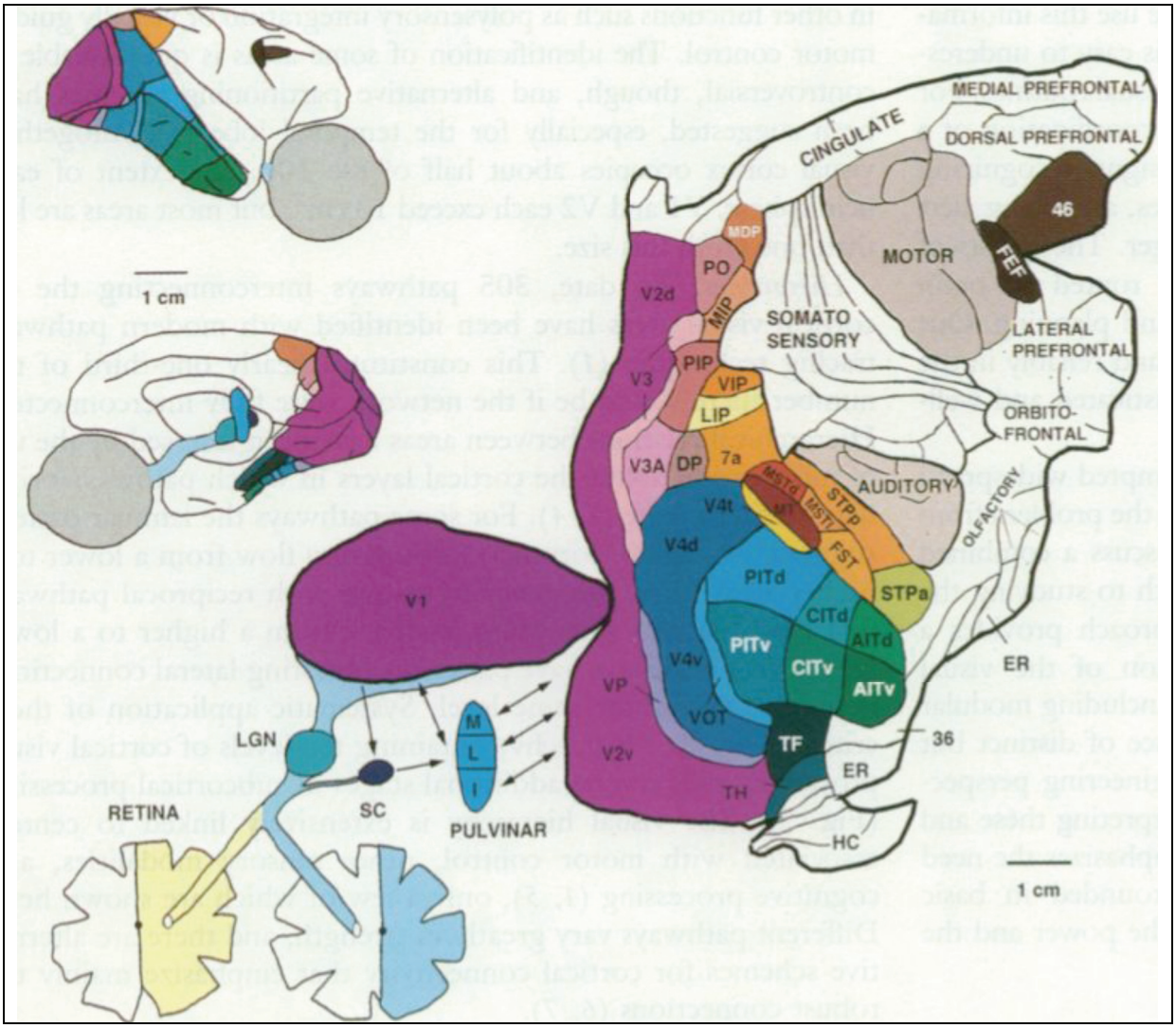

Figure 2: Overview of the macaque visual system (from Van Essen et al. (1992)); visually responsive areas are shown in color. In comparison with Figure 1, V1 corresponds roughly to OC, V2 to OB, V3A, V4, and MT/MST to OA. VIP, LIP, and area 7a correspond to PG, PITd and PITv to TEO, and CITd, CITv, AITd and AITv to TE. FEF and area 46 correspond to FD.

All these facts led Ungerleider and Mishkin (1982) to the hypothesis that the macaque visual system is hierarchically divided into two functional pathways: a 'ventral stream' involved in object vision, starting in striate cortex and extending along the inferior temporal cortex; and a 'dorsal stream' involved in spatial vision, extending from striate cortex over anterior prestriate cortex into posterior parietal cortex. The ventral stream at closer look thus starts with projections from V1 to V2, and from there to V3 and V4; V4 then projects into both TEO and TE in the inferior temporal cortex. The dorsal stream also begins with projections from V1 to V2, and continues from there into area V5 or MT (middle temporal), and from then into adjacent areas in the upper bank (and fundus) of the superior temporal sulcus (STS) and the intraparietal sulcus (IPS). Based on the different functional specializations they dubbed the ventral stream as processing the 'what', while the dorsal stream processes the 'where' of visual information.

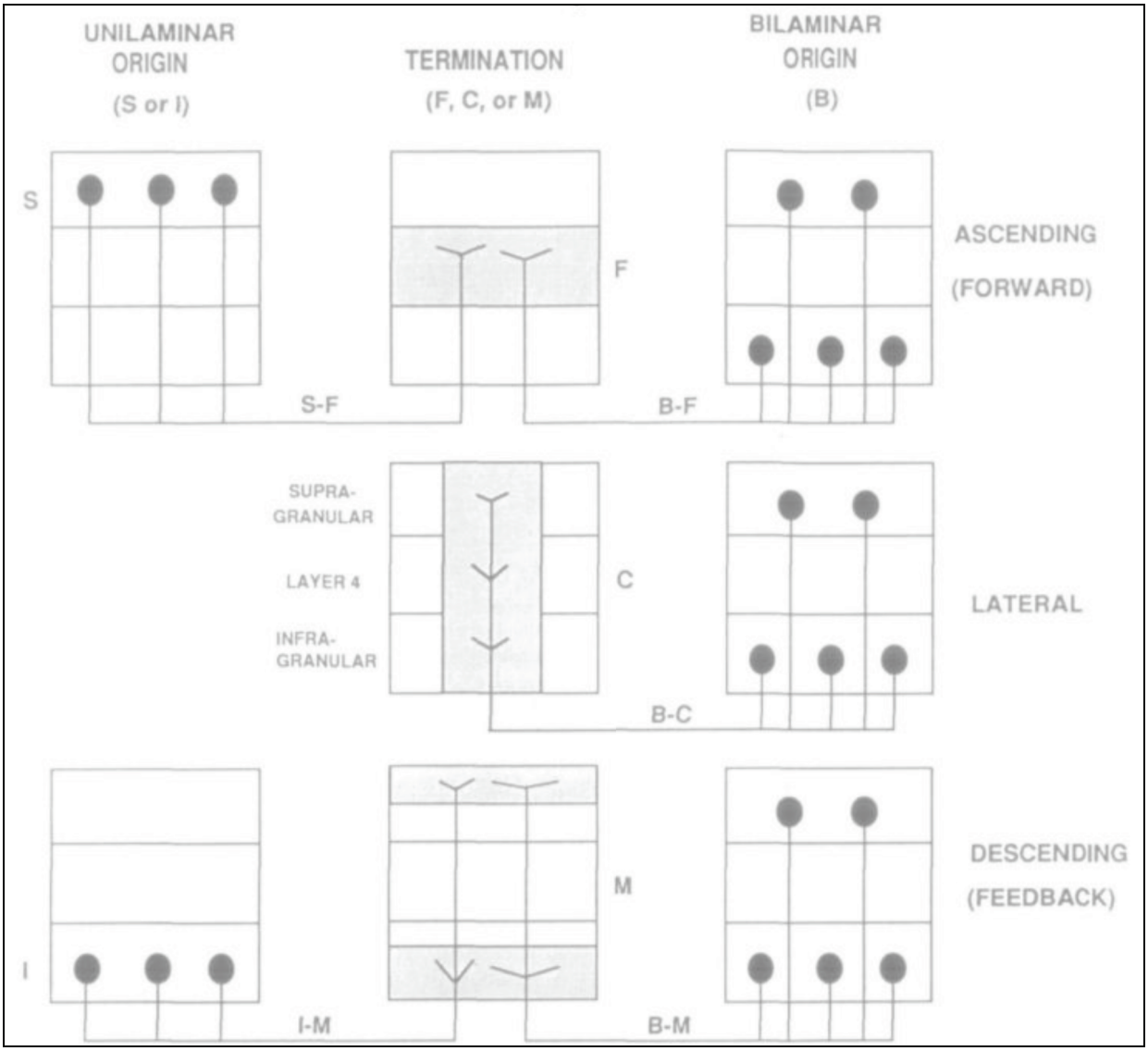

Figure 3: Classification schematic for cortico-cortical connections (from Felleman and Van Essen (1991)). Using this classification it is possible to assign a direction for connections between cortical areas, in turn allowing the areas to be ordered in a hierarchy.

In an attempt to parcellate the visually responsive cortex Felleman & Van Essen (1991) remapped the results of a large number of anatomical studies onto one reference hemisphere to elucidate the cortical wiring of the visual system. The first result of this work, a template map of the macaque visual system with boundaries for 32 visually activated areas is shown in Figure 2. At the time of publication this map could be considered to be an almost complete map of the visual system. The extent of all visual areas in this scheme closely corresponds to the autoradiography mapping by Macko et al. (1982) as seen in Figure 1.

Mainly using specific connection patterns between the areas (using cortical layers of neuronal somata and the axon terminals as 'fingerprints') they then generated a tentative hierarchy of those 32 visual areas. The 'fingerprinting' used the known projection patterns to assign each connection to one of the three categories: ascending, lateral and descending. Since layer 4 is the main input layer of cortex, projections mainly terminating in layer 4 were classified as ascending feed-forward connections; projections terminating in all layers were

considered columnar lateral connections; and projections terminating both in supragranular and infragranular layers were classified as descending feedback connections. Figure 3 shows the projection patterns and the classification scheme.

This study upholds the distinction between a ventral stream, whose input is mainly relayed by V4, and a dorsal stream, mainly relayed through V5/MT. In addition it reveals considerable information exchange between the pathways, that is, laminar connectivity patterns show hierarchically higher areas of the two pathways to directly interact.

Using the area connection data from Felleman & Van Essen (1991), Malcolm P. Young (1992) calculated a topological representation of the visual areas, using a multidimensional scaling technique. This approach yields a two dimensional plot showing all areas and their connections; the technique places elements close together, that are well connected, and spatially separates elements, that are only loosely connected. This approach, as shown in Figure 4, 'naturally' results in a common input cluster and two separated clusters, a ventral and a dorsal one. The area comprising the clusters match the two-pathway model (Ungerleider & Mishkin (1982)) quite well. In addition, the prefrontal convergence in area 46 matches prefrontal area FD_V, as identified by Macko et al. (1982).

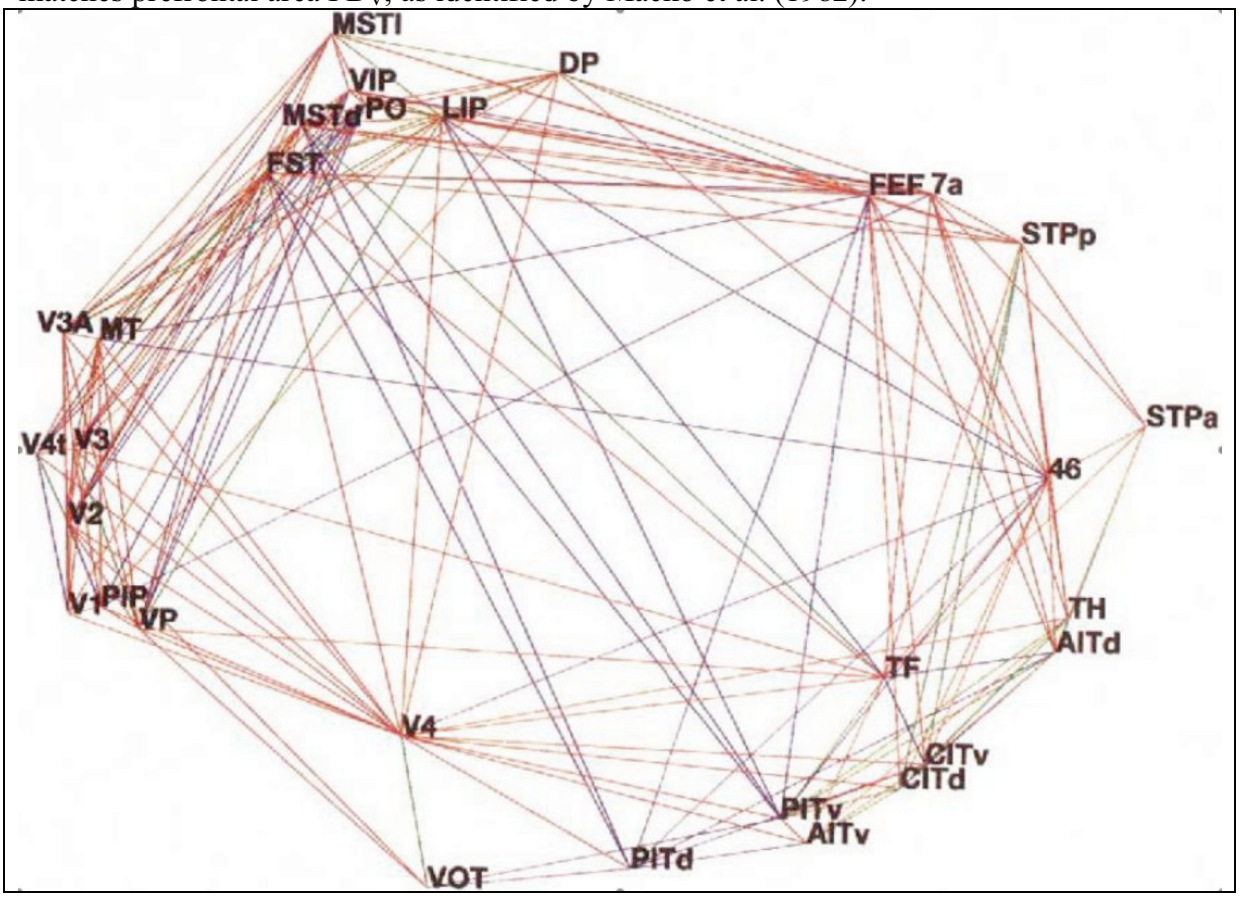

Figure 4: The topological organization of the macaque cortical visual system (from Young (1992)). Areas are clustered by their connectional distance, known projections are displayed as lines (red bidirectional, green and blue unidirectional). Note the three main clusters, a striate-prestriate cluster at the left containing mainly occipital structures; a parietal cluster at the top; and a inferior temporal cluster at the lower right. Also note the convergence of the two extra-occipital clusters at area 46 (prefrontal cortex close to FD_V in Figure 1) and STPa (the anterior superior temporal polysensory area). Area names as in Figure 2.

In humans lesions of visual cortex produce different symptoms depending on their precise location. Lesions of occipitotemporal cortex can create object agnosia (including prosopagnosia, or face-blindness, a specific inability to recognize faces) and achromatopsia; while occipitoparietal lesions can create, amongst other things, optic ataxia and visuospatial neglect (Ungerleider and Haxby (1994)). Unlike the targeted lesions used in monkeys, human data relies more or less on accidental lesions, whose precise location and extent is variable.

To further scrutinize the large-scale organization of human visual cortex, Haxby, et al. (1991) performed measurements of regional cerebral blood flow (rCBF) using positron emission tomography (PET). Subjects performed a spatial discrimination task and an object recognition task. Figure 5 shows the main results from these experiments; the spatial vision task activated lateral occipital and superior parietal cortex, while the object vision task activated lateral occipital and occipitotemporal cortex.

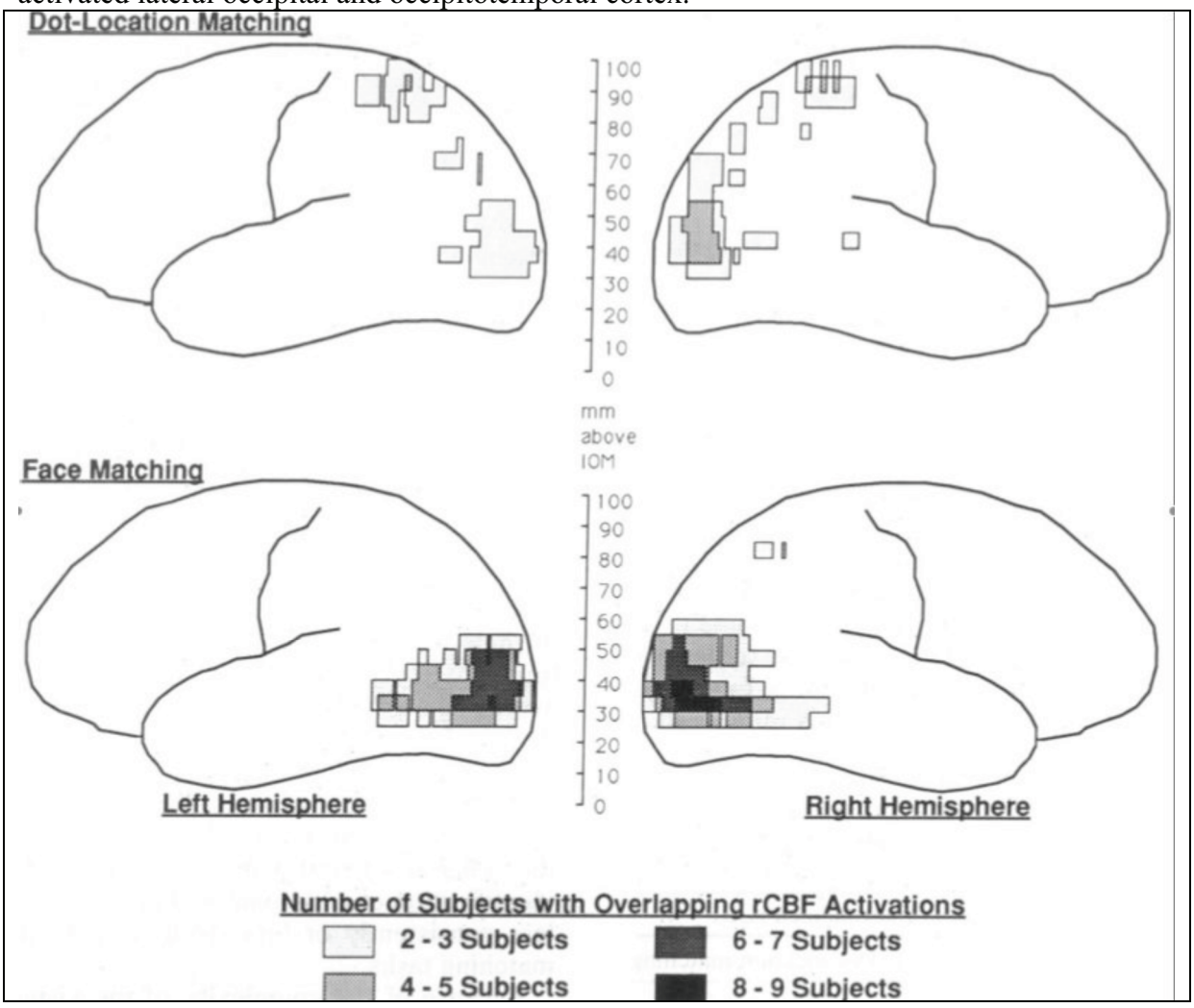

Figure 5: Divergence of 'what' and 'where' in human visual cortex (Haxby et al. (1991)). Shown are cortical regions that were activated (as measured in increased rCBF compared versus a sensorimotor control task). The gray level codes the number of subjects showing increased blood flow in those areas (all individual data co-registered onto a standard atlas brain). The dot-location matching task (top) requires parsing of the spatial relationship between stimuli, while the face matching (bottom) requires parsing of faces to match identity. Both tasks activate lateral occipital cortex, the spatial

task also activates superior parietal cortex, the object identification task also activates occipitotemporal cortex.

Combined, the human lesion analyses and the PET-studies indicate, that the large scale organization of human visual cortex is a division of visual processing into two pathways, one dorsoparietal for spatial vision, and one occipitotemporal for object vision, with both pathways sharing a common input. This organization is very similar to the macaque's, as can be seen in Figure 6.

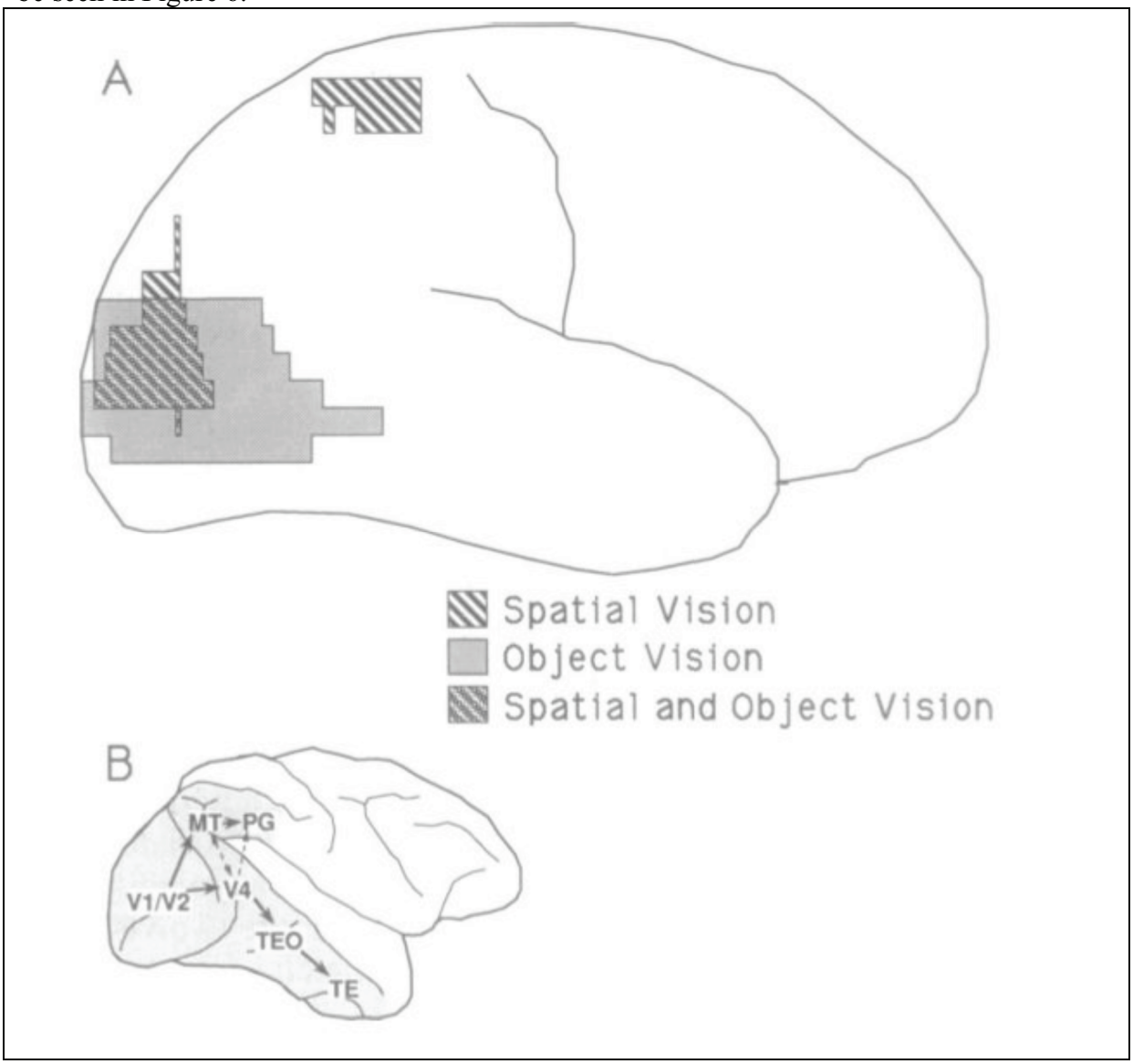

Figure 6: Similarities in the organization of the visual system of humans and macaques (from Haxby et al. (1991)). Humans (A) and macaques (B) process visual information in similar ways; occipitotemporal early visual cortex (V1, V2) processes all inputs, while later processing is divided into two branches; a more dorsal spatial 'where' stream (containing MT and PG in the macaque) and a more ventral 'what' stream (containing V4, TEO and TE in the macaque).

In the early 1990s Ogawa et al. (1990) noted that magnetic resonance properties of blood depend on its oxygenation level; and, since the blood oxygenation depends on neurophysiological events, measuring this signal allows inferences about the physiological

state. Kwong et al. (1992) showed, that the BOLD signal can be used to map the activity of the human brain *in vivo*. Since then this non-invasive method, functional Magnetic Resonance Imaging (fMRI), has been used extensively to map the human brain (as well, as the brains of other primates and rodents). Several experiments that probe the dichotomy of the visual system have been performed in human and monkeys, using similar, or even the exact same stimuli, allowing a very detailed comparison of the brain organization of theses species.

Figure 7 shows the activation, caused by a spatial visual stimulus (a disparity-defined checkerboard), between monkey and human. Both species show activation along structures of the occipitoparietal cortex. They also show some activity in early visual areas. These results agree nicely with the lesion and PET experiments, showing that processing of spatial variables, like depth, is mainly performed by the dorsal pathway.

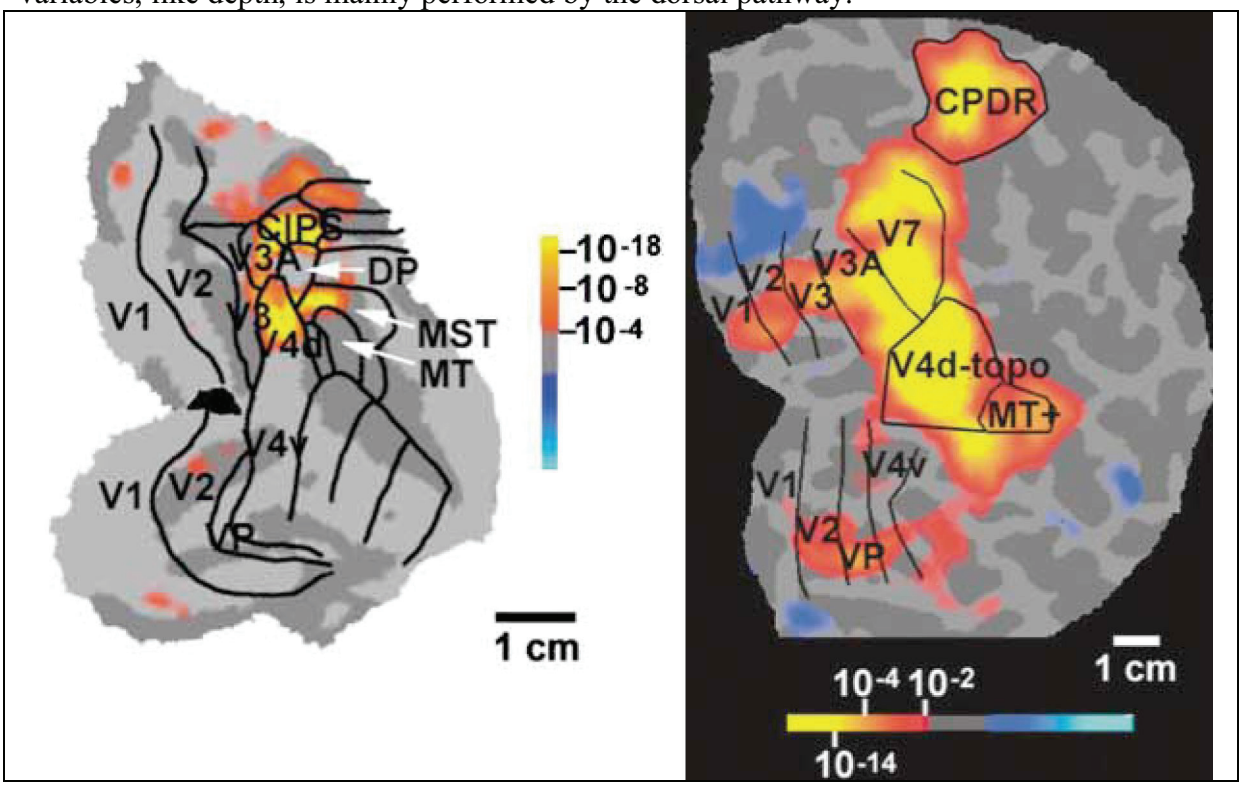

Figure 7: Localization of disparity-sensitive cortical areas in macaque (left) and human (right) (compiled from Tsao et al. (2003a). Both sides show statistical activation maps, comparing cortical activation to a checkerboard stimulus, defined by binocular disparity in a random dot field, versus activation to a flat random dot field. The activation is overlaid on a flat representation of the cortical surface of the occipital pole (dark gray: sulcal depth, light gray gyral heights). Black lines mark borders between the labeled visual areas. Both species clearly show activation of structures of the dorsal pathway. Abbreviations: CIPS, caudal intraparietal sulcus; CPDR, caudal parietal disparity region.

In comparison, Figure 8 shows the activation pattern, caused by object processing, for monkey and man. The maps show that in both species processing intact images of objects compared to unrecognizable scrambled versions mainly involves temporal cortex.

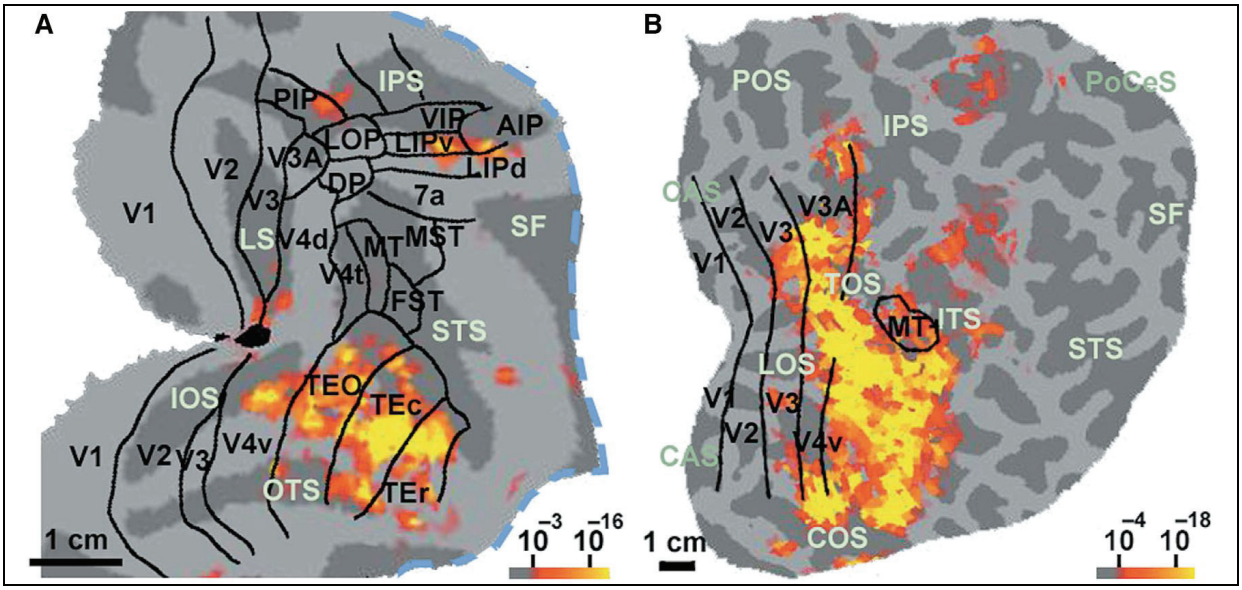

Figure 8: Localization of object-sensitive cortical areas in macaque (A) and human (B) (compiled from Tsao et al. (2003b)). Statistical activation maps shown overlaid on flattened maps of the posterior part of the brain. Contrasted is the activation by images of objects versus scrambled versions of the same images. The main activation is located along the inferior temporal region for both species. Abbreviations: LS, lunate sulcus; IOS, inferior occipital sulcus; OTS, occipitotemporal sulcus; IPS, intraparietal sulcus; STS, superior temporal sulcus; SF, Sylvian Fissure; AS, arcuate sulcus; ITS, inferior temporal sulcus; POS, parietooccipital sulcus; CAS, calcarine sulcus; COS, collateral sulcus; TOS, transoccipital sulcus; LOS, lateral occipital sulcus; PoCeS, postcentral sulcus.

It is of interest to note, that the fMRI results show areas that are differentially activated by the stimulus conditions compared; therefore areas activated equally under a specific contrast do not appear on the activation contrast maps. Since early visual areas like V1 and V2 show no real preference for either objects over scrambles, or disparity checkerboards over a flat stimulus, they are not activated in Figure 7 and Figure 8; however, compared to a blank screen whole and scrambled objects, as well as zero disparity and disparity checkerboard random dot fields, do elicit modulation of activity in V1 (see Tsao et al. (2003a) and Tsao et al. (2003b)).

Since the large-scale organization of visual cortex is very similar in macaque and man even though these two have been separated for several million years, comparing the actual layout of visual areas between the species should allow insights into the fine-scale organization of these areas as well. Van Essen et al. (2001) developed and refined a method to overcome inter-subject and even inter-species differences in cortical layout, by warping surface representations of the cortical sheet. The warping simultaneously conserves the neighbor relations between close points on the cortical sheet, while aligning more coarsely spaced landmarks between the input surfaces.

Taking a combination of anatomical landmarks (like the central sulcus), conserved functional landmarks (like the borders of area V2), and less conserved functional landmarks (shape driven activation), Denys et al. (2004) created a representation of macaque object sensitive areas overlaid on a flat map of human cortex. Figure 9 shows how macaque higher visual areas map to human cortex (and Brodmann areas) under these registration constraints.

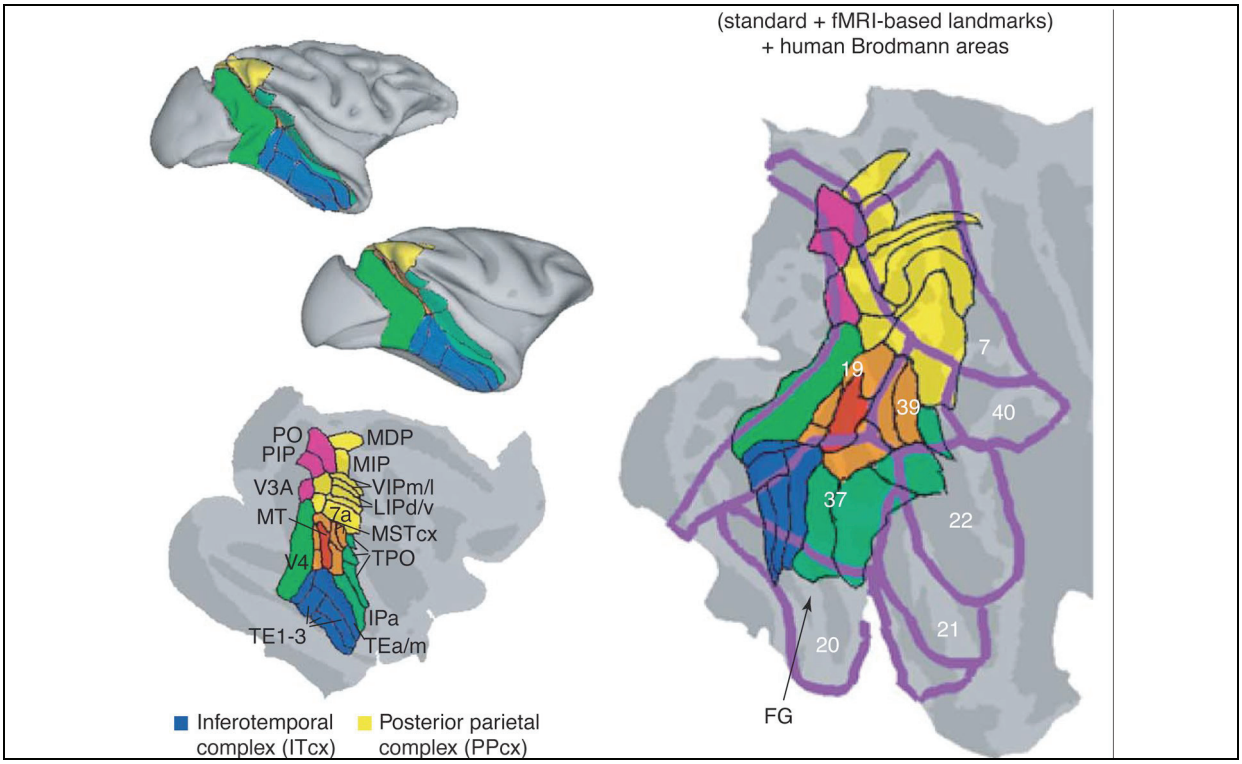

Figure 9: Comparing higher visual areas in human and monkey (compiled from Orban et al. (2004)). The left half shows higher visual area borders on an inflated monkey brain, the flatmap representation is also labeled. The right side shows the same macaque areas mapped over a human flatmap atlas; for reference the human Broadman areas are overlaid. Note how the macaque inferotemporal complex becomes mainly confined to (temporal) area 37, while most of the posterior parietal complex ends up in (parietal) area 7.

2. Modularity in early visual areas

Retina and lateral geniculate nucleus

In primates, the axons of the retina ganglion cells (RGCs) divide at the optic chiasm and separate according to the visual hemi-field of the environment their receptive fields belong to. Receptive field is the name given to the area in the visual surround that a given neuron responds to; RGCs usually have round receptive fields that are organized in a center-surround fashion and increase in size from the central part of the retina, the fovea, to the periphery. Center-surround organization means the neuron prefers opposite stimuli parameters in its center part compared to its more peripheral part. Cells which respond to stimuli presented left of the (current) point of fixation are routed to the right hemisphere of the brain, and vice versa cells responding to stimuli right of the fixation point are routed to the left half of the brain. Both retinae have an overlapping coverage of the visual surround (except for the far periphery, which is only represented monocularly). Therefore, at the chiasm two (almost) complete representations of the visual world get rerouted into two representations of each half of the visual surround, with (almost) all parts of the half world covered by axons from both eyes.

In the retinogeniculate visual pathway, the one mainly responsible for conscious visual perception in primates, the first relay station is the lateral geniculate nucleus (LGN) in the thalamus.

The LGN organizes the input from the RGCs in an orderly fashion, keeping the two dimensional topographic representation established in the retinae. There seem to be two main determinants for organizing inputs into distinct layers: first, the type of the source RGC input (and therefore also receptive field type), and second, the source eye (input from the ipsi- or contralateral eye). Figure 10 shows an exemplary histological section through a macaque's LGN.

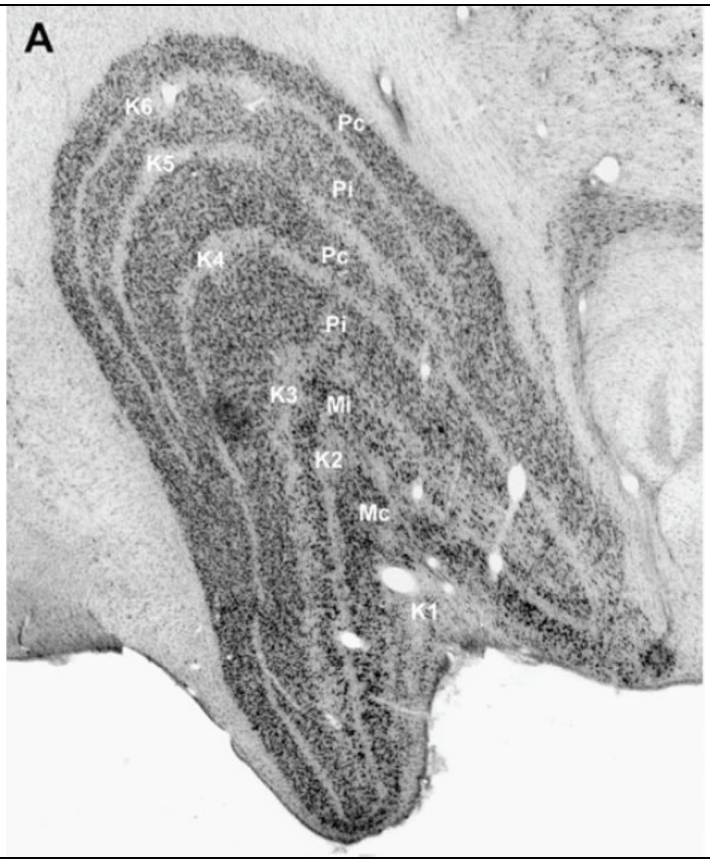

Figure 10: Organization of the lateral geniculate nucleus of the macaque monkey (taken from Casagrande et al. (2007)). The coronal, Nissl-stained section nicely shows the structure of the nucleus. Abbreviations: M, magnocellular; P, parvocellular; K koniocellular; c, from contralateral eye; i, from ipsilateral eye; numerals denote the different koniocellular layers. All layers have complete representations of the contralateral visual surround that are tightly in register.

Reviewed in Dacey (2000), the parvocellular layers (P) receive input mainly from midget ganglion cells; the magnocellular layers (M) receive input from parasol ganglion cells, and the koniocellular layers (K) from small bistratified ganglion cells. All other RGC types have not been traced to the LGN, their stratification is therefore unknown. The inputs to the P layers convey red and green (on and off) information from the fovea, as well as luminance (on and off) information from the periphery; the M layers convey luminance (on and off) information; the K layers convey at least blue (on) information. Each of the two M layers receives input from only one eye; for the four P layers the input eye changes between every layer; the source eye organization of the K layers is not well known.

Like in the retina, geniculate neurons have round receptive fields that increase in size from fovea to periphery. In primates, Wiesel and Hubel (1966) described four main receptive field / response categories. According to their nomenclature type I cells have center-surround fields and opponent-color responses, that is, when stimulated with white light, they show a ‘simple’ center-surround organization with excitatory center and inhibitory surround (or vice versa). At the same time, when stimulated with filtered light, center and surround respond only to different wavelengths. The center might be driven by red light, while the surround only reacts to green light, such that covering the center or center and surround with red light will drive the neuron maximally (as the surround is ‘blind’ for red light); covering center and surround with green light will cause short transient off-responses as well as inhibit the neuron

below its default firing rate. Presenting green only in the center does not change the default firing rate. Type II cells, in contrast, only show opponent-color responses without center-surround organization. That is, such neurons respond to optimally colored stimuli in their receptive field and they are inhibited by stimuli of the opponent-color independent whether the stimuli cover the whole receptive field or only a small fraction in the center. Interestingly type II neurons do not change their default firing rate when presented white light stimuli (small or full field). Type III cells only show center-surround organization without any preferred wavelength for center or surround. (And finally, type IV cells show excitatory center and inhibitory surround, with a chromatically rather unselective center and a surround that changes from complete inhibition at short to medium wavelength light to a decrease in firing compared to the default rate for red light.) Neurons in the four dorsal parvocellular layers typically are of types I, II or III. Neurons in the two ventral magnocellular layers typically are of type III or IV.

The LGN is reciprocally connected with the visual cortex, mainly with Brodmann area 17, also known as primary visual cortex (V1) or striate cortex (because of its hallmark unique strong staining of cortical layer 4).

Primary visual cortex

From the late 1950s on, the physiology of V1 has been the focus of much scrutiny. In a series of experiments in cat and in monkey, Hubel and Wiesel established the groundwork for our current understanding of the functional architecture of V1 (concisely summarized in the Ferrier Lecture (Hubel and Wiesel (1977)).

Receptive fields in V1, like in those in earlier stages, are smallest in the fovea and get increasingly larger towards the periphery; cells close to each other not only have similar receptive fields diameters, they also represent areas located close in the visual surround, in other words, V1 maintains the topology already found in LGN and retina. It takes roughly one to two millimeters of distance between V1 neurons (measured on the cortex surface) for their receptive fields not to overlap (which is a direct corollary of the orderly increase in receptive field sizes from center to periphery).

One striking difference between LGN and V1 neurons is the organization of their receptive field and the optimal stimulus configuration. All LGN cells have concentric receptive fields, with or without center-surround type differences in excitatory and inhibitory subfields. Primary visual cortex, in comparison, shows (at least) four classes of increasing complexity. The least ‘refined’ neurons in striate cortex, ‘circular symmetric’ cells (Hubel and Wiesel (1977)), have concentric center-surround receptive fields that resemble those of the LGN. Most V1 neurons, however, show a more elaborate structure in the receptive field. The next class of neurons was named ‘simple’ cells by Hubel and Wiesel (1959). These cells are not optimally activated by the small spots of light, that work well in retina and LGN, but respond to small bars of light (or edges) of a certain orientation. Each cell has only a narrow range of orientations that cause responses and a small displacement of the stimulus inside the receptive field will decrease the response. ‘Complex’ cells is the name of neurons that also only respond well to oriented bars or edges, but do not show the dependency on the exact position of the stimulus inside the receptive field, as ‘simple’ cells. Finally, ‘hypercomplex’ cells are very similar to complex cells, in that they respond well to bars or edges of a certain orientation anywhere in their receptive field, but in addition they also are sensitive to the total length of the edge or bar. Also called ‘end-stopped’ cells, they only respond well, if one or both ends of an oriented stimulus do not extend beyond a certain region. The less complex cells of type ‘circular symmetric’ can be found mainly in cortical layers 4C and ‘simple’ cells in 4B (and 6), layers receiving direct input from LGN neurons; ‘complex’ and

'hypercomplex' cells are mainly found in layers 2, 3, 5, and 6, layers receiving only little direct LGN input (more details later). Simple, complex, and hypercomplex cells represent the result of true processing in V1; only 'circular symmetric' cells can already directly be explained by the properties of LGN neurons.

Recordings performed perpendicular to the cortex surface always yield neurons that prefer the exact same stimulus orientation from layer 1 to 6 (with the exception of layer 4C, which shows no orientation selectivity); these neurons (from all four types) have very similar receptive field centers. Horizontal electrode tracks (ideally restricted to just one layer) yield an orderly procession of preferred orientations at roughly 10° per 20-50µm. The first observation shows that V1 is organized in small modules, called orientation columns; the second shows, that these columns are arranged in a regular fashion. Initial attempts to describe this arrangement based on reconstructed electrode tracks led to a model of swirls of iso-orientation slabs. Because of the relative coarse sampling by the reconstructed tracks this initial model always was considered preliminary. Bonhoeffer and Greenvald (1991) reassessed this model again using *in vivo* optical imaging of intrinsic signals. This technique exploits the fact that optical refraction of neural tissue depends on its electric or metabolic activity; actual measurements are taken from several square millimeters of cortex simultaneously with a maximum resolution of 50 µm and are therefore well suited for mapping orientation column organisation. The refined model shows that columns of the same orientation are arranged like pinwheels. V1 has several singularities in which columns of all orientations meet. Today, two photon calcium imaging allows optical imaging at the resolution of individual neurons; Ohki, et al. (2006) show that even at the center of a pinwheel a neuron's preferred orientation can be predicted from the 'orientation sector' it belongs to. Figure 11 shows exemplary maps of the larger organization of orientation columns in cat striate cortex, for intrinsic-signal optical imaging and a close-up of the center from calcium imaging experiments.

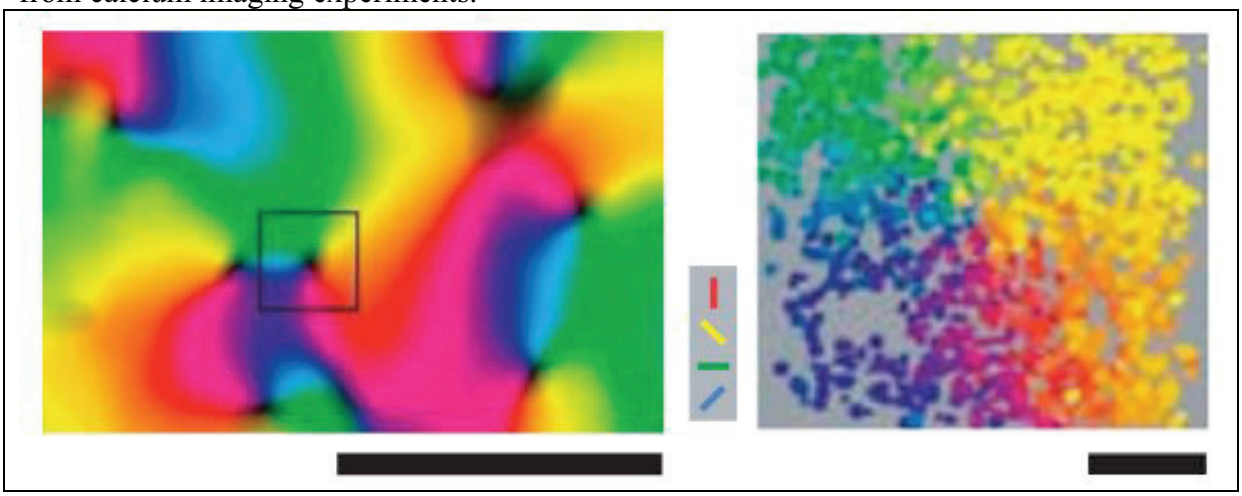

Figure 11: The topology of orientation columns in cat primary visual cortex (compiled from Ohki, et al. (2006)). The left shows mapping of orientation pinwheels using intrinsic-signal optical imaging (scale bar 1 mm). Colors code the optimal orientation of the columns. The small middle inset shows the common orientation legend. The square approximates the area targeted for two-photon calcium imaging. The right shows the result of measuring the orientation preferences for nine depths (from 130 µm to 290 µm below pial surface, scale bar 100µm). Even close to the very center of the pinwheel the preferred orientation of single cells is well in register with its orientation sector.

In addition to their orientation tuning, many V1 neurons also differ from LGN neurons in that they respond to signals from both eyes. In layer 4C, the major input from the LGN, neurons are still monocular, but neurons in other layers of V1 can be activated by visual stimuli in either eye, showing again the results of the processing performed by V1. Nevertheless, most neurons are mainly driven by one of the eyes, a phenomenon called ocular dominance by Hubel and Wiesel. Recordings perpendicular to the cortex surface show, that the ocular dominance for each cortical column is equal to the eye activating the monocular cells in layer 4C. This shows that cortical cells are organized in ocular dominance columns. Horizontal recordings show that the dominating eye changes periodically, roughly every 400 μm; defining the width of the dominance columns. Since ocular dominance columns are mainly caused by the anatomical separation of monocular LGN inputs in layer 4C, it turned out that they can be detected using anatomical staining methods. Based on differences in axonal patterns caused by ipsi- and contralateral input LeVay et al. (1975), created an ocular dominance map of the macaque primary visual cortex. Figure 12 shows a typical ocular dominance map for the operculum of the macaque. Both types of stripes contain complete representations of the contralateral visual world. Each ocular dominance region contains several complete orientation pinwheels so that in effect both systems combine into one complete visual representation.

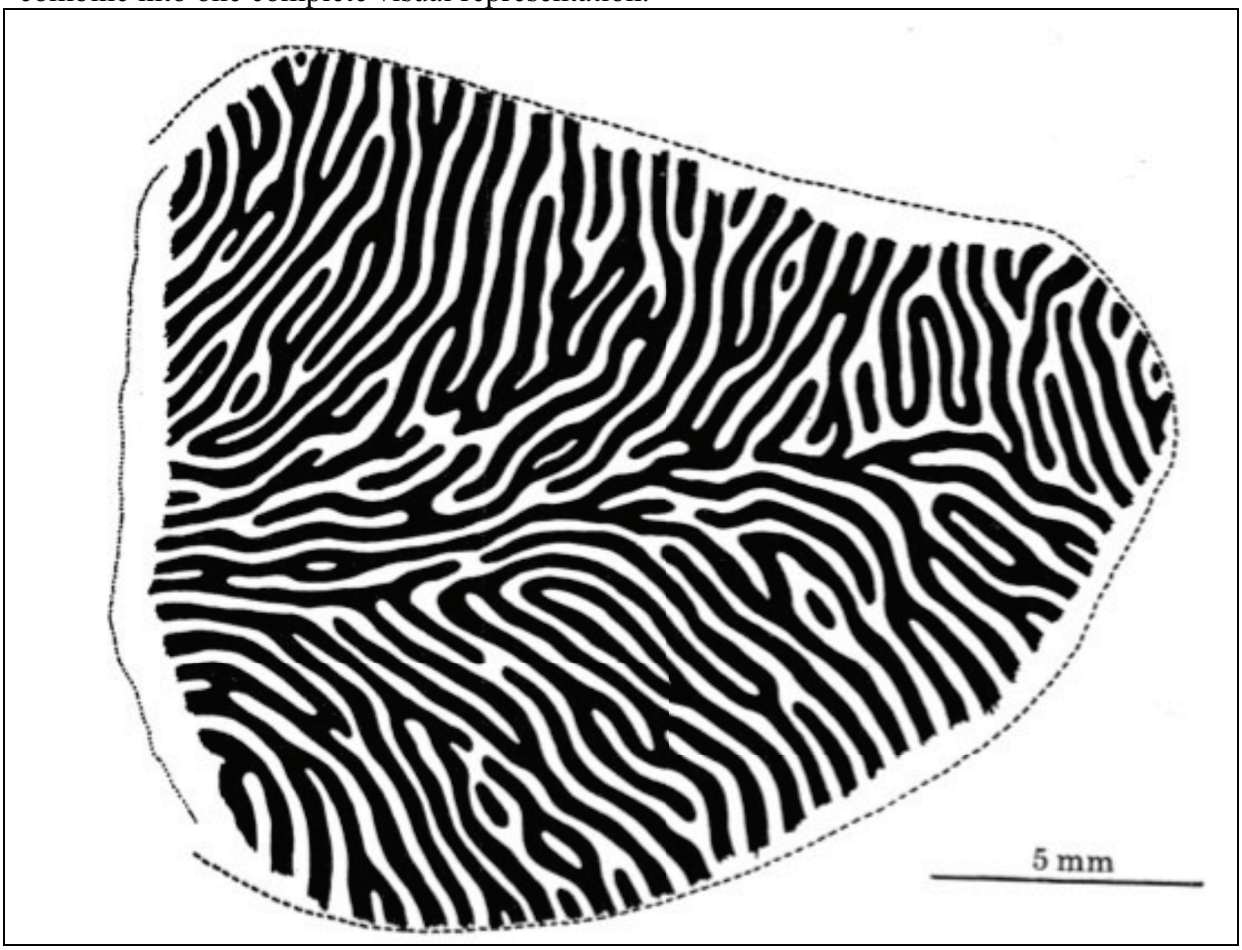

Figure 12: Ocular dominance columns of the operculum of macaque striate cortex (data from LeVay et al. (1975), adapted from Hubel and Wiesel (1977)). The dashed line on the right represents the border of V1 to the next visual area V2. The fovea is at the right end. Ocular dominance columns are organized into two inter-digitated patterns of ipsi- and contra-lateral preference.

An additional organizing structure in primary visual cortex is an evenly distributed pattern of patches of cytochrome oxidase (CO) rich compartments, mainly in layers 2/3, called blobs (Horton and Hubel (1981)). Neurons inside these blobs are color selective, while cells outside the blobs, in the inter-blob area are much less color selective (Livingstone and Hubel (1984)). Figure 13, from Lu and Roe (2008), shows how well aligned color selective regions and CO blobs are in macaque V1 (using combined in vivo optical imaging (of intrinsic hemodynamic signal) with CO histology. Closer analysis also shows that CO blobs or color domains are located mainly along the center of ocular dominance columns, and that color blobs are located in areas of low orientation selectivity away from the centers of the orientation pinwheels (see Lu and Roe (2008)).

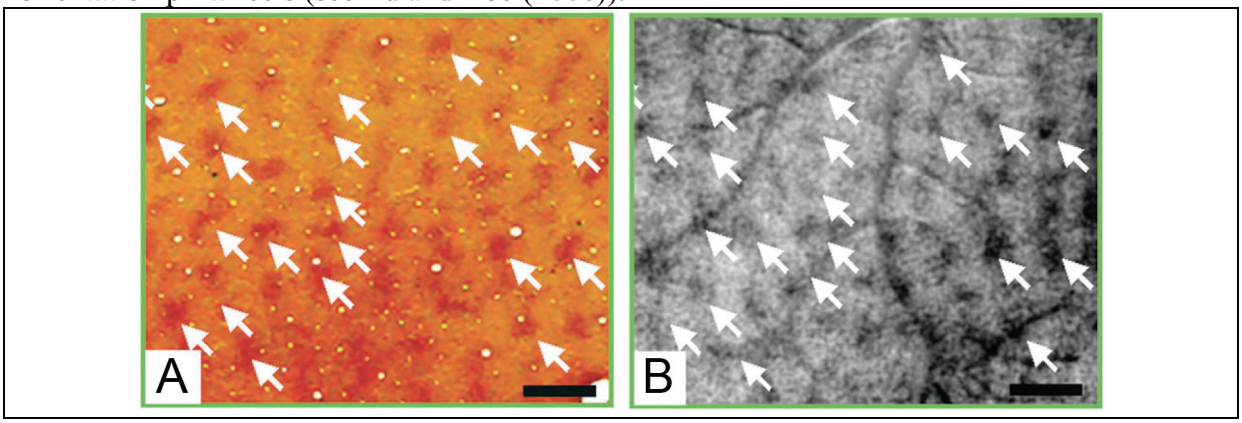

Figure 13: CO blobs align well with areas of color selectivity (modified from Lu and Roe (2008)). The left (A) shows a histological CO map; the right (B) shows color selective areas of Macaque V1 as dark spots. The white arrows show matching cytochrome oxidase and color 'blobs'. Histological sections were aligned to the optical imaging data, using affine transformation guided by the vascular patterns visible in both maps to correct for distortions caused by tissue fixation and flattening. Size bar: 1mm.

Initially it was assumed that the diversity of response types from the different RGC types maintained in the LGN, is also maintained inside V1 and V2 (Livingstone and Hubel (1988)). Based on the known anatomical connections and a series of elegant psychophysical experiments with humans, the model of three separated channels, shown in Figure 14, emerged. The beauty of the model is, that it effortlessly accounts for the later separation in ventral and dorsal streams, as the tentative input modalities for both streams are kept separated from the earliest possible stage. The separation into the three 'channels', movement/stereo, color, and form, however proved to be not as strict as this tripartite model demands.

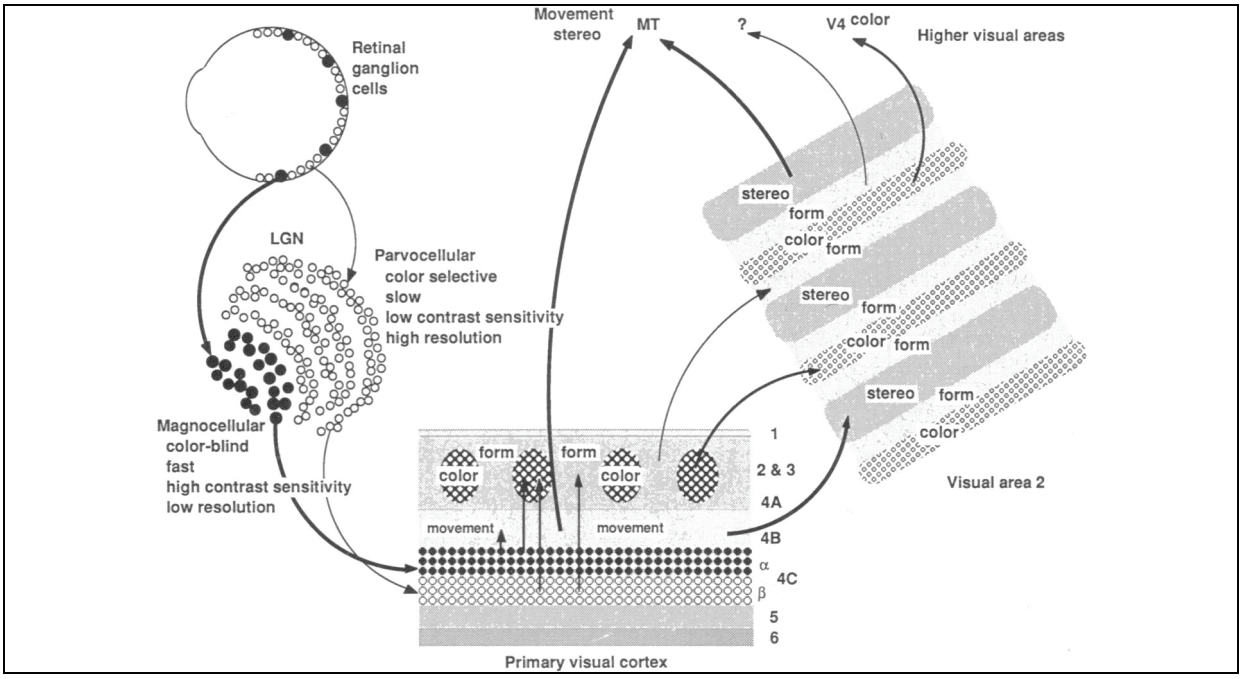

Figure 14: Schematic view of the early visual areas as a functionally segregation of three channels (from Livingstone and Hubel (1988)).

In the LGN the separation is still very strict; also the projection patterns of the three LGN cell types into V1 maintains the separation; intra-cortical connections in V1, however, mix all three LGN input channels. The connection distance between the projection layers is maximally two synapses (Figure 15). These cross connections show that the three 'channels' are less independent than previously thought.

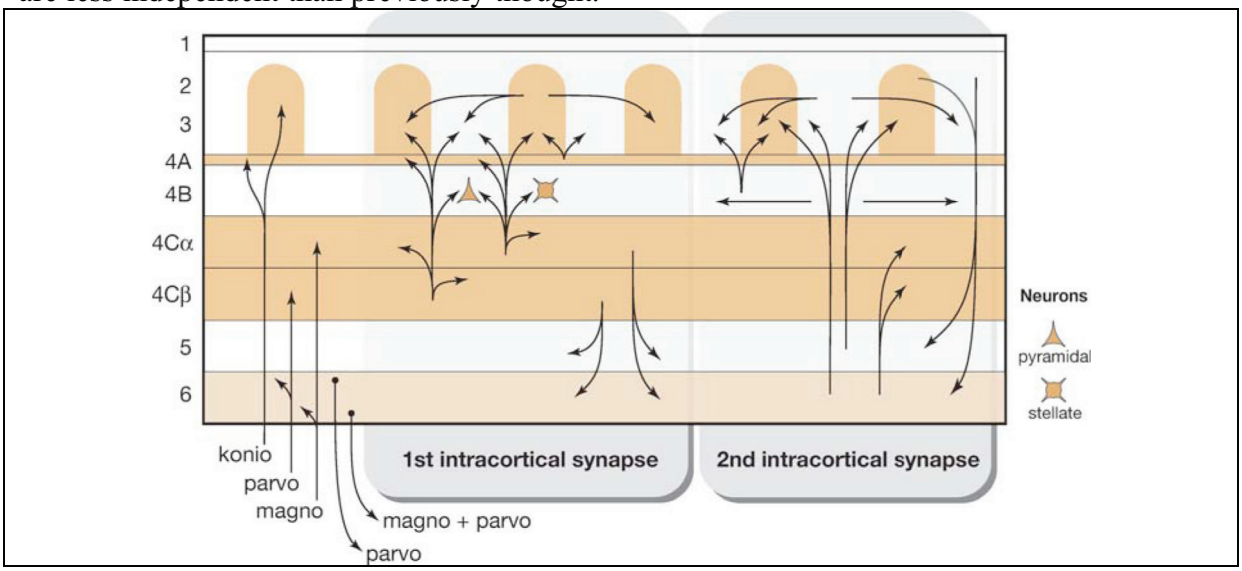

Figure 15: Intra-cortical connections of V1 (from Sincich and Horton (2005)). The three geniculate cell types project to distinct layers in V1. The distance between these layers, however, is only 2 intra-cortical synapses.

Secondary visual cortex

Under CO staining, V2, the cortex just adjacent/surrounding V1, shows a peculiar sequence of stripes consisting of alternating 'thick' and 'thin' stripes of dark labeling; interleaved

between any pair of dark stripes are ‘interstripes’ with almost no label, also called ‘pale stripes’. Following Hubel and Livingstone (1987), neurons in thick stripes are selective for orientation and also for binocular disparity; neurons in thin stripes show weak orientation selectivity, but show color-opponency; and finally, pale stripes show orientation selectivity and in addition many neurons there are also show ‘end-stopped’ responses. Each of the three stripe sets contains a complete representation of the visual surround, similar to the ocular dominance columns in V1 (Shipp and Zeki (2002)). Interestingly, the amount of CO staining in V2 is inversely correlated with the amount of projection the different stripes receive from V1, and directly correlated with the amount of projections from the pulvinar (Sincich and Horton (2002)).

Connections between V1 and V2

The tripartite model was based partly on the existence of three discrete projections from V1 to V2, to maintain the initial parallelism (Figure 14). The current model only maintains two separate channels from V1 to V2 (see, Sincich, Jocson, and Horton (2007)); Figure 16 shows, that V1 color sensitive domains, the CO blobs, project mainly to V2 thin stripes. Thin stripes, unlike orientation sensitive pale and thick stripes, also contain a large fraction of color sensitive neurons. Orientation sensitive V1 inter-blobs project to equally orientation sensitive V2 stripe types. The main difference between the orientation sensitive V2 pale and thick stripes is that thick stripes also respond to binocular disparity (Chen, et al. (2008)).

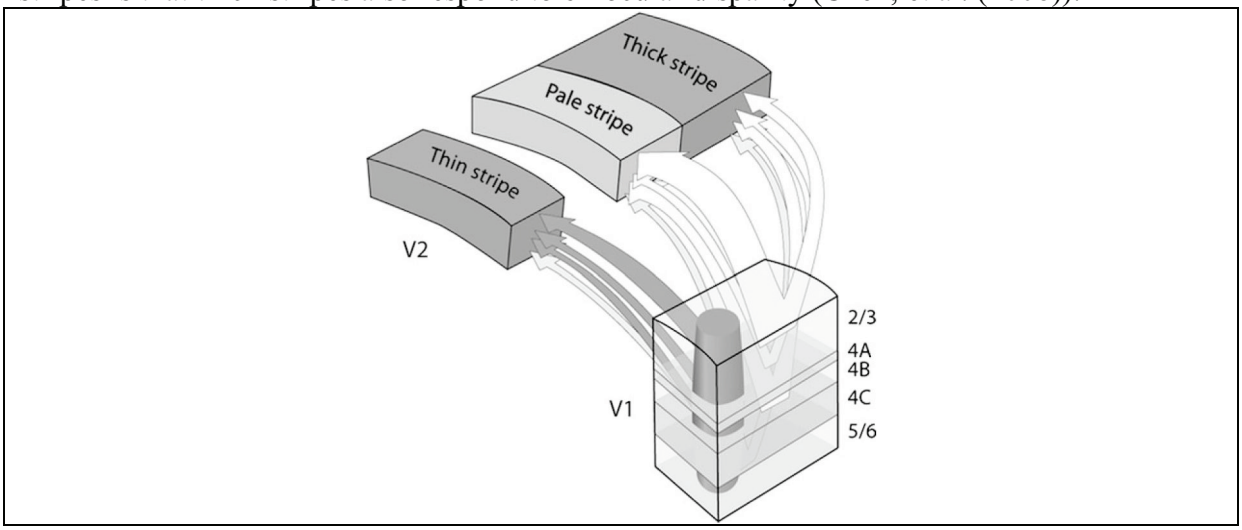

Figure 16: Anatomically distinct channels connect V1 and V2 (from Sincich, et al. (2007)). ‘Color’ information is relayed from V1 blobs to V2 thin stripes. Interblob V1 projects to orientation sensitive thick and pale stripes.

The magno-cellular LGN input to V1 terminates in layer 4C and then projects to layer 4B; 4B then projects to all V2 stripe types (though least to thin stripes), and it also directly projects to the motion sensitive area MT (Sincich and Horton (2005)). The 4B projections reaching V2, in turn, project either directly from V2 thick stripes to MT or via the third visual area (V3).

3. Modularity in higher visual areas

Motion

In the macaque, area MT, also called V5, is located in the superior temporal sulcus (STS). In combination with area V3A, MT represents the major entry stage for the dorsal visual pathway (see Figure 4). Figure 17 shows the input channels from earlier processing stages. In the main input channel, spiny stellate neurons project directly from layer 4B in V1 into MT. In a second input channel, a different population of neurons from V1 layer 4B (as well as all other layers) is relayed via V2 (thick stripes) to MT. The sub-cortical projections from the superior colliculus (SC) and the LGN are thought to be involved in the phenomenon 'blindsight' (Sincich et al. (2004)). Blindsight is the remaining visual capacities of individuals with complete destruction of primary visual cortex and/or the optic radiation that relays input from the LGN to V1 (see Stoerig and Cowey (1997)). Generally affected subjects do not consciously perceived these remaining capacities in location, discrimination or detection of visual stimuli, yet they perform tests well beyond chance level.

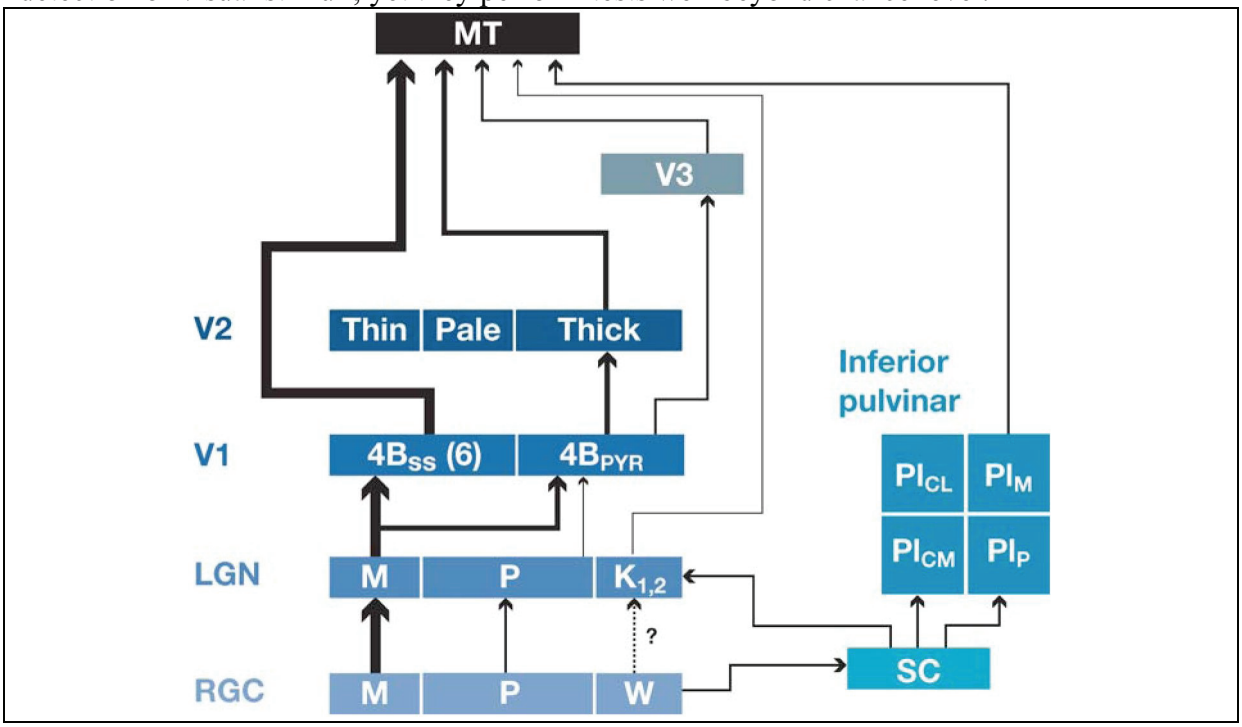

Figure 17: Cortical and sub-cortical inputs to area MT (from Born and Bradley (2005)). The rectangles represent individual sources (stacked by tentative hierarchy) the line thickness represents the magnitude of the input. MT's main input is from the magnocellular-dominated spiny stellate cells in V1 layer 4B. The input from V2 thick stripes (originating mainly from pyramidal cells in V1 layer 4B) is the second largest. Abbreviations: RGC, retinal ganglion cell; LGN, lateral geniculate nucleus; SC, superior colliculus; PI, inferior pulvinar; (CL, central lateral nucleus, M, medial nucleus, CM, central medial nucleus, P, posterior nucleus)

Area MT contains a complete representation of the contralateral visual surround. Neurons are tuned for direction of movement, with highest activation towards stimuli moving in the preferred direction and minimal activation towards stimuli moving in the 180° opposite direction (termed null-direction). In addition many MT neurons have a preferred speed of motion. Cells with similar preferred direction are stacked orthogonal to the cortical surface,

building a system of direction columns. Similar to the orientation columns in V1, direction columns in MT are organized in a topological map with small changes of preferred direction between columns interrupted by occasional sudden reversals by 180°. In addition to direction, many MT neurons also possess a preferred binocular disparity. See Born and Bradley (2005) for a recent review of these properties.

If both eyes focus on any point in space, stimuli at the focus plane/sphere are activating exactly corresponding 'locations' on both retinae; stimuli slightly out of focus produce retinal activations that are slightly horizontally shifted. The direction of his shift depends on, whether the stimulus is in front of the fixation point ('near') or behind of the fixation point ('far'). Measuring the amount and direction of this shift allows measuring the depth of stimuli relative to the fixation. DeAngelis and Newsome (1999) showed that disparity-selective neurons are organized as bands/clusters interleaved with areas of low disparity selectivity. The resulting functional organization of area MT is shown in Figure 18.

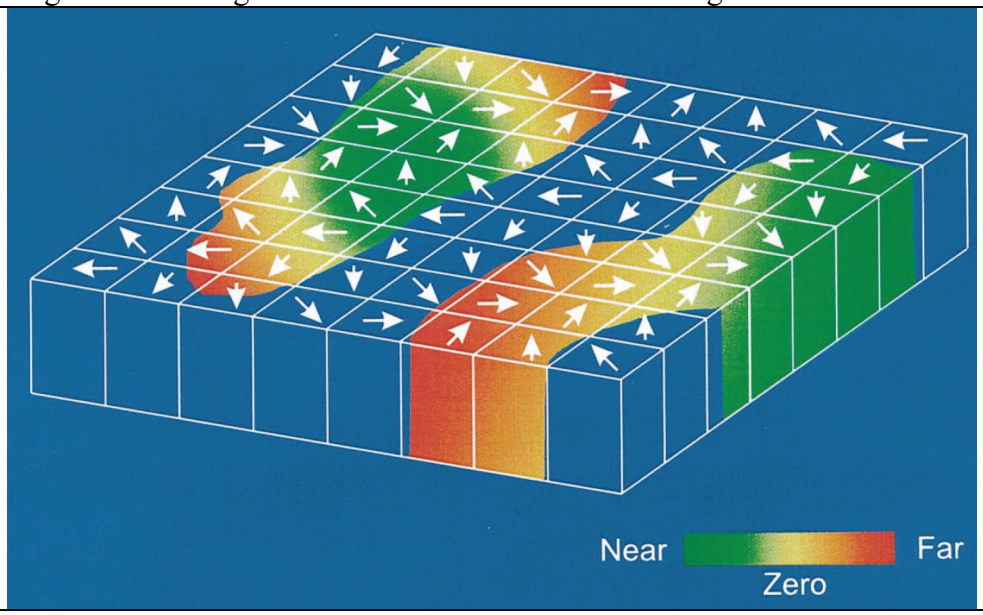

Figure 18: The functional organization of area MT (from DeAngelis and Newsome (1999)). The slab represents the cortical sheet. Direction columns are mainly organized as a map of small changes between columns (the simplified graphic does not show any interruption). Disparity-tuned patches show an orderly representation of preferred disparities with smooth transitions from near over zero to far.

V1 neurons projecting to MT show similar selectivity for direction of motion, as do MT neurons; disparity tuning in MT is much broader than in V1 (and more similar to V2 disparity tuning). Ponce, Lomber and Born (2008) reversibly inactivated areas V2 and V3 by cooling, while recording from MT. Cooling decreased disparity tuning in MT more than direction tuning, indicating that MT's disparity representation relies on the 'indirect' inputs, while the direction columns are driven mostly by the 'direct' V1 input. Interestingly, V2 thick stripe neurons, that most likely project to MT disparity regions, show only very little direction tuning (just orientation and disparity). MT disparity regions seem to combine direction and coarse disparity as co-registered maps for the first time in the visual hierarchy (DeAngelis and Newsome (1999)).

The activity of MT neurons predicts the ability of monkeys to perform coarse discrimination of absolute disparities (Uka and DeAngelis, reviewed from Roe et al. (2007)), as well as the reported percept in ambiguous 'structure from motion' stimuli (see Born and Bradley (2005) & Roe et al. (2007) for references). Inactivation of MT in macaques impairs

coarse depth discrimination and direction discrimination abilities. Discrimination of fine depth differences, however, might be mediated by area V4 (see Roe et al. (2007) for reference), the main entry point into the ventral visual pathway. MT's preferred stimulus properties, depth and direction of motion make it well suited to feed the dorsal stream of spatial vision.

Color

In the animal kingdom all chromatic vision is linked to different photoreceptors each with a unique spectral selectivity; in macaques and humans there are three different cone types in the retina, with absorption maxima in short (S), middle (M), and long (L) wavelengths (in addition the achromatic rod system has an absorption maximum between the M and L cones) (Dacey (2000)). The absorption spectra of the three cones are not discrete, but they have wide regions of overlap. Each light source will drive all three cones differentially, that is each wavelength (or combination of wavelengths in mixed light sources) will result in a signature activation pattern of the three color photoreceptors. RGCs combine the cone inputs selectively to create two channels of opponent colors; red-green (L vs. M cones) and blue-yellow (S vs. L+M cones). These RGCs transfer color information into the P and K layers of the LGN. These layers, in turn, project to the V1 CO-blobs, and then the V2 thin stripes. Achromatic V2 thick stripes project to 'dorsal' area MT, while chromatic thin stripes project to 'ventral' area V4 (Shipp and Zeki (1985)).

Taking opponent color properties (receptive fields organized with excitatory and inhibitory zones with different wavelength selectivity) as criterion, Zeki (1978) reported that; the dorsal stream entry points MT, V3 and V3A show almost no color tuned neurons, V2 shows less then 10%; V4, however, contains as much as 54% color tuned neurons. Initial recordings in (anatomically defined) V4 led Zeki (1973) to the assessment that 'in every case the units have been color coded, responding vigorously to one wavelength and grudgingly, or not at all, to other wavelengths or to white light at different intensities'. The other neurons in V4 are orientation selective (more so than the color cells) and are thought to be involved in form/shape processing. Both orientation and color are thought to be processed and combined by V4 to parse complex forms.

Perception of colors is more complicated than it appears at first sight, though. Intuitively one thinks that measuring the spectral content of light coming from each point in the visual surround should suffice to assign the property 'color' to each point. A direct consequence of this read-out would be that the perceived color of an object depends strongly on the spectral composition of the illumination. For 'pure' monochromatic illumination that observation holds true, e.g. under red light blue objects simply appear to be dark red while red objects appear to be very light red. For 'richer' light sources activating all cone types, though, the color percept dissociates from the actual flux of light, that is a red object continues to appear red, even if the actual wavelength composition of the reflected light would match the 'true' reflection of a different color (say yellow) under different lighting conditions (results from Land's 'retinex' experiment, see Zeki (1980)). This property of color perception is termed color constancy. Theoretically, the 'true' color of an object can be deduced from taking the relative activity maps for the three cone types over a larger area and compare them with each other, as illumination wavelength composition will affect all objects equally.

Some of the color-coding cells in macaque V4 show a response profile that correlates well with a percept of constant colors in the 'light' of changing illumination. Zeki (1983) used visual 'Mondrian' color stimuli to drive cells in macaque V4. The stimuli were initially designed by Land to test color constancy in humans; they consist out of abstract intersections of differently colored rectangles, resembling geometric images by Piet Mondrian (hence the

moniker). Together with spectrally controlled illumination this makes it possible to control the reflected wavelength composition of the color rectangles and compare that to the perceived color in humans. Figure 19 shows an example of a macaque V4 cell that responds according to the perception (of a human observer) that only one of the four stimuli actually was red and not according to the physical composition of the light-source in the receptive field of the cell. The existence of this neural specialization, and the lack of similar color constancy coding responses from other cortical areas make V4 the best candidate region for color processing in the macaque.

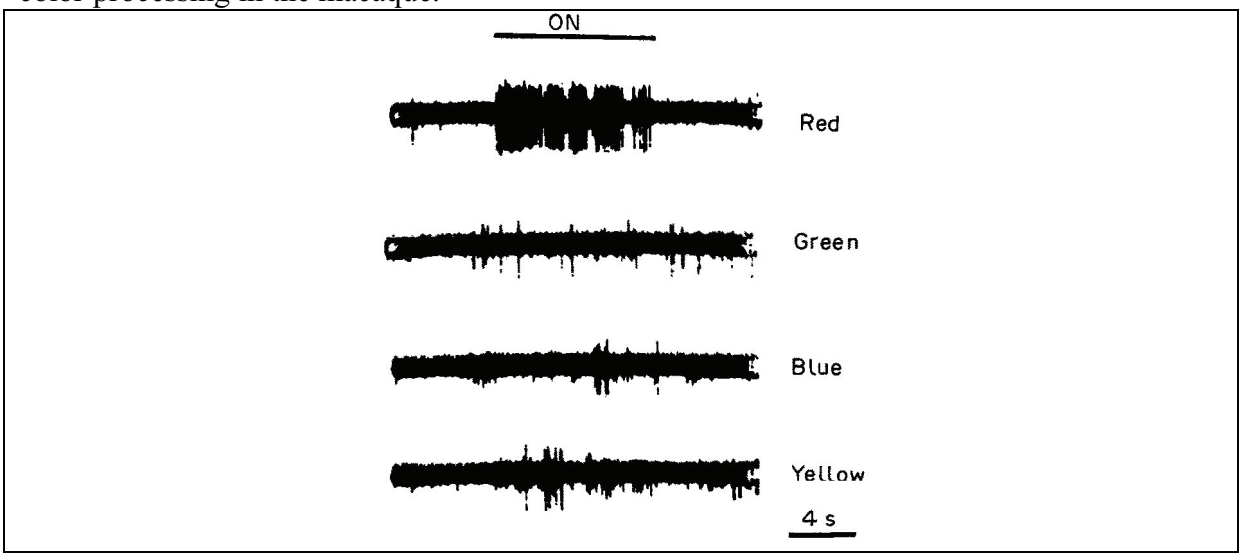

Figure 19: Responses of red cell in macaque V4 to the exact same spectral stimulus depend on the integration of reflectance (from Zeki (1983)). The four traces show the responses of a red selective cell in V4 to Mondrian patches of four different colors. For each recording the illumination was selected such that all four patches, even though they appeared to be different in color, reflected the exact same light in spectral composition. The cell therefore must have compared its input with information from outside its receptive field to assign the label 'red' only to one of the patches; showing that V4 contains neurons that correspond not to the physical input but to the actual percept.

Functional MRI studies of macaques revealed several areas in the vicinity of V4 that preferentially respond to color stimuli versus achromatic stimuli. Figure 20 shows the distribution of color selectivity in early visual areas of the macaque (Conway and Tsao (2006)). The localizer experiment did not select for color constancy but for wavelength selectivity, explaining the strong effect in V1 and V2.

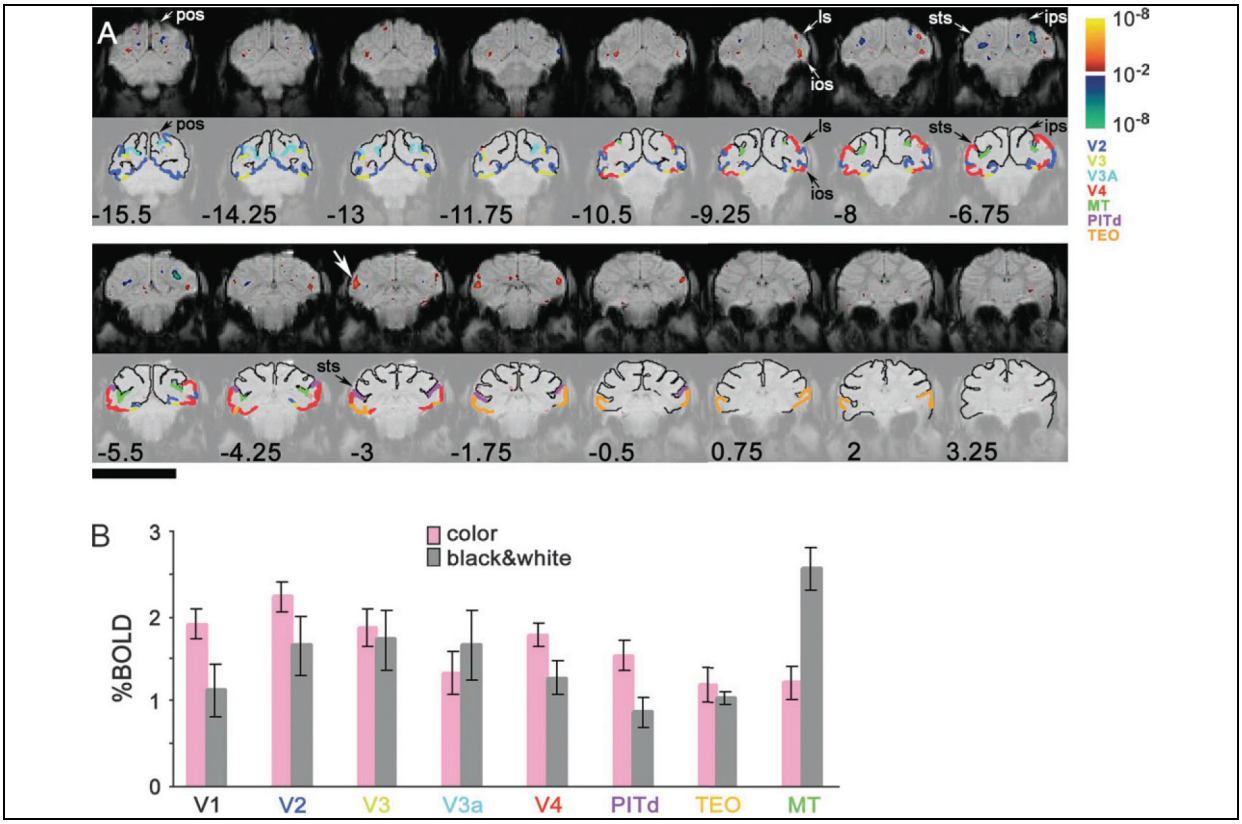

Figure 20: Color areas in macaque monkey (from Conway and Tsao (2006)). Rows 1 and 3 in A) show activation maps comparing BOLD activity to moving isoluminant red-blue gratings to black and white achromatic gratings; areas responding to color are overlaid in warm colors, areas responding to the achromatic stimulus are in cold colors. Rows 2 and 4 show visual areas in color taken from macaque brain atlas (color legend right of row 2, slice positions in mm relative to the interaural line is shown in black). For each defined area the bar graph in B) shows the mean percent change of the BOLD response for black and white and color gratings (compared to stationary grey); error bars show the standard error. Color responsive areas are V1, V2, V4 and PITd and TEO. Note that PITd as well as posterior TEO are considered to be part of the V4 complex by Zeki.

Human color vision has first been assessed by studying the effect of accidental lesions on the reported perception of subjects. Briefly reviewed in Bartels and Zeki (2000) lesions in areas in the posterior fusiform gyrus, anterior of ventral V3 and ventral of hMT+, a location that roughly matches the position of the macaque V4 complex, produce a number of color specific impairments: ranging from achromatopsia, the complete loss of color perception in the hemifield contralateral to the lesion, over a selective inability to perceive color constancy under changing illumination, to a remaining ability to discriminate different wavelengths without the ability to assign colors to the stimuli.

With the advent of fMRI in the 1990s, color vision, like other mental capacities, became accessible to measurement in healthy human subjects, (as well as patients with specific disorders) (Hadjikhani et al. (1998), Bartels and Zeki (2000), Wade et al. (2008)). Early studies found color specific activation anterior of ventral V3 and inferior of MT in the area of human cortex that could well be homologue to macaque V4. One study by Hadjikhani et al. (1998), however, combining color and luminance contrast mapping using the traveling wave method, found a color specific area in humans anterior of their retinotopic mapping of V4,

that also showed a retinotopic representation of the complete hemifield (see Figure 21). Based on this data they postulated a new retinotopic cortical area V8 in the collateral sulcus that selectively processes color information in humans. That interpretation though hinges upon a mapping of V4 that only represents a quarterfield, similar to the macaque.

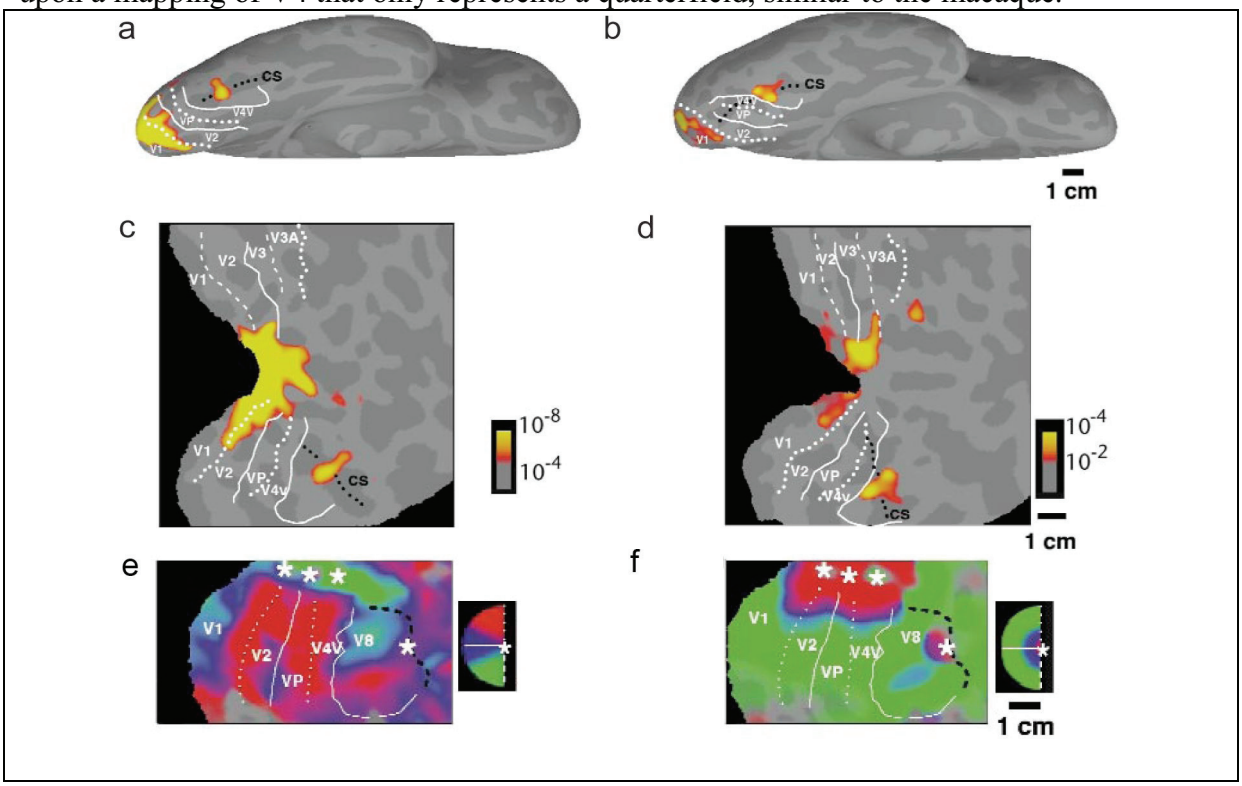

Figure 21: Color selective cortex in humans (modified from Hadjikhani et al. (1998)). Ventral views of inflated hemispheres (A), B)), showing the activation contrast color > luminance contrast in warm colors. White lines show borders of retinotopically defined visual areas. C) and D) same data shown on flattened maps of the occipital pole region. For one subject E) shows the result of the traveling wave meridian localization experiment, F) the result from the eccentricity mapping.

In contrast, Bartels and Zeki (2000) interpret the data shown in Figure 22, as a human V4-complex based color system, consisting of two clusters per hemisphere; a posterior cluster termed V4, that contains a hemifield representation for color stimuli, and a more anterior discontinuous cluster termed V4a, that also contains a representation of the contralateral hemifield. This anterior hV4a has Talairach coordinates very close to the ones reported for V8 by Hadjikhani et al. A recent review by Wandell and collegues (2007), reconciles both views to some degree, by giving support to hV4 being a hemifield representation (located in 'ventral' cortex) like Bartels and Zeki, but also giving support to a more anterior retinotopic hemifield representation (which they call VO-1). Unlike macaque V4, which consists of two quarterfield representations, one ventral and one dorsal, hV4 contains a ventral hemifield representation. (It should be noted, that group analysis by Wade et al. (2008), does indicate the possibility for the existence of a vestigial dorsal part of hV4).

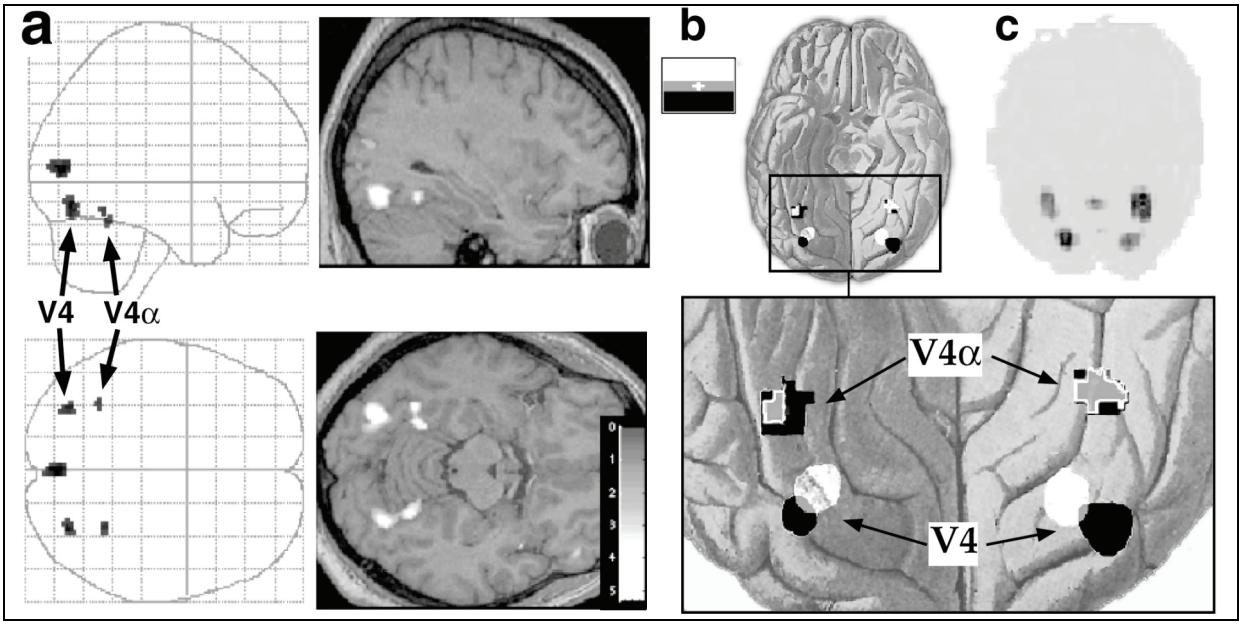

Figure 22: Color selective cortex in humans (from Bartels and Zeki (2000)). A) Glass-brain representation of color selective areas (group analysis from 4 subjects). The right of A) shows the activation chromatic > achromatic for a representative subject overlaid on the anatomical scan. B) shows the result of an chromatic up-down mapping of the visual field representation, especially in the magnification (bottom right) it seems clear, that Zeki's hV4 contains a complete representation of the contralateral hemifield; and even the anterior hV4a (that shares Talairach coordinates with Hadjikhani's V8) contains upper and lower field representation. C) shows the four members of the color area to emerge as a single component in independent component analysis.

While spatial vision is (almost) color blind, object vision depends on extracting chromatic information from visual input (see Livingstone and Hubel (1987)). Especially the ability to assign constant colors to objects independent of changing illumination conditions (that differ between morning and evening, between sun and shade) should help object categorization immensely by canceling out a source of visual signal variability.

Form

Since the late 19th century it was clear that there are at least two different forms of blindness. Munk defined 'cortical blindness', as the total absence of any vision following the complete removal of occipital cortex, and contrasted this to 'psychic blindness', the absence of higher visual recognition capabilities after localized lesions (Mink 1881, cited from Gross (1994)). In the early 20th century Klüver and Bucy realized, that bilateral lesions of temporal lobe produce a set of specific symptoms, now known as the Klüver-Bucy syndrome. The first among the symptoms of temporal lobe lesions, and the most important one for this section, was "… psychic blindness or visual agnosia … the ability to recognize and detect the meaning of objects on visual criteria alone seems to be lost although the animal exhibits no or at least no gross defects in the ability to discriminate visually" (Klüver 1948, cited from Gross (1994) see there for further references). All this implicates the temporal lobe as part of the machinery that parses visual forms and 'translates' them into perceptual objects.

Bruce et al. (1981) recorded from single units in macaque superior temporal sulcus (STS). 30% percent of the recorded neurons showed a highly specific tuning for complex objects, like hands and faces. Figure 23 shows the responses of a unit that responded best to

human and monkey faces. Note how 'scrambling' the image, dividing the original into 4 by 4 squares and rearranging their order randomly, completely abolishes the unit's activity. Similarly, Perrett et al. (1982) recorded from neurons in the fundus of the STS, yielding 48 face-selective cells out of 497. Desimone et al. (1984) found few face selective cells while systematically surveying IT neurons for their stimulus selectivity, but also describe a cluster of such cells in the lower bank of the STS close to the fundus. In addition, they also showed neurons that selectively respond to images of hands. These early experiments show that the temporal cortex contains units that are suitable for detecting and representing complex objects.

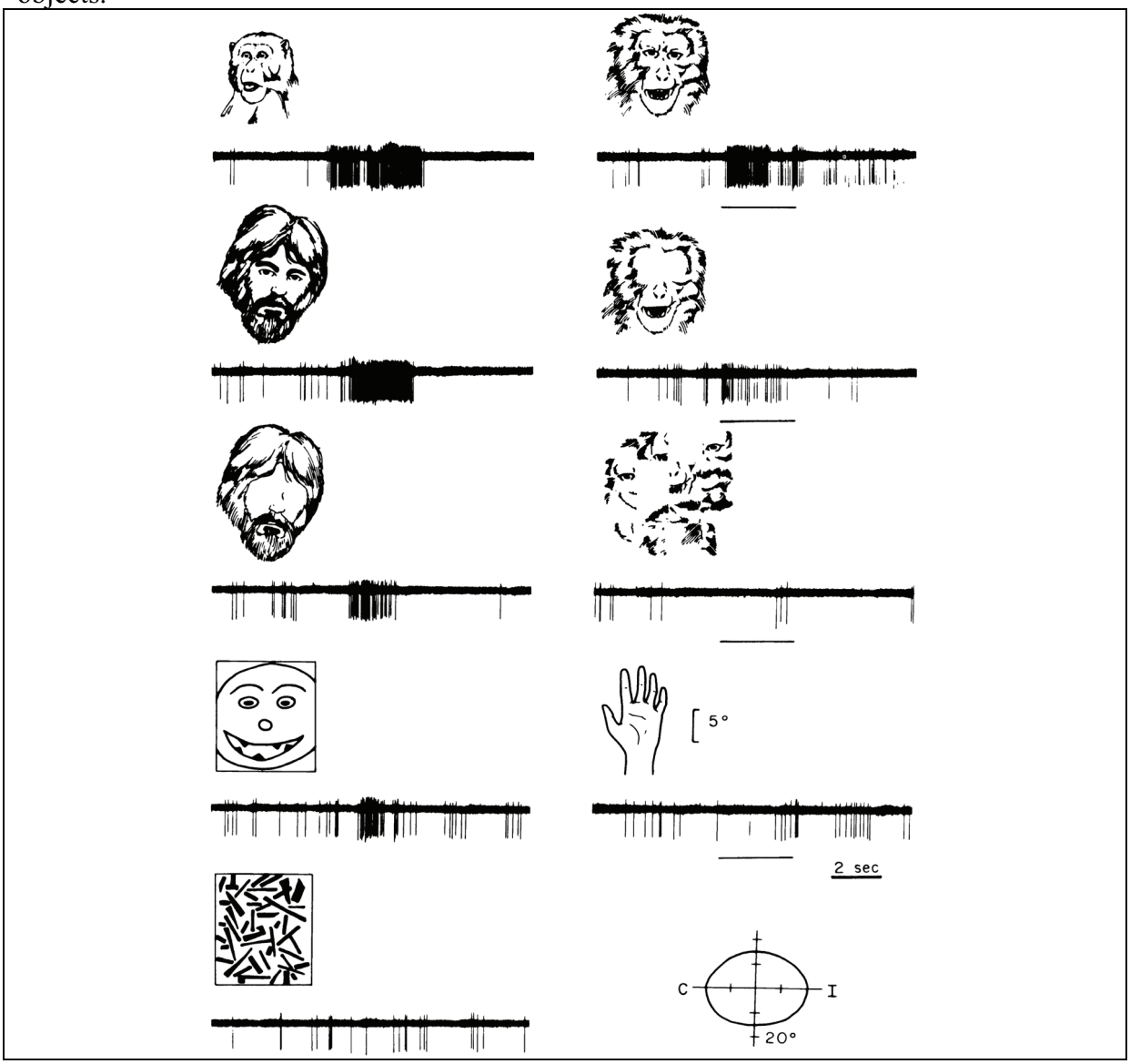

Figure 23: Response of an object-selective unit in IT cortex (Bruce et al (1981)). Each trace shows the neuronal response of the unit to the image just above the trace. The lower right inset shows the position of the receptive field. The unit responded to any image resembling a face.

Interestingly, Ó Scalaidhe and colleagues (1997) also found face selective units in prefrontal cortex (Figure 24).

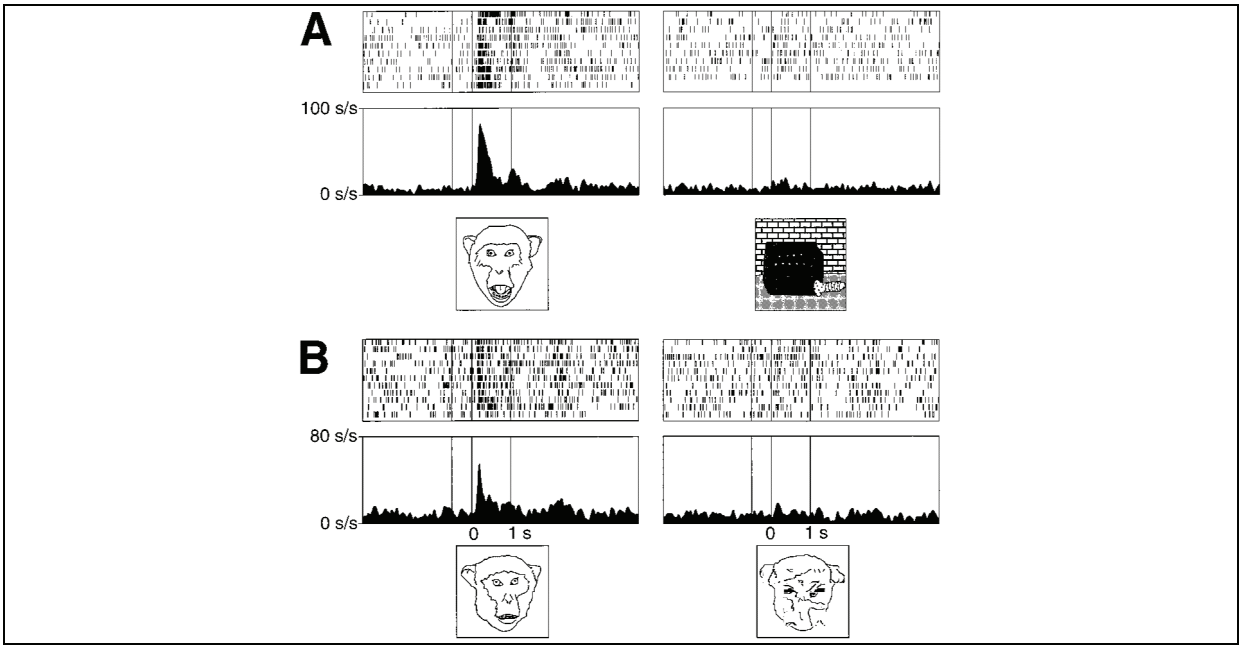

Figure 24: Response of a face-selective neuron in prefrontal cortex (Ó Scalaidhe et al. (1997)). A) shows the response of the neuron to the best stimulus (a face) and the worst stimulus. B) shows the response of the same unit to a different face and the scrambled version of the same face. All plots show dot raster diagrams for individual trials above the spike density function for all trials.

Tanaka and colleagues (1991) explored the optimal stimuli for 725 neurons in IT cortex, by trying to find the simplest two-dimensional stimulus for each unit that still produces maximal activation. They termed this the 'critical' feature of the cell. They showed that IT cortex can be segmented into a posterior and an anterior compartment based on the distribution of receptive field sizes and optimal stimuli. Posterior IT (that corresponds to anatomically defined area TEO) shows small receptive fields and a high percentage (72%) of 'primary' cells, while anterior IT (that corresponds to TE) shows much larger receptive fields and a low percentage (12%) of 'primary' cells. In their nomenclature 'primary' cells respond to slits or spots of a certain orientation, size and color; that show stimulus selectivity similar to earlier visual areas. TE is therefore the area that is most likely responsible for detailed object recognition, while TEO most likely represents TE's input area. Non-primary cells either preferred simple textures or more elaborate shapes. Most 'elaborate' cells respond to a specific (but abstract) combination of simpler components (see Figure 25), but some only respond to images of human or monkey faces or hands. Tanaka et al. suggest that every real world object should activate a hallmark combination of only few active elaborate cells, each coding for a part of the overall shape. They further propose that faces and hands are represented as separate entities in IT cortex.

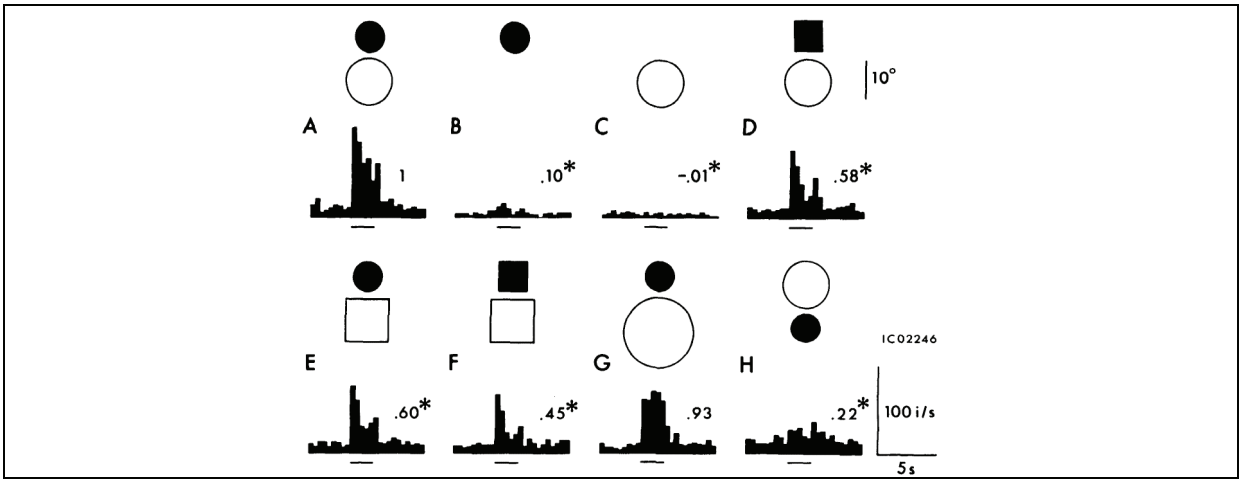

Figure 25: Example of an elaborate neuron in anterior IT cortex (Tanaka et al. (1991)). The cell's optimal stimulus could be reduced to a dark disk above a light disk; either component alone fails to activate the unit.

Comparing the procession of 'critical features' between neighboring neurons in perpendicular and tangential recording tracks in anterior IT cortex Fujita et al. (1992) found a columnar organization of feature selectivity. That is, cells in perpendicular electrode tracks show similar critical features over the whole cortical thickness (up to 2.5 mm), while tangential recordings showed that clustering of similar selectivity only extends for roughly 0.4 mm. This organization closely resembles the organization of earlier visual areas like V1 into orientation columns (or into orientation hypercolumns) and ocular dominance columns. Fujita et al. estimated that area TE might house 1300 to 2000 individual columns involved in object processing.

Wang, Tanaka, and Tanifuji (1996) used optical imaging in anterior IT cortex. They first started with an electrophysiological recording to define the critical feature of the recording site, and then used that exact stimulus while simultaneously measuring the intrinsic signal over several square millimeter of cortex (Figure 26). Around each recording site there is an area that is significantly activated by the same critical stimulus. For each stimulus there are also remote areas that respond significantly.

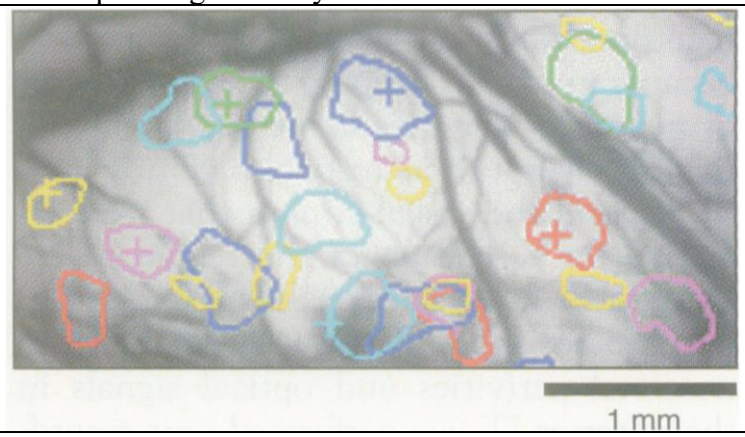

Figure 26: Different visual stimuli drive intrinsic signal changes in a patchy distribution in IT cortex (Wang et al. (1996)). The image shows crosses at sites where critical features were mapped, outlines in the same color show areas of IT cortex that were significantly modulated by the same stimulus ($P < 0.05$). Areas around the recording site always respond to the same critical feature, showing the columnar organization of

anterior IT cortex. In addition, there exist remote patches that are also significantly modulated by the same stimuli (see outlines without cross).

Interestingly, they also found face-selective patches in anterior TE that slowly changed position in relation to the rotation of the shown head. This shows that faces, like other objects, are represented by columns and that there exists at least one example for an orderly representation of a high-level feature like view direction.

The existence of columns selective for 'critical features' together with the fact that these features typically are quite abstract shapes that do not reflect real objects (with the notable exception of faces and hands), led Tanaka et al. (1991) to the combination–coding hypothesis. That is, any real object can be described by the activation of a few feature columns. Tsunoda et al. (2001) set out to test this hypothesis, combining electrophysiological recordings with optical imaging. First, they established that each optical defined feature-patch contains neurons that respond well to the same stimuli that were used to localize the patches. Figure 27 shows the differences in the pattern of activated feature columns caused by different objects (a) and by simplification of complex objects.

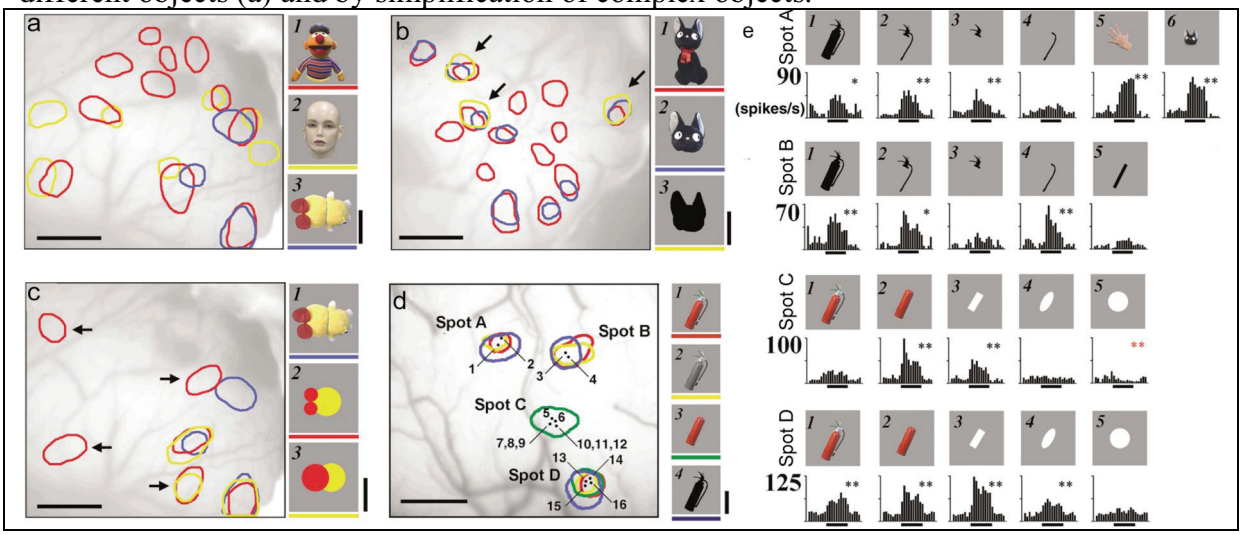

Figure 27: Complex objects produce specific activation patterns in TE (Tsunoda et al. (2001)). A) Shows outlines for significantly activated patches of IT cortex for three different objects. Different objects recruit overlapping and distinct patches. B) Simplification of objects can reduce the number of recruited feature columns; it can also lead to the recruitment of additional patches (black arrows in C), green outline in D)). Numbers in D) denote electrode tracks. E) Responses of 4 neurons in the four labeled spots of D). Note, how the neuron in Spot C selectively responds to a white tilted rectangle, as well as the fire extinguisher reduced to its barrel (closely resembling a tilted rectangle), but not to the complete image.

The observation that simplification of objects does not necessarily just reduce the number of recruited patches (from the initial set), led Tsunoda et al. (2001) to the hypothesis that object identities are coded in the activation of a few feature columns, but that active and inactive columns are part of the code used in TE.

Another line of evidence for a columnar or patchy organization of object representation in TE can be found in the anatomical connections. Saleem et al. (1993) injected anterograde tracer into area TEO to study the organization of the connections from TEO to TE. Figure 28 shows a typical result, individual tracer injections label a few sites in TE. Labeled sites show up as columns that extend though all cortical layers. This organization where single TEO

locations project to several distinct TE columns matches well the pattern of distributed columns with similar stimulus selectivity as shown in Figure 26.

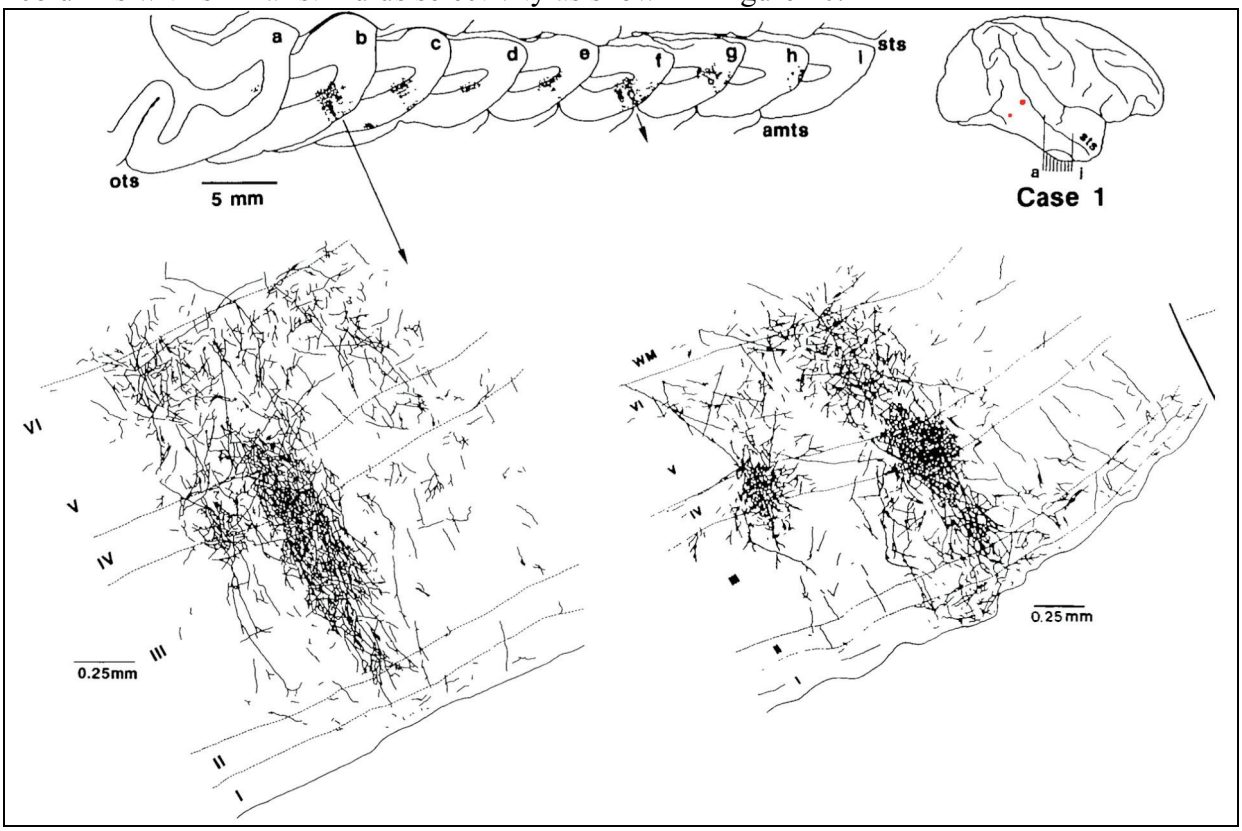

Figure 28: Area TEO projects to TE in a patches (compiled from Saleem et al. (1993)). Top right: lateral view of the individual brain, injection sites of the anterograde tracer in TEO are shown in red. Top left: projection pattern of the labeled terminals. Below are *camera lucida* drawings of two fully labeled TE columns. TEO injection typically yield two to five discrete labeled foci in TE that span the full cortical thickness.

Fujita and Fujita (1996) showed, that injections in TE cortex label the whole cortical column at the injection site, and they also produce distinct labeled columns up to 4 mm away. Figure 29 shows an exemplar remote labeled column at the left, and the pattern of laterally connected patches of columns on the right.

The extent of the TE columns labeled from TEO as well as the extent of TE columns labeled from TE are close to the size of TE feature columns as measured either by electrode penetrations (Tanaka et al. (1991)) or by optical imaging (Wang et al. (1996)). Both the pattern of the inputs from TEO as well as intra-TE cross-connections are likely involved in shaping the exquisite selectivity for forms of TE neurons.

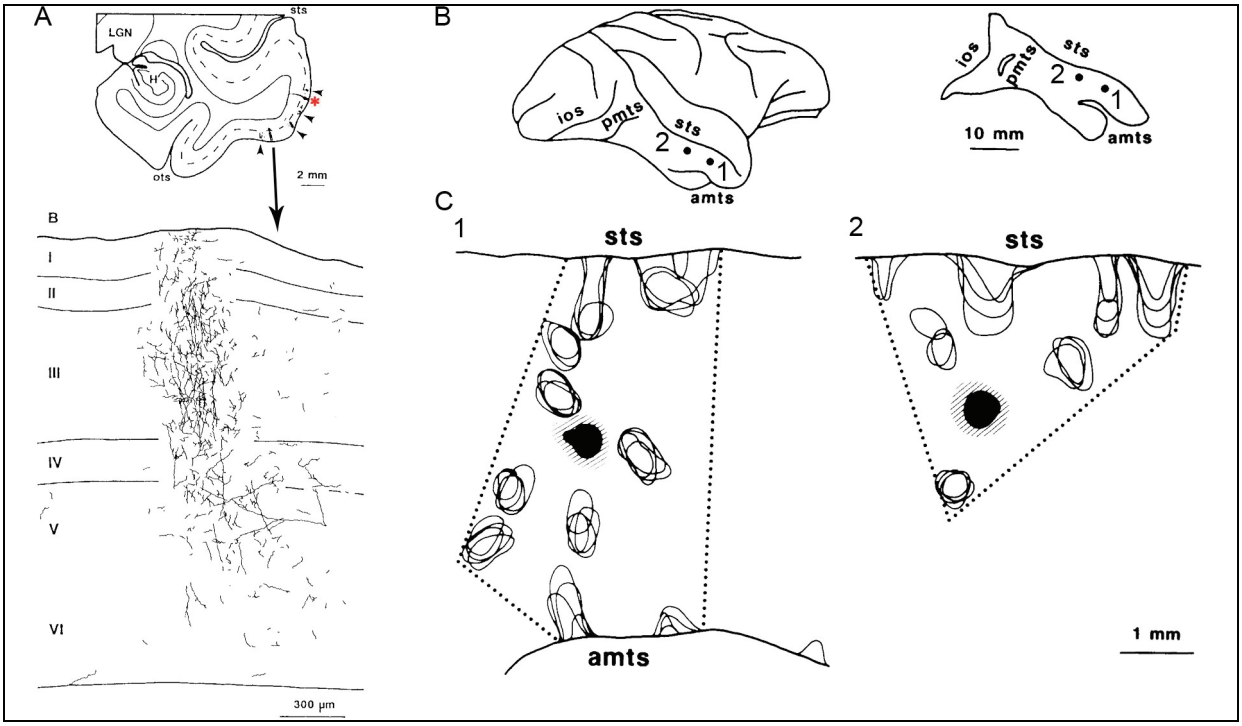

Figure 29 : Intrinsic connections in TE are patchy (Fujita and Fujita (1996)). A) Coronal section showing TE; the injection site is maked with a red asterisk. A) bottom magnification of one projection; almost the whole cortical column is labeled. B) Overview of two injection sites. C) Tangential reconstruction of projection zones from two injections. The injections are marked black, projection zones are shown as outlines.

In humans the machinery responsible for object recognition/processing was elusive for a long time, due to the difficulty in measuring neurophysiological data with sufficient temporal and spatial resolution. The advent of functional magnetic resonance imaging (fMRI) 18 years ago changed this situation significantly. As an alternative to the tedious 'detective' work required to correlate specific 'visual recognition' deficits with specific accidental lesions, fMRI made possible planned experiments to understand the basis of object vision.

The existence of face blindness (prosopagnosia) in humans without a generalized blindness for all other objects supports the hypothesis that faces are processed as a separate class of objects by a dedicated machinery in the brain. In 1997, Kanwisher, McDermott and Chun used fMRI to probe healthy subjects for cortical regions that responded stronger to images of faces than to images of other objects. Initially they found robust face-selective activation in the right mid-fusiform gyrus. Figure 30 shows the result of more extensive 'face-localization' experiments in a human subject. In addition to bilateral activation in the fusiform gyri, two additional bilateral activated locations appear, the occipital face area (OFA) and a face-specific patch in the STS (fSTS). Following Kanwisher and Yovel (2006), the OFA is involved in representing the physical aspects of a face; FFA is involved in processing of face identity, while fSTS seems to be involved in procession of viewpoint, gaze and facial expression.

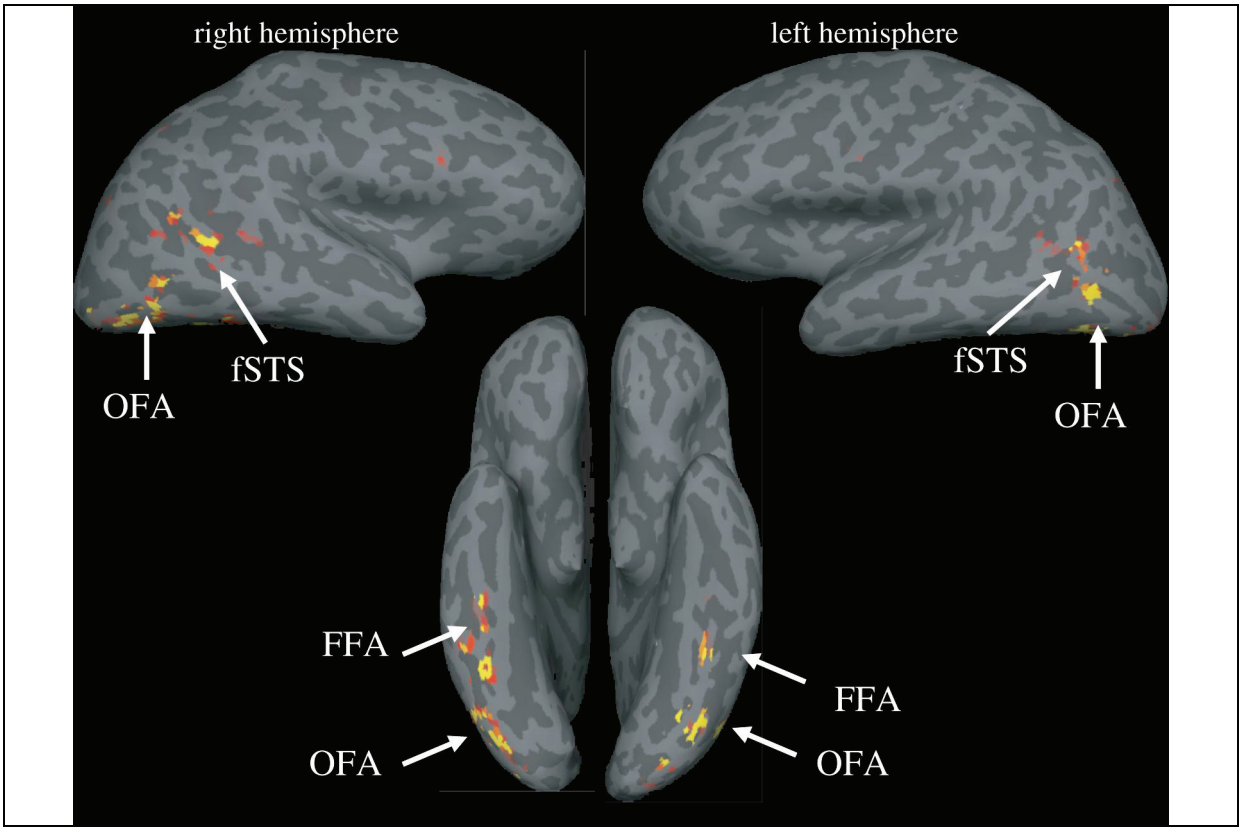

Figure 30: Human face-selective regions (Kanwisher and Yovel (2006)). Functional overlay contrasting activity for faces versus other objects in yellow-red over inflated human hemispheres. Top: lateral views of both hemispheres, bottom: ventral view of the same hemispheres. Abbreviations: OFA, occipital face area; FFA, fusiform face area; fSTS, face-speific superior temporal sulcus.

Further mapping experiments identified human bodies as an additional category that is processed in two dedicated areas: the extrastriate body area (EBA) (Downing et al. (2001)) and the fusiform body area (FBA) (Schwarzlose et al. (2005)). Interestingly, the FBA is located in the fusiform gyrus just adjacent to the FFA, necessitating high spatial resolution for separating both modules in fMRI.

Tsao et al (2003b) showed for the first time in similar fMRI localization experiments that face-selective activation is clustered into distinct modules in macaques as well. In addition they showed that body-selective modules are located just adjacent to the face-selective patches similar to the arrangement in the human fusiform gyrus (later confirmed by Pinsk et al. (2005)). Figure 31 shows the results for face and body-selective patches in macaque temporal cortex. It is noteworthy that monkeys, like humans possess several distinct areas of face selective cortex.

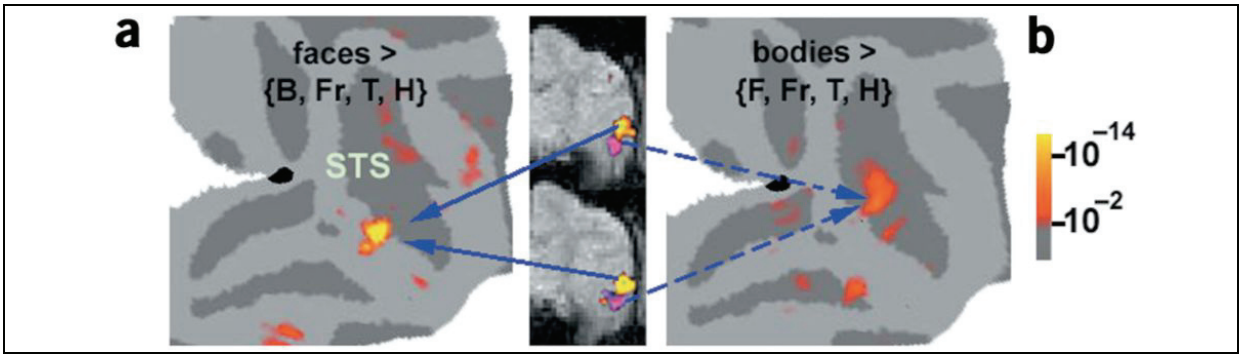

Figure 31: Face and body selective patches in macaque IT cortex (modified from Tsao et al. (2003b)). A) activation map contrasting faces versus all other objects, B) activation map comparing bodies versus all other objects. Middle two partial functional slices overlaid with the same contrast, face-selective regions red-yellow, body selective regions pink. Abbreviations: B, bodies; Fr, fruit; T, gadgets; H, hands; F, faces.

Electrophysiological recordings targeted to one of the fMRI-identified face-selective patches showed that almost all visually responsive neurons were selective for faces (see Figure 32). The extent of the electrophysiologically-defined face patches was several mm and thereby larger than would be expected for a feature column (diameter around 0.5 mm). These results suggest that fMRI-identified human face areas should also contain many face-selective neurons.

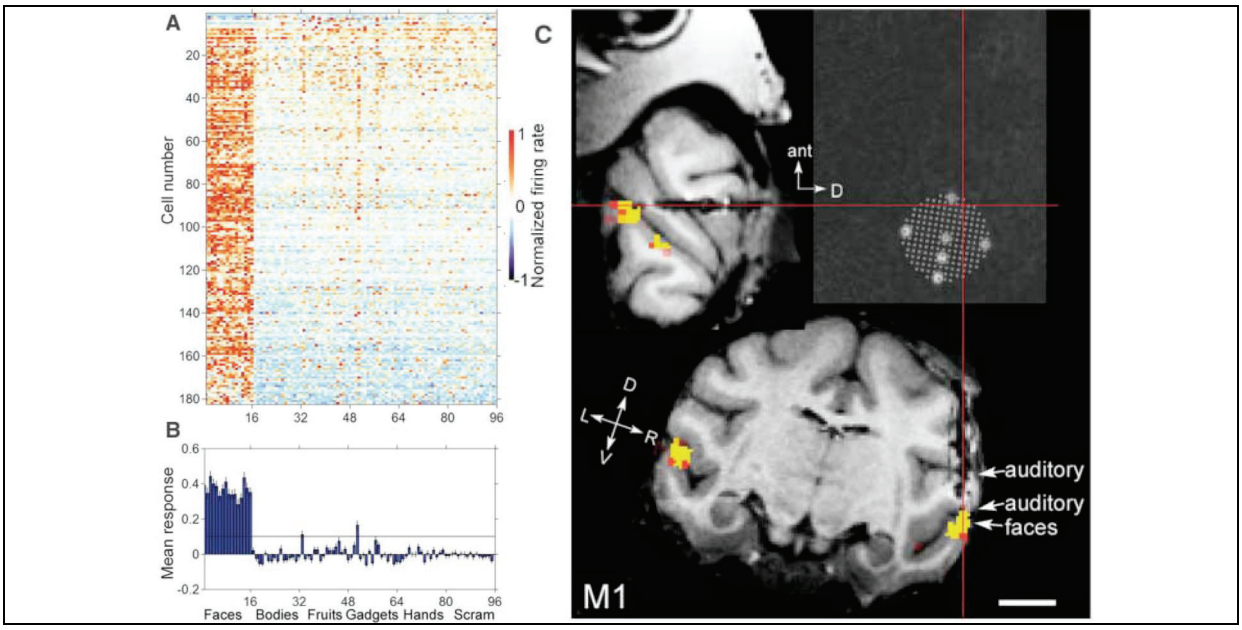

Figure 32: Neurons inside fMRI-identified face patches are highly selective for faces (modified from Tsao et al. (2006)). A) Selectivity profile for 182 neurons recorded in monkey M1. Each unit is represented by one row, each column represents one image, the first 16 images are faces. Roughly 97% percent of all visually responsive units recorded in the face patch were face-selective. B) Same data collapsed over all cells, each bar represents the mean population response to each of 96 images. Again images of faces yield a consistently higher response than all other images. C) Activation contrast showing faces > objects overlaid on a structural scan of monkey M1. The red lines in the sagittal view and in the coronal view represent the electrode access vector used to reach the face patch.

Haxby et al (2001) measured activation of human temporal cortex to a set of 8 different object categories. They then divided the data set in two halves and analyzed the two halves separately. They calculated activation contrasts comparing each object category with the mean response to all categories. Correlations between the activation maps from the two halves showed that the maps for the same category were always more strongly correlated with each other, than with any other object's activation map. Interestingly, excluding the voxels maximally activated by the relevant category before calculating the spatial correlations, did not change the correlations by much. Haxby et al. interpret this as follows: each category produces a signature activation in all of temporal cortex, and even when sub-regions of highest selectivity for that object category are excluded, the activation pattern still faithfully encodes the category. In other words, they hypothesize that every object is encoded in a distributed manner in all of temporal cortex. They pose this 'object form topography' against the interpretation of domain specific modules that exclusively process individual object categories like faces and bodies. Interestingly, Tsao et al. (2003b) confirmed in a similar analysis of monkey data that the distributed pattern in all visual cortex without face-selective voxels could still discriminate faces from other objects.

Overview of experiments

The central question I address in my thesis is: what is the circuitry for face processing in the macaque brain. Experiments to understand how face and object vision are organized in the ventral visual stream have led to three different views. There is evidence for a distributed and overlapping object representation by the concurrent activity of the whole visual temporal lobe ('object form topography' Haxby et al. (2001)); there is also evidence for a less global object representation by recruitment of different sets of feature columns that together 'describe' the presented object, the 'combination coding scheme' (Tanaka et al. (1991), Wang et al. (1996), Tsunoda et al. (2001)); and finally there is evidence for a modular 'domain specific' organization for faces and bodies, in which specific modules exclusively represent objects of a single category (Kanwisher et al. (1997), Tsao et al. (2003)). The face-selective feature columns found by Wang et al. (1996)) next to columns selective for simpler object shapes show that even in a combinatorial coding scheme, some complex stimuli are processed in a more integrated fashion. Thus it remains unclear how face and object perception are organized in the continuum from fully distributed to purely modularized.

One prediction of a distributed organization is that any site in object cortex is connected to most other sites, either completely or, more likely, in a spatially graded fashion, with stronger connections to nearby cortex. On the other hand, the hallmark of a modular hierarchical system is that any column or patch is only connected to a few other sites, based on common functional properties. Which of these two possibilities is the organizing principle of visual object cortex? To address this, it is necessary to identify the anatomical projections of sites with known functional properties (e.g., an individual face patch) and then to measure the functional properties of these projection sites. Classical neuro-anatomical tracer methods offer high spatial resolution, and tracer injections can be targeted to electrophysiological characterized locations, but they lack the capability to characterize the response profiles of neurons at the projection sites, as they require sacrificing the animal before the projections are identified.

Tolias et al. (2005) introduced an elegant new experimental method for in vivo tract tracing by combining electrical microstimulation with fMRI. Electrical microstimulation serves to activate cortical areas around an electrode site and fMRI serves to measure the activation caused by the stimulation. Since stimulation electrodes also allow electrophysiological recordings, this method allows one to precisely measure stimulus preferences at stimulation sites. The fMRI data acquisition can easily cover the whole brain, thereby allowing one to detect even widespread 'projection patterns'. And, since projection sites are identified in vivo, projection sites discovered in one session can be targeted for further recordings and even used as new stimulation sites.

The central goal of my thesis was to address the question: how are the macaque face patches organized? The face processing system of macaque monkeys offers an ideal preparation for dissecting the large-scale functional architecture of object vision, since almost all monkeys have a set of face-selective regions that can be easily localized with fMRI and targeted for anatomical and electrophysiological experiments (following Tsao et al (2003b) and (2006)). I used combined microstimulation with fMRI as the method to ask whether the face patches are integrated into a distributed object representation or whether they constitute a separate system of modules? The former would predict that stimulation of a particular face patch should lead to wide spread activity in inferotemporal cortex; the latter would predict that stimulation of a particular face patch should only activate other face patches.

The results of my experiments argue strongly that the face-patches in macaque temporal cortex form a tightly coupled modular system. The face-patches are strongly connected to

other face patches but not to surrounding non face-selective cortex; they are also connected to subcortical structures including the amygdala. Around the stimulation site in each face patch, there was always an activated area larger than the patch itself, either caused by passive spread of the stimulation current or by 'lateral' connections from each patch to the embedding cortex. Interestingly, microstimulation outside of the face patches also elicited very specific patchy projection patterns. This suggests that modular structure might be found in all object cortex, even though the features that 'bind' these non-face patches remain elusive.

The second goal of my thesis was to compare the organization of face-selective modules in macaques and humans. Macaques show a robust pattern of six distinct face patches, extending along the entire extent of the temporal lobe; in humans the most anterior face-selective module, the FFA, lies in the middle of the temporal lobe. This raises the question, whether the use of anterior temporal cortex for face processing is unique to macaques. And, since the face processing system can be loosely considered a landmark system for the hierarchical organization of object vision, this might indicate how close both species are in the organization of the ventral visual stream.

Two differences between human and macaque fMRI experimental designs made revisiting this difference worthwhile. On the one hand, macaque face-patch localization experiments are routinely performed using contrast agents that increase the signal 3 to 5 fold and are done with many repetitions of the same visual stimulus set to increase statistical significance of activation maps. On the other hand, the anterior temporal cortex in humans is notoriously hard to access with fMRI, due to signal loss caused by susceptibility artifacts induced by the air filled ear canals; also, human experiments usually use as few repetitions as possible. To account for these differences we optimized MR measurement parameters (voxel size and slice position) and used a very high number of repetitions of measurement sessions in each subject, and scrutinized activity patterns in individual human subjects (many human fMRI studies perform group averaging, which suppresses small, spatially variable activated regions).

Our study revealed the majority of human subjects showed one or two additional face patches in the temporal lobe anterior to the FFA, which might correspond to the set of three anterior face patches in the macaque. Thus the large-scale organization for face processing seems to be conserved between macaques and humans, even though the exact number of modules might differ.

The third and final goal of my thesis was to determine whether the face patch system is restricted to the temporal lobe. Previously, face-selective neurons were reported in prefrontal cortex (Ó Scalaidhe et al. (1997)). Are these cells organized into distinct face-selective patches as in temporal cortex? The aim was to map the organization of face selectivity in frontal cortex using the functional MR methods that have worked so well in temporal cortex.

We found that macaques typically show three patches of face-selective cortex in prefrontal cortex. Prefrontal face patches were more strongly modulated by the expressive content of faces than temporal face patches. This result fits well with the role of prefrontal cortex in social behavior, for which detection of the emotional state of other individuals is essential.

The experiments

The central goal of my thesis was to elucidate the connectivity of the macaque face-patch system using combined microstimulation and fMRI. These experiments are described in the paper "Patches with links: A unified system for processing faces in the macaque temporal lobe" by Moeller, Freiwald, and Tsao (Science 320: 1355-1359). I performed this project under the supervision of Doris Tsao and with scientific consultation by Winrich Freiwald. I took part in the initial study design (with both advisors), established the method of combining targeted electrical microstimulation with fMRI, performed all measurements and analysis, created all figures, and wrote a first draft for the manuscript. All further refinement and iterations of the manuscript were in close co-operation with D. Tsao and W. Freiwald.

The second question I addressed is how similar is the organization of the face representation system in macaques and humans. The results of this project are described in the paper "Comparing face patch systems in macaques and humans" by Tsao, Moeller & Freiwald (PNAS, 2008, in press). I performed all data acquisition and data analysis for this paper.

The third question I pursued is whether face-selective patches exist in macaque prefrontal cortex. This work is described in the paper "Patches of face-selective cortex in the macaque frontal lobe" by Tsao, Schweers, Moeller, and Freiwald (Nature Neuroscience 11: 877-879). I created the visual stimuli, analyzed the data, created parts of the figures, and participated in writing the manuscript.

The following chapters faithfully reproduce the text and the figures of the published papers.

Patches with links: A unified system for processing faces in the macaque temporal lobe

(Science 320: 1355-1359)

Sebastian Moeller, Winrich A. Freiwald, Doris Y. Tsao*

Institute for Brain Research and Center for Advanced Imaging, University of Bremen, P.O.B. 330440, D-28334 Bremen, Germany

*To whom correspondence should be addressed. E-mail: doris@nmr.mgh.harvard.edu

The brain processes objects through a series of regions along the ventral visual pathway, but the circuitry subserving the analysis of specific complex forms remains unknown. One complex form category, faces, selectively activates six patches of cortex in the macaque ventral pathway. To identify the connectivity of these face patches, we used electrical microstimulation combined with simultaneous functional magnetic resonance imaging (fMRI). Stimulation of each of four targeted face patches produced strong activation specifically within a subset of the other face patches. Stimulation outside the face patches produced an activation pattern that spared the face patches. These results suggest that the face patches form a strongly and specifically interconnected hierarchical network.

An essential step to understand the neural mechanism underlying any percept is to identify its anatomical substrate. For example, many theoretical models of object recognition propose a hierarchical architecture (*1, 2*), but it remains unclear if and how such hierarchical models are actually implemented by the brain.

The face processing system of macaque monkeys provides an ideal preparation for dissecting the large-scale functional anatomy of object recognition. Almost all macaques have a set of face-selective regions that can be easily identified by fMRI (*3, 4*) and readily targeted for anatomical experiments (*5*). Understanding their connectivity should provide important insights into the large-scale circuitry used by the brain to perceive a complex form.

It is debated whether face processing relies on a sequence of dedicated processing stages (*6*) or whether it relies on distributed representations (*7*). The former model predicts that face-selective regions show strong connections to each other but not to surrounding non-face-selective temporal cortex, while the latter predicts strong connections between face-selective regions and surrounding non-face-selective temporal cortex (*8*).

Tracer injections made into the macaque temporal lobe reveal a patchy connectivity pattern (*9-14*). For example, Saleem et al. found that injections into TEO produce labeling in TE restricted to between two to five discrete foci (*10*). However, the functional properties of cells at injection and termination sites were not identified in these studies. In general, to dissect functional anatomy, it is necessary to combine connectivity maps with functional topography (*15, 16*). Specifically, the connections of the macaque face patches cannot be deduced from previous studies. To identify the anatomical connections of the macaque face patches, we used fMRI-guided electrical microstimulation combined with simultaneous fMRI (*17-19*).

Macaque monkeys typically have six discrete, bilateral patches of face-selective cortex (Fig. 1, Fig. S1). These patches are organized into: one posterior patch on the lateral surface of area TEO (which we will refer to as “PL”, for posterior lateral), two middle face patches in

posterior area TE, one located in the fundus of the superior temporal sulcus (STS) ("MF", for middle fundus) and one on the lower lip of the STS ("ML", for middle lateral), and three patches in anterior area TE, one located near the fundus of the STS ("AF", for anterior fundus), one on the lower lip of the STS and adjacent gyrus, in area TEad ("AL", for anterior lateral), and one more medially on the ventral surface, just lateral and anterior to the anterior middle temporal sulcus (AMTS), in area TEav ("AM", for anterior medial) (*20*).

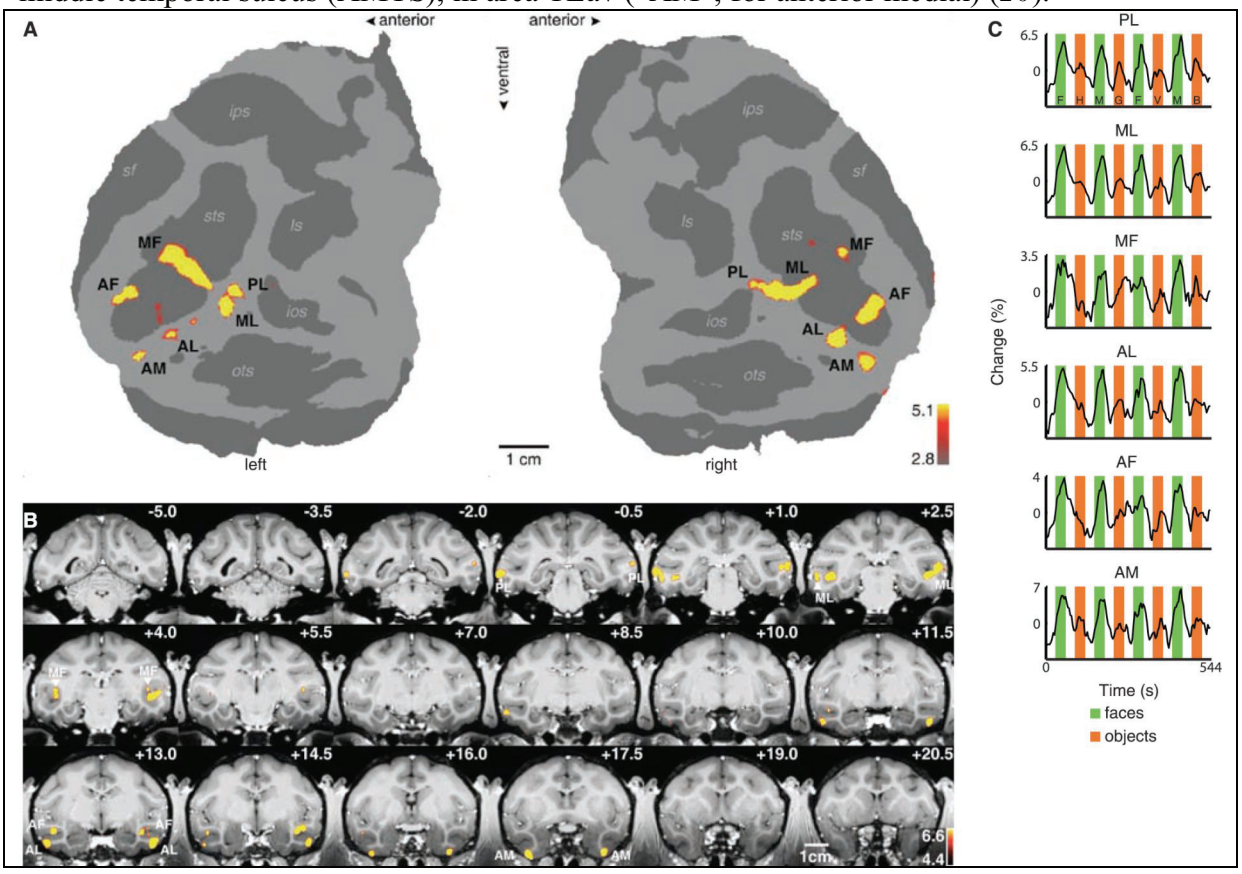

Fig 1. Face-selective patches in monkey M1. (A) The flattened cortical surfaces ("flatmaps") from both hemispheres show regions significantly more activated by faces than by other objects. Computational flattening involves distorting the spatial arrangement of the data, and under-estimates the size of the sulci (shown in dark grey). Anatomical labels: *sts:* superior temporal sulcus, *sf:* Sylvan fissure, *ips:* intraparietal sulcus, *ls:* lunate sulcus, *ios:* inferior occipital sulcus, *ots:* occipitotemporal sulcus. (B) The same contrast overlaid on high resolution coronal slices from monkey M1. The anterior-posterior position of each slice in mm relative to the interaural line is given in the top right corner; the left hemisphere is shown on the left. The face patches are labeled as in (A). (C) Mean time courses extracted from the six face patches of the right hemisphere. Three different visual stimulation conditions were presented: faces (green epochs, F: human faces, M: monkey faces), objects (orange epochs, H: hands, G: gadgets, V: vegetables and fruits, B: monkey bodies), and scrambled versions of the same images (white epochs).

We identified the locations of face patches in four monkeys (M1 – M4) by scanning them with a standard face localizer stimulus (*3*). Individual animals and hemispheres exhibited slight variations on the prototypical pattern just described. Figures 1A, B show face patches in the left and right hemispheres of monkey M1 on flattened maps of the posterior 2/3 of the brain excluding prefrontal cortex and in coronal slices; this animal had five discrete

face regions in the right hemisphere (PL and ML were confluent). Time courses from the face patches confirm the face selectivity of each patch (Fig. 1C). Figure S1 shows the face patches of the three other animals (M2 – M4) used in this study.

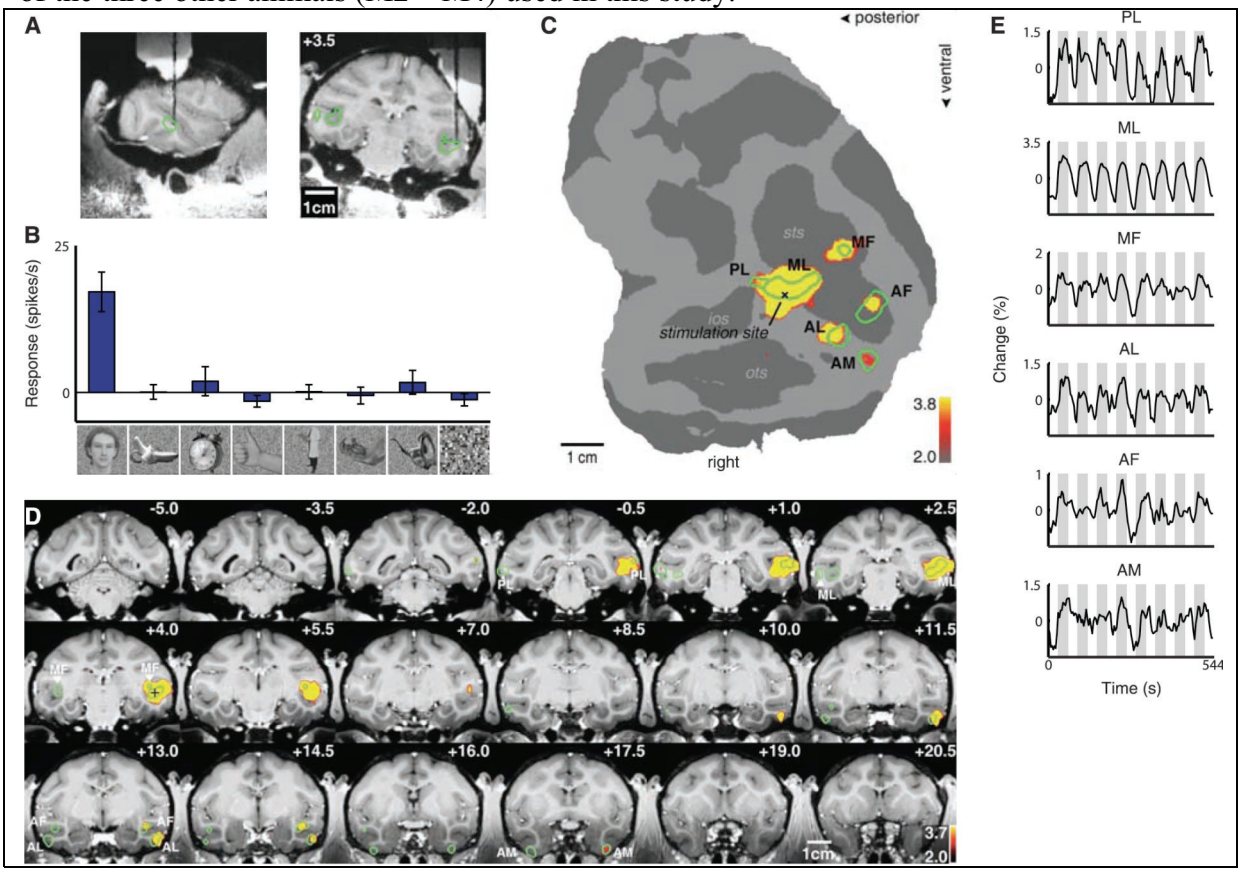

Fig 2. Brain regions activated by microstimulation in the lateral middle face patch (ML) of monkey M1. (A) The position of the electrode in relation to the face patches (indicated by green outlines) in sagittal and coronal MRI slices; the tip of the electrode was located 3.5 mm anterior to the inter-aural line. (B) Selectivity profile of the last neuron recorded before stimulation. The bars show the mean response of this unit to images from eight different image categories (faces, fruits, gadgets, hands, bodies, monkey body parts, monkey bodies, and scrambles), error bars 95% confidence intervals. (C) Areas significantly activated by microstimulation versus no microstimulation overlaid on the flatmap. The face patches (cf. Fig. 1) are indicated by the green outlines. The stimulation site inside ML is marked by an "x". (D) The same functional contrast overlaid on coronal slices. The face patches are indicated by green outlines. The "+" indicates the approximate stimulation site (the slice containing the actual stimulation site, at +3.5, is not included in this mosaic). (E) Mean time courses from the six face patches in the right hemisphere. Microstimulation blocks (gray epochs) were interleaved with fixation only blocks (white epochs).

We then targeted a subset of the face patches for microstimulation combined with simultaneous fMRI. We first verified that the electrode correctly targeted each face patch by recording spiking activity. We then transferred the animal to the scanner for microstimulation. We stimulated a total of four different face patches (ML, AL, AM, and AF), several inferotemporal (IT) sites neighboring the face patches, and a site in the upper bank of the STS (Table S1).

We first targeted ML in monkey M1. Figure 2A shows MR images of the electrode descending into ML, in sagittal and coronal planes. Figure 2B shows the response profile of the last cell recorded from this patch prior to microstimulation; this cell was highly face selective (as were neighboring ones above it). The location of the electrode tip, marked on the flat map, confirms that stimulation was within ML (Fig. 2C). Comparing activation with and without microstimulation revealed five discrete regions in the temporal lobe (Fig. 2C). Stimulation resulted in a large spread around the electrode tip, a stretch of 4 mm with little activity, and then three discrete anterior patches located 6 - 11 mm anterior to the stimulation site. These patches coincided with the three anterior face patches of this monkey (compare Fig. 1A with Fig. 2C, and Fig. 1B with Fig. 2D). This activation pattern was reproducible across scan sessions, and was not sensitive to the choice of significance threshold (Fig. S2). Time courses from the six face patches confirm strong activation during microstimulation epochs (Fig. 2E).

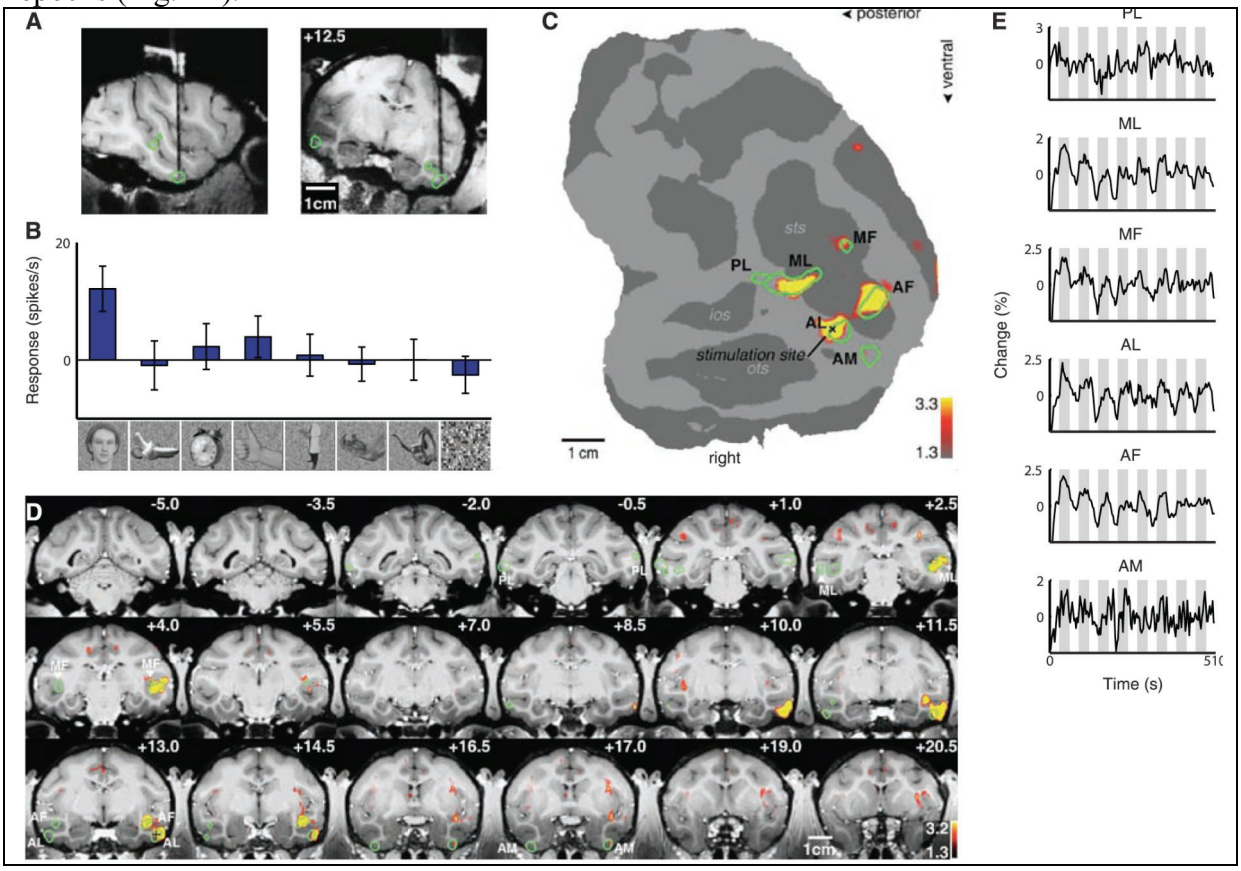

Fig 3. Brain regions activated by microstimulation in the anterior lateral face patch (AL) of monkey M1. Same conventions as Fig. 2. (A) Electrode position in AL. (B) Example of neuronal selectivity. (C) The contrast microstimulation versus no microstimulation revealed microstimulation-induced activity in four discrete patches in the temporal lobe coinciding with AL (the stimulation site), AF, ML, and MF, as well as a fifth patch of faint activation coinciding with AM. PL was the only face patch not activated. (D) The same contrast overlaid on coronal slices. (E) Time courses from the six face patches of the right hemisphere.

Figure S3 shows the results of stimulating ML in two additional animals (M2 and M3). In monkey M2, stimulation in ML elicited activation in three other face patches: MF, PL, and AL. In monkey M3, stimulation in ML elicited activation in two other face patches: PL and

AL. Results from the three animals show that ML is strongly connected to PL and AL, and more weakly/variably to the remaining face patches.

If fMRI activity is driven principally by the energy demands of transmitter release during synaptic activity (*21, 22*) then these electrical stimulation-induced activations likely reflect orthodromic (rather than antidromic) spike propagation. Activations could result from direct or indirect connections (*23*).

Microstimulation-induced activations were usually much stronger in the hemisphere ipsilateral to the stimulation site, but we sometimes observed activation in contralateral face patches as well. Figure S4 shows contralateral activations induced by stimulation in the right hemisphere ML of monkeys M1 and M2. These contralateral activations were confined to the face patches PL, ML, and MF.

ML was strongly connected to AL in all three animals. To follow the circuit, we next targeted AL (Fig. 3A). Figure 3B shows that the last cell recorded before moving the animal to the scanner was face selective. In addition to spread around the stimulation site, stimulation in AL produced strong activation in ML, MF, and AF, and weak activation in AM (Fig. 3C-E). In contrast to stimulation in ML, stimulation in AL produced no activation in PL. In a second animal (M4), stimulation of AL elicited activation in ML, MF and AM, but not AF or PL (Fig. S5). Thus AL appears to be robustly connected to ML, MF, and AM, and more variably to AF.

We next targeted AM, the most anterior of the six face patches. In monkey M1, stimulation in AM induced activity in ML, AL, and AF (Fig. S6A-E). In monkey M2, stimulation in AM induced activity in ML and AL (Fig. S6F-J; this animal lacked an AF in the stimulated hemisphere, see Fig. S1A). Thus AM appears to be robustly connected to AL and ML.

Finally, we stimulated the third of the anterior face patches, AF, in one animal (M1, Fig. S7). This experiment showed that AF is strongly connected to MF, and more weakly to ML.

In the experiments described so far, the animal fixated a blank gray screen during microstimulation. To test for interactions resulting from combining microstimulation with visual stimulation (*24, 25*), we combined electrical and visual stimulation in a stimulus sequence composed of six conditions: faces, faces + microstimulation, objects, objects + microstimulation, blank, and blank + microstimulation. We ran two monkeys (M1 and M2) on this stimulus sequence, microstimulating in ML. This experiment revealed that: 1) the strength of activation elicited in the face patches by microstimulation in ML was comparable to that elicited by viewing faces, and 2) there was only a weak interaction between responses to microstimulation and those to visual stimulation (Text S1).

If the circuitry of IT cortex follows a single scheme, then stimulating just outside a face patch should yield an activation pattern similar to that obtained by stimulating inside a face patch. If, on the other hand, the face patches constitute a unique system within IT cortex, then stimulating outside the face patches may yield a qualitatively different activation pattern. In particular, a distributed mechanism for coding non-face objects might predict that stimulation outside a face patch should lead to widespread activity throughout IT cortex.

We therefore stimulated three different sites just outside the face patches. First, we stimulated a site just posterior to ML, on the lower lip of the STS, in monkey M1 (Fig. 4A). The last cell recorded from this site responded only to scrambled patterns (Fig. 4B). Stimulation at this site produced a large spread of activity within the STS around the stimulation site (which spared both PL and ML), as well as a discrete patch of activity in the lower bank of the STS, anterior to ML and 7 mm anterior to the stimulation site (Fig. 4C-E). This result suggests that IT cortex outside the face patches also exhibits discrete patchy connectivity, consistent with previous anatomical tracer studies (*10, 13, 26*). Figure S8 shows

the result of microstimulating outside ML in monkey M2. In addition to a large spread around the stimulation site (which included PL but largely spared ML), there was activity in a discrete region just posterior to AL, on the outer surface of the inferotemporal gyrus. Finally, Figure S9 shows the result of stimulating just posterior to AM in monkey M2. This produced spread around the stimulation site as well as activity in a discrete posterior projection site within the ventral bank of the STS and a discrete anterior projection site within the fundus of the STS.

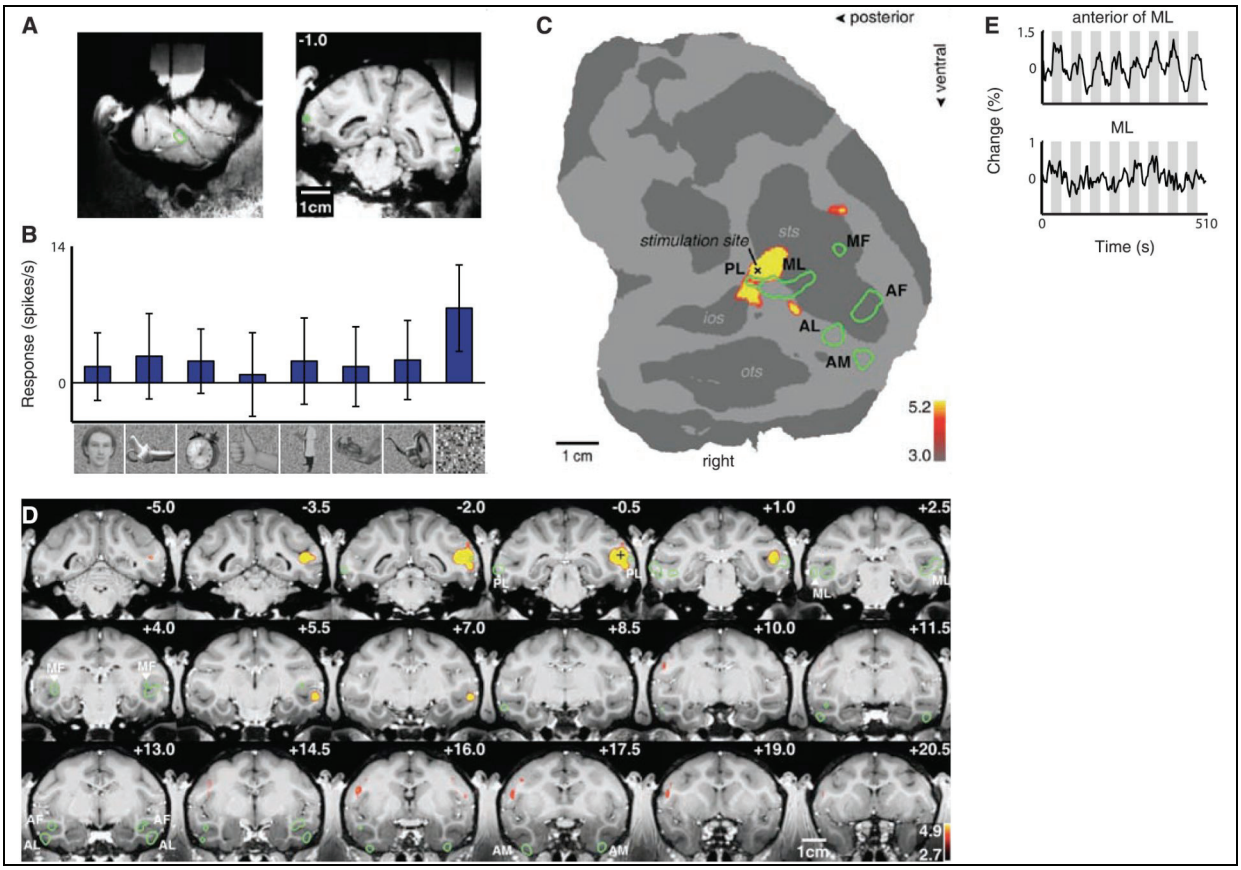

Fig 4. Brain regions activated by microstimulation outside the lateral middle face patch (ML) in monkey M1. Same conventions as Fig. 2. (A) Electrode position just posterior to ML. (B) Example of neuronal selectivity. (C) The contrast microstimulation versus no microstimulation revealed microstimulation-induced activity around the stimulation site as well as in a distinct patch anterior to ML. (D) The same contrast overlaid on coronal slices. Note how the activation spared most of PL and the other face patches. (E) Time courses from the patch just anterior to ML and from ML.

Face cells have been found in both the upper and lower banks of the STS (*27*). To compare connections of the upper versus lower banks of the STS, we stimulated a site in the upper bank of the STS in monkey M1 at approximately the same AP position as ML (Fig. S10A-E). Stimulation at this site produced a different activation pattern from stimulation in the lower bank: instead of discrete clusters of activation, we observed a large swath of activity extending from -5 to +20 within the upper bank and fundus of the STS, as well as activation in cingulate and somatomotor cortex (Fig. S10F-J, second monkey). This experiment shows that the technique of fMRI combined with microstimulation is capable of detecting highly distributed connectivity patterns. Furthermore, the result suggests that microstimulation is capable of activating cells more than one synapse away (it seems unlikely that all of the areas activated in Fig. S10 were directly connected to the stimulation site). If

true, this strengthens our main finding concerning the specificity of connections between face patches, since it implies that cells two synapses or more away from the stimulation site were also located within the face patch system.

We did not observe any other cortical regions consistently activated besides those described (*28*). However, we did consistently observe stimulation-induced activation in three subcortical regions: the amygdala, claustrum, and pulvinar. Stimulation in AM elicited activation in the lateral nucleus of the amygdala and laterally adjacent claustrum in both monkeys tested (Fig. S11A, B). Stimulation outside but close to AM also activated the lateral amygdala and claustrum (Fig. S9C, slice at +20.5), suggesting that these two structures receive inputs from a larger region within ventral IT (*29*).

We observed activation of the inferior pulvinar in response to microstimulation of both ML (Fig. S11C) and AL (Fig. S11D), as well as IT foci outside the face patches (data not shown). Thus, the inferior pulvinar appears to be strongly connected to a large portion of IT cortex (*9*). Because the pulvinar, claustrum, and amygdala were the only non-face-selective brain structures consistently activated by stimulation of the face patches, we hypothesize that these structures may constitute three bottlenecks for communication between the face patches and other regions of the brain (*30*).

In this study, we imaged brain regions activated by microstimulation of four different macaque face patches (ML, AL, AM, and AF). The results suggest that the six macaque face patches form a tightly and specifically interconnected system, as summarized in Fig. S12 and Table S2. The existence of an interconnected circuit consisting of six nodes, likely dedicated to coding the same Gestalt form, shows that functional specialization in IT exists not only at the level of isolated columns (*31*) or patches (*3*), but extends to the level of connected, distributed networks.

Our results extend previous findings of functional specialization in early visual cortex, where modules processing the same visual attribute have been shown to be specifically connected (*32*), e.g., color-specific blobs in area V1 with color-specific thin stripes in area V2 (*33*). The face patch network likely represents a stable structural network, since the connections were apparent across three very different functional states: without visual stimulation, with visual stimulation by faces, and with visual stimulation by non-face objects (Text S1). However, functional connectivity within the face patch system and between the face patches and other brain areas may depend on behavioral and perceptual state (*24, 34*).

Of all the face patches, we know most about the functional properties of the two middle ones, ML and MF. Single-unit recordings show that almost all visually responsive cells in this region are face selective (*5*), implying that the step of face detection has been accomplished. Because microstimulation of ML activated three anterior face patches (Fig. 2C), this suggests the existence of a sequence of dedicated face processing stages following face detection. Such an architecture would be consistent with computational models of object recognition in which a detection stage precedes individual recognition (*35*). However, our results suggest an important role for feedback in face processing. Stimulation of AL led to feedback activation of ML (Fig. 3) with a strength and spatial precision comparable to the feedforward activation of AL by ML stimulation (Fig. 2).

Is the circuitry of the face patches unique, or a theme that is recapitulated in surrounding non-face-selective cortex? The results of microstimulating outside the face patches (Figs. 4, S8, and S9) suggest that there do exist largely self-contained networks of modules, outside the face patches, for processing shape. Since non-face objects elicit highly distributed fMRI response patterns in IT cortex (*7*), these networks of non-face modules likely represent aspects of form present in almost all objects, such that any object would activate multiple

networks. But given their size, there may exist only a finite set of macroscopic shape processing networks.

References and Notes

1. S. Ullman, *Trends Cogn Sci* **11**, 58 (Feb, 2007).
2. M. Riesenhuber, T. Poggio, *Nat Neurosci* **2**, 1019 (Nov, 1999).
3. D. Y. Tsao, W. A. Freiwald, T. A. Knutsen, J. B. Mandeville, R. B. Tootell, *Nat Neurosci* **6**, 989 (Sep, 2003).
4. M. A. Pinsk, K. DeSimone, T. Moore, C. G. Gross, S. Kastner, *Proc Natl Acad Sci U S A* **102**, 6996 (May 10, 2005).
5. D. Y. Tsao, W. A. Freiwald, R. B. H. Tootell, M. S. Livingstone, *Science* **311**, 670 (2006).
6. V. Bruce, A. Young, *Br J Psychol* **77 (Pt 3)**, 305 (Aug, 1986).
7. J. V. Haxby *et al.*, *Science* **293**, 2425 (Sep 28, 2001).
8. J. D. Cohen, F. Tong, *Science* **293**, 2405 (Sep 28, 2001).
9. M. J. Webster, J. Bachevalier, L. G. Ungerleider, *J Comp Neurol* **335**, 73 (Sep 1, 1993).
10. K. S. Saleem, K. Tanaka, K. S. Rockland, *Cereb Cortex* **3**, 454 (Sep-Oct, 1993).
11. K. S. Saleem, K. Tanaka, *J Neurosci* **16**, 4757 (Aug 1, 1996).
12. K. Cheng, K. S. Saleem, K. Tanaka, *J Neurosci* **17**, 7902 (Oct 15, 1997).
13. K. S. Saleem, W. Suzuki, K. Tanaka, T. Hashikawa, *J Neurosci* **20**, 5083 (Jul 1, 2000).
14. W. Suzuki, K. S. Saleem, K. Tanaka, *J Comp Neurol* **422**, 206 (Jun 26, 2000).
15. W. H. Bosking, Y. Zhang, B. Schofield, D. Fitzpatrick, *J Neurosci* **17**, 2112 (Mar 15, 1997).
16. L. C. Sincich, G. G. Blasdel, *J Neurosci* **21**, 4416 (Jun 15, 2001).
17. A. S. Tolias *et al.*, *Neuron* **48**, 901 (Dec 22, 2005).
18. L. B. Ekstrom, G. Bonmassar, R. B. H. Tootell, P. R. Roelfsema, W. Vanduffel, paper presented at the SFN Annual Meeting, Washington D.C. 2005.
19. This technique is not as sensitive as classical tracer injection followed by post-mortem histology and may therefore miss weak, diffuse projections. But as an in vivo method, it possesses several important advantages for correlating anatomy to function: 1) since the results come in the form of fMRI activity maps, they can be precisely compared to the pattern of fMRI-identified face patches, 2) the technique allows for repetitions, 3) it allows for combination with electrophysiological experiments, and 4) it allows for the use of many stimulation sites in the same animal, enabling a detailed, sequential characterization of connectivity.
20. K. S. Saleem, N. K. Logothetis, *A combined MRI and histology atlas of the rhesus monkey brain in stereotaxic coordinates* (Elsevier, London, 2007).p.
21. C. Mathiesen, K. Caesar, N. Akgoren, M. Lauritzen, *J Physiol* **512 (Pt 2)**, 555 (Oct 15, 1998).
22. N. K. Logothetis, J. Pauls, M. Augath, T. Trinath, A. Oeltermann, *Nature* **412**, 150 (Jul 12, 2001).
23. For example, in Fig. 2C, the activation in AM could be due to a direct connection from ML to AM, or an indirect connection from ML to AL to AM.
24. S. L. Fairhall, A. Ishai, *Cereb Cortex* **17**, 2400 (Oct, 2007).
25. When the animal is viewing non-face objects, cortex representing non-face objects could exert a strong inhibitory influence on the face patches, thereby reducing or eliminating the effect of microstimulation on the face patches. Alternatively, if

processing within face patches and non-face-selective cortex proceeds in parallel, then viewing non-face stimuli should not strongly affect microstimulation-induced activity within the face patch system.
26. B. Seltzer, D. N. Pandya, *J Comp Neurol* **290**, 451 (Dec 22, 1989).
27. G. C. Baylis, E. T. Rolls, *Exp Brain Res* **65**, 614 (1987).
28. Tracer studies show that IT cortex is connected to ventrolateral prefrontal cortex (*36*) and area V4 (*37*). Prefrontal connections may have been missed in the current study because prefrontal cortex was not covered by the slice prescription during AM stimulation (prefrontal cortex was covered during stimulation of ML in monkeys M3 and M4, and stimulation of AL in monkey M4). Tracer studies show that connections between V4 and TEO are stronger than those between V4 and TE (*14, 37*). Thus V4 connections may have been missed because PL (located in TEO) was not stimulated.
29. M. J. Webster, L. G. Ungerleider, J. Bachevalier, *J Neurosci* **11**, 1095 (Apr, 1991).
30. J. M. Chein, W. Schneider, *Brain Res Cogn Brain Res* **25**, 607 (Dec, 2005).
31. K. Tanaka, *Annu Rev Neurosci* **19**, 109 (1996).
32. D. J. Felleman, Y. Xiao, E. McClendon, *J Neurosci* **17**, 3185 (May 1, 1997).
33. M. S. Livingstone, D. H. Hubel, *J Neurosci* **4**, 309 (Jan, 1984).
34. C. Summerfield *et al.*, *Science* **314**, 1311 (Nov 24, 2006).
35. B. Epshtein, S. Ullman, paper presented at the CVPR, New York 2006.
36. M. J. Webster, J. Bachevalier, L. G. Ungerleider, *Cereb Cortex* **4**, 470 (Sep-Oct, 1994).
37. L. G. Ungerleider, T. W. Galkin, R. Desimone, R. Gattass, *Cereb Cortex* **18**, 477 (Mar, 2008).
38. We are grateful to the late David Freeman and to Margaret Livingstone who programmed and designed the visual stimulus presentation software RF3, to Nicole Schweers, Katrin Thoss, and Ramazani Hakizimana for technical support, to Stefan Everling for advice on microstimulation, to Margaret Livingstone and K.S. Saleem for comments on the manuscript, and to Guerbet for providing Sinerem. This work was supported by a Sofia Kovalevskaya Award from the Alexander von Humboldt Foundation, by the German Science Foundation (DFG FR1437/3-1), and by the German Ministry of Science (Grant 01GO0506, Bremen Center for Advanced Imaging).

Supplementary material

Materials and Methods

All animal procedures complied with the NIH Guide for Care and Use of Laboratory Animals, regulations for the welfare of experimental animals issued by the Federal Government of Germany, and stipulations of Bremen authorities.

Overview.

Four male rhesus macaques were implanted with MR-compatible headposts and trained to fixate for a juice reward both inside and outside the scanner. After initial training, face-selective cortical areas were localized using fMRI. Then MR-compatible recording chambers were implanted to allow access to specific face patches in each monkey. The face selectivity of cells inside and outside the face patches was characterized by extracellular recordings to confirm successful targeting. We then stimulated specific sites inside the scanner, while the animal fixated a small fixation cross over a gray background for juice reward. See (*1, 2*) for details on fMRI procedures and (*3*) for details on fMRI-guided targeting and extracellular recording procedures.

Surgery.

Surgical procedures followed standard anesthetic, aseptic, and postoperative treatment protocols which have been described in detail elsewhere (*4*). The headpost was implanted in two surgical procedures separated by several weeks recovery time. First, the monkey was anesthetized (Ketamin / Medetomidine, 8mg/kg / 0.04mg/kg), then intubated and switched to a maintenance regime of oxygen (30 %), nitrous oxide (70 %) and isoflurane (0.5-2 %). The monkey's head was postioned in a stereotaxic frame, and the skull was exposed and cleaned (peroxide 30% and saline). Projections of the estimated chamber border and headpost were marked on the skull, and positions for 20 ceramic screws were marked. After drilling and thread cutting, the screws were inserted and covered with several layers of acrylic cement, as was all of the exposed skull area. Anesthesia was ended and the monkey was given a period of six weeks or longer to recover. In a brief second surgery, an MR-compatible headpost was attached to the initial implant using acrylic cement.

After computing the chamber location and angle allowing access to the desired face patch, we implanted the recording chamber using the same two-step anesthesia regime described above. A Cilux chamber was positioned using a stereotaxic frame and custom-made manipulators that allowed us to specify the center position of the chamber on the skull as well as rotation and tilt. The chamber was fastened using acrylic cement.

Prior to extracellular recording, a craniotomy was made inside the chamber under Ketamin / Medetomidine anesthesia; the diameter of the craniotomy was initially kept small and was enlarged as required.

Monkey fMRI.

All scanning was performed on a 3T MR scanner (Allegra, Siemens). For each monkey we acquired 10 anatomical volumes at high spatial resolution (0.5 mm isometric) for surface reconstruction and activity visualization. We used a T1 weighted inversion recovery sequence (MPRAGE). These scans were performed under Ketamin / Medetomidine anesthesia to reduce motion artifacts.

For all functional imaging, a contrast agent, ferumoxtran-10 (Sinerem, Guerbet; concentration: 21 mg Fe/ml in saline; dosage: 8 mg Fe/kg) was injected into the femoral vein

prior to each scan session. Sinerem is the same compound as MION, produced under a different name (*5*). Sinerem/MION increases signal-to-noise and gives finer spatial localization than BOLD (*6, 7*).

Unlike BOLD, Sinerem results in a signal reduction at activated voxels; for all presented functional data we inverted the signal, to allow easy comparison to BOLD data. All functional data was acquired in coronal slices. We used a multi-echo sequence (EPI, TR 3 or 4 s, TE 30 or 25 ms, 64 x 64 matrix). In combination with a concomitantly acquired fieldmap, this allowed high fidelity reconstruction by undistorting most of the B0-field inhomogeneities (*8, 9*).

For the initial fMRI experiment to localize face patches, we used a block design. Data for each animal was acquired over several scan sessions (M1: 15 runs in 2 sessions, M2: 18 runs in 3 sessions, M3: 35 runs in 3 sessions, M4: 23 runs in 3 sessions). In these localizer experiments we acquired 136 volumes per run (28 slices, spatial resolution 1.25 mm isometric, TR 4 s). The slice volume was adjusted for each monkey to cover the temporal lobe.

For all microstimulation experiments (with the exception of the experiment shown in supplementary text), the monkey fixated a small cross (0.36° diameter) on a plain gray background for a juice reward. We used either 21 slices at 1.25 mm isometric resolution (TR 3 s, block length 30 s, 170 volumes/run), or 28 slices at 1.5 mm isometric resolution (TR 4 s, block length 32 s. 136 volumes/run, or TR 3 s, block length 30 s, 170 volumes/run), or 42 slices at 1.5 mm isometric resolution (TR 4 s, block length 32 s, 136 volumes/run); the last prescription covered almost the whole brain.

In the experiment combining external visual stimuli with electrical microstimulation (supplementary text) we used the following scan parameters: 28 slices at 1.5 mm isometric resolution, TR 3 s, 200 volumes / run.

Targeting the face patches.

Targeting of face patches required a two-step procedure: 1) computing the skull position and orientation of a recording chamber to allow access to the face patch, and 2) computing which grid angle and grid hole to use within the chamber. To accomplish step 1, we used a custom MATLAB program to position a virtual chamber such that it would reach the desired face patch and the rim of the chamber would lie over the skull. This yielded coordinates specifying the center of the chamber axis on the skull as well as two angles for this axis (in the coronal and sagittal planes; in most instances the angle in the sagittal plane was 0°). To accomplish step 2, we acquired an anatomical scan of the monkey's brain with a recording grid positioned inside the cylinder whose holes were filled with MR-visible silicone. Registering the face patch localizer data to this anatomical scan allowed us to determine which grid hole to use to reach the desired face patch. The use of angled grids allowed us to reach face patches lying outside the direct projection of the chamber. Thus, for example, we were able to target four different face patches (ML, AL, AM, and AF) from the same recording chamber in monkey M1.

Electrophysiological recording.

We used standard non-magnetic tungsten electrodes (FHC) of low impedances (0.5 or 1 MΩ at 1 kHz). To allow scans of the electrodes *in situ* we used MR-compatible grids and guidetubes. We used a tungsten rod as indifferent electrode, which we lowered into the saline-filled grid and chamber. A custom all-plastic advancer was used to advance the electrode.

Extracellular signals were amplified and fed into a dual window discriminator to separate up to two units. The low impedance stimulation electrodes almost exclusively recorded multi-unit activity. Spikes were stored as time stamps at a temporal resolution of 1 ms.

Microstimulation.

To map the connectivity of the face patches, we stimulated pre-targeted sites in the temporal lobe. The stimulation protocol followed a block design. We normally interleaved 9 blocks of fixation-only with 8 blocks of fixation plus electrical microstimulation; we always started and ended with a fixation-only block. During microstimulation blocks we applied one pulse train per second, lasting 200 ms with a pulse frequency of 300 Hz. Bipolar current pulses were charge balanced, with a phase duration of 300µs and a distance between the two phases of 150µs. In the early phase of the project, we used a nominal current amplitude of 100 µA; we later switched to 300 µA since this yielded stronger activations. Due to the capacity of electrode and cable, only ~ 50-90 % of the nominal charge was actually delivered into the tissue (the unloading of this capacity could be observed as an inverted current at the end of each rectangular half-pulse on the control oscilloscope).

We used a programmable constant voltage impulse generator to drive a constant current stimulus isolator, which interfaced with different and indifferent electrodes through a coaxial cable. All stimulus generation equipment was stored in the scanner control room; the coaxial cable was passed through a wave guide into the scanner room.

Visual stimulation.

We used four visual stimulation protocols, one for unit characterization and three for MRI experiments. In all protocols the monkey's task was to maintain fixation on a central fixation spot (0.36° diameter); the required fixation duration to earn a drop of juice was lowered from 4 s to 1 s in each session. Gaze was measured in all experiments using an infra-red based system.

Face patch localizer:

The face patch localizer stimulus followed a block design. Blocks lasted 32 seconds, and included the following image categories: human faces (F), monkey faces (M), hands (H), gadgets (G), fruits and vegetables (V), and headless human bodies (B). There were 16 different images in each category. Each image block was preceded by a block consisting of scrambled versions of the same images (S), resulting in the following sequence: S F S H S M S G S F S V S M S B R (the final block consisted of a gray random dot pattern). Each image subtended 12° visual angle (10.4 cm diameter at 49 cm distance), and was presented for 0.5 s.

Unit characterization:

For electrophysiological recordings, we used a set of 128 images representing 8 different categories (16 images per category): faces, fruits and vegetables, gadgets, hands, headless human bodies, monkey body parts, headless monkey bodies, and finally, block-scrambled images. The images measured 100 x 100 pixels and spanned 7.6° visual angle (6 cm diameter at 45 cm distance). The images were presented in random sequence (duration 200 ms followed by 200 ms of gray background).

Microstimulation without visual stimulation:

To keep the animals awake and fixating during pure microstimulation sessions (i.e., all microstimulation experiments except that shown in supplementary text), we presented a fixation spot on a plain gray background through the experiment.

Microstimulation with visual stimulation:

For the experiment shown in the supplementary text, we combined visual and microstimulation. Visual stimulation consisted of faces (F, 64 images), objects (O, 32 images, 16 gadgets and 16 fruits and vegetables), and pure gray (G, full screen). Stimuli followed the sequence: G (60), F (30), G (60), F* (30), G (60), O (30), G (60), O* (30), G (60), G (30), G (60), G* (30), G (60) (duration in seconds indicated after each block, the asterisk indicates that electrical stimulation was also applied). Each image subtended 12° visual angle.

During MRI sessions, visual stimulation was performed using custom code utilizing the Psychophysics Toolbox (*10*). The stimuli were displayed at 60 Hz with a resolution of 1280 x 1024 pixels, using a video beamer and a back projection screen. During unit characterization outside the scanner, visual stimulation was performed using RF3 (a custom data acquisition program designed by the late David Freeman and by Margaret Livingstone). Stimuli were displayed at 60 Hz with a resolution of 640 x 480 pixels.

Electrophysiological data analysis.

To compute the selectivity profile of recorded single- and multi-units, we sorted the recorded data by image category, calculated the mean activity to each category (over 100 ms, starting 100 ms after onset) and then subtracted the mean baseline activity (the mean activity during the first 75 ms after stimulus onset). If the response of a unit to faces was at least twice as large as that to the next-best category, we considered it to be face selective. Only data obtained during stimulus presentations in which the monkey's eye position was within a window of +/- 4.5° around the fixation spot for at least 95% of the presentation duration (to allow for blinks) was analyzed.

fMRI data analysis.

We used FreeSurfer (http://surfer.nmr.mgh.harvard.edu) to reconstruct cortical surfaces and to create flat representations of each monkey's visual cortex, as if sampled at the cortex-white-matter boundary. The resulting flatmaps give an overview of the spatial distribution of fMRI activation maps.

We used FS-FAST for functional data analysis. Table S1 summarizes the number of runs used to generate each of the figures presented in the paper. Runs in which there was excessive motion were discarded. Data were motion-corrected with the AFNI motion correction algorithm (*11*), and intensity normalized. This preprocessed data was then analyzed using a generalized linear model (GLM) approach. To define face-selective areas we calculated the contrast faces versus all other objects (without scrambled images). To define areas activated by microstimulation, we contrasted activity during microstimulation epochs versus fixation-only epochs. All color scale bars show the significance of the contrast maps as negative common logarithm of the probability of error.

Each monkey's face localizer data was used to generate a mean functional volume, which defined the common functional space for the monkey. All subsequent functional data was registered to this common functional space using a custom registration program (written by Joe Mandeville), and all regions of interest (ROIs) were defined in this common functional space.

Mean time courses from each ROI were extracted using custom Matlab code. The mean time series across all voxels within the ROI was detrended with a second order polynomial. To analyse the interaction between visual and electrical microstimulation, we extracted the mean GLM beta values (scaled to percent signal change) for all voxels of each ROI.

To analyze the data presented in the supplementary text, we only included volumes recorded at time points during which the monkey kept his gaze inside a window +/- 3 degrees around the fixation spot for at least 80% of the TR length (to allow for blinks); to account for hemodynamic delay, we assumed that affected volumes were delayed by 5 s.

Supplementary text: Effect of combining visual and electrical stimulation

To test for interactions between visual and electrical stimulation, we combined the two in a stimulus sequence composed of six conditions: faces, faces + microstimulation, objects, objects + microstimulation, blank, and blank + microstimulation. We ran two monkeys on this stimulus sequence, microstimulating in ML. Supplementary Text Figure 1 shows the fMRI activation to these six conditions within each of the six face patches in monkey M1.

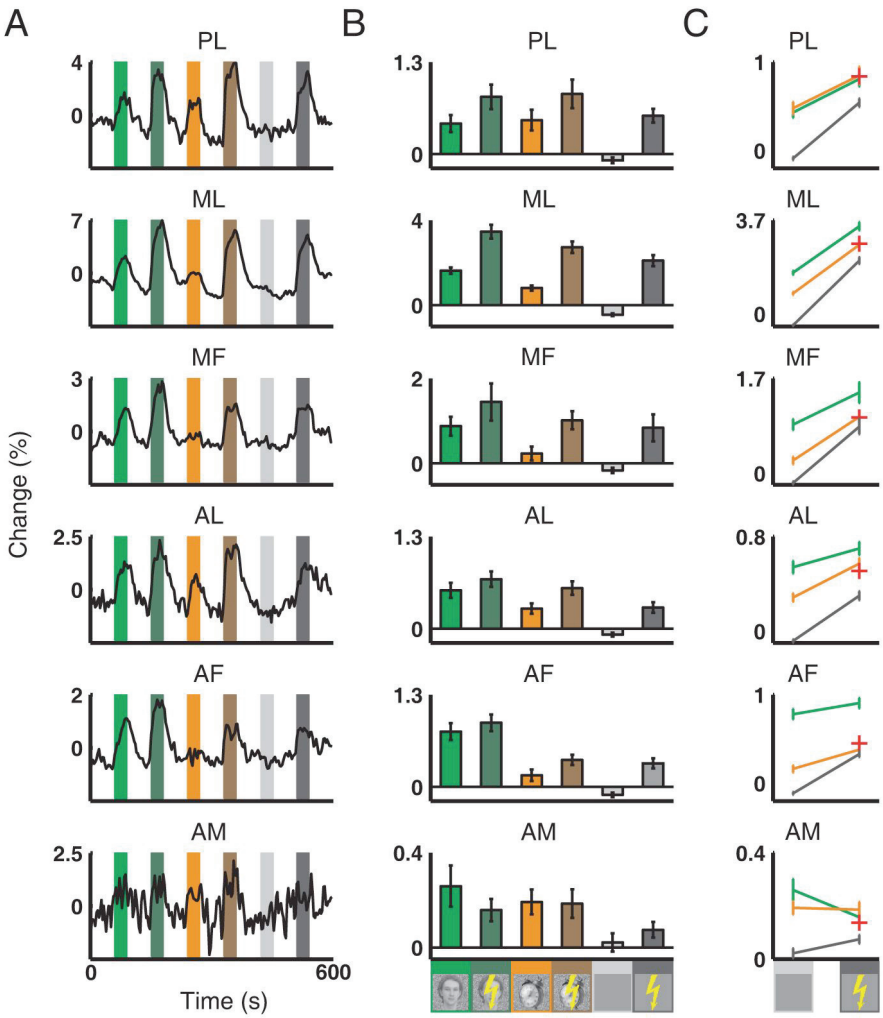

Supplementary Text Figure 1. Effects of combining visual and electrical stimulation. (A) Average time course from each face patch ipsilateral to the stimulated hemisphere. The color code for the six conditions (faces, faces and microstimulation, objects, objects and

microstimulation, blank, blank and microstimulation) is given below the bar graphs in (B). The time course from AM was noisy due to signal extinction at the temporal pole in this experiment. **(B)** Mean activation to the six stimulation conditions (error bars indicate 95 % confidence intervals). **(C)** Activation to blank, faces, and non-face objects, with (right) and without (left) microstimulation (same data as (B), plotted in a different format). The "+" indicates the predicted level of activation to objects plus microstimulation, assuming a model in which visual and electrical stimulation exert independent effects.

The results appear qualitatively consistent with a model of independent effects of visual and electrical stimulation, since activity in PL, ML, MF, AL, and AF increased during microstimulation epochs, regardless of whether the monkey was viewing faces, objects, or a blank screen (Supplementary Text Figure 1). ANOVA analysis with two factors (visual stimulation condition and microstimulation condition) showed that both main effects were highly significant in all face patches, with the exception of the effect of microstimulation in AM (due to poor signal-to-noise ratio in the region of AM in this experiment). The ANOVA analysis revealed only weak interactions between visual and electrical stimulation that reached significance in only two patches at p = 0.01 (p values indicated in the table below).

Patch	Significance of microstimulation	Significance of visual stimulation	Significance of interaction
AF	p<<0.001	p<<0.001	p=0.0008
AL	p<<0.001	p<<0.001	p=0.03
AM	p=0.39	p<<0.001	p=0.02
MF	p<<0.001	p<<0.001	p=0.16
ML	p<<0.001	p<<0.001	p=0.002
PL	p<<0.001	p<<0.001	p=0.1

Below, we assume a model of independent effects to estimate the fraction of neurons activated by visual versus electrical stimulation.

A model of independent effects of visual and electrical stimulation:

Let us assume: 1) that visual and electrical stimulation activate independent fractions of neurons, and 2) that a neuron's state is binary, i.e., activated or not activated (although not essential, this assumption simplifies the equations). Let M denote the maximal activation of a face patch, let B, O, and F denote activations to a blank screen, objects, and faces, respectively, in the absence of microstimulation, and let B*, O*, and F* denote corresponding activations to visual stimuli in the presence of microstimulation.

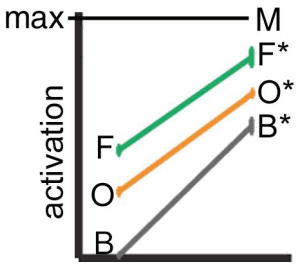

Each activation value can be expressed as a fraction of the theoretical maximum, M:

$$
\begin{aligned}
B &= f_1 \times M \\
B^* &= f_2 \times M \\
O &= f_3 \times M \\
O^* &= f_4 \times M \\
F &= f_5 \times M \\
F^* &= f_6 \times M
\end{aligned}
\qquad (1)
$$

If electrical and visual stimulation are fully independent, then the activity elicited in response to combined visual and electrical stimulation can also be described using the following formulas:

$$
\begin{aligned}
O^* &= \left(f_2 + f_3 - \left(f_2 \times f_3\right)\right) \times M \\
F^* &= \left(f_2 + f_5 - \left(f_2 \times f_5\right)\right) \times M
\end{aligned}
\qquad (2)
$$

This is because activated fractions are independent (see figure below); the subtraction term ensures that the fraction of neurons activated by both visual and electrical stimulation is counted only once.

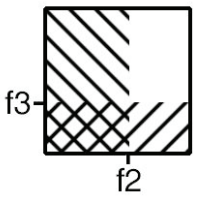

Combining equations (1) and (2) yields five equations in four unknowns (f_2, f_3, f_5, M):

$$
\begin{aligned}
B^* &= f_2 \times M \\
O &= f_3 \times M \\
F &= f_5 \times M \\
F^* &= \left(f_2 + f_5 - \left(f_2 \times f_5\right)\right) \times M \\
O^* &= \left(f_2 + f_3 - \left(f_2 \times f_3\right)\right) \times M
\end{aligned}
\qquad (3)
$$

Combining the first four equations in (3) yields:

$$
F^* = \left(\frac{B^*}{M} + \frac{F}{M} - \left(\frac{B^*}{M} \times \frac{F}{M}\right)\right) \times M \qquad (4)
$$

which can be rearranged into:

$$
M = \frac{B^* \times F}{B^* + F - F^*} \qquad (5)
$$

Thus M can be computed from experimentally measured values for B*, F, and F*. Then, f_2, f_3, and f_5 can be computed using the first three equations in (3). Finally the model allows us to *predict* a value for O* using the last equation in (3).

To obtain values for O, F, B*, O*, and F*, we extracted the mean hemodynamic response strength for the six patches to the six different stimulation conditions

(Supplementary Text Figure 1B). We then used these measurements to compute predicted values of f_2, f_3, f_5, M, and O*, as outlined above.

The following table summarizes the results of these computations. The subscript *m* denotes measured values, the subscript *c* denotes computed values, and the subscript *p* denotes the predicted value. All values are scaled to percent signal change, except the three values f2, f3, f5, which are unit-less fractions of the maximum M.

Patch	B^*_m	O_m	F_m	F^*_m	$f2_c$	$f3_c$	$f5_c$	M_c	O^*_m	O^*_p
AF	0.33	0.16	0.78	0.90	0.26	0.13	0.62	1.25	0.38	0.45
AL	0.30	0.28	0.54	0.70	0.26	0.25	0.47	1.15	0.57	0.51
AM	0.07	0.19	0.26	0.16	0.68	1.76	2.37	0.11	0.19	0.14
MF	0.84	0.23	0.87	1.45	0.30	0.08	0.32	2.76	1.01	1.00
ML	2.10	0.80	1.63	3.47	0.16	0.06	0.13	12.78	2.73	2.77
PL	0.54	0.48	0.43	0.81	0.38	0.33	0.30	1.43	0.85	0.84

Predicted values of O^* (indicated by +'s in Supplementary Text Figure 1C) always fell close to actually measured values, demonstrating the consistency of the model with experimental results. The paradoxical values computed for AM reflect the fact that microstimulation of ML did not produce significant activation in AM in this experiment. Discounting the results from AM, the fraction of neurons activated by microstimulation ($f2_c$, mean = 0.27) was always larger than that activated by viewing non-face objects alone ($f3_c$, mean = 0.17), and in several cases comparable to that activated by viewing faces alone ($f5_c$, mean = 0.37).

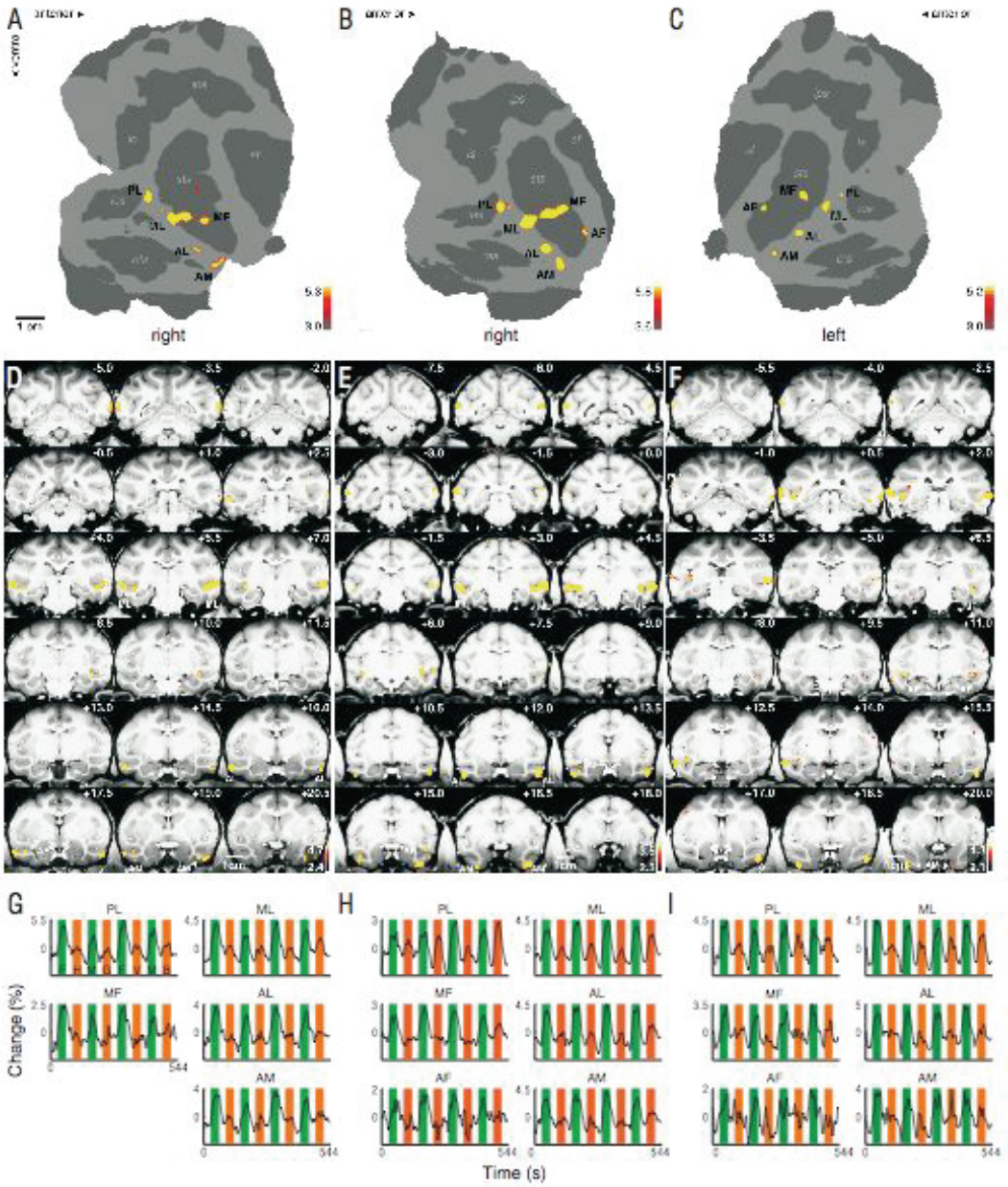

Fig. S1. Face selective patches in monkeys M2, M3, and M4. Same conventions as in Fig. 1. Flatmaps and timecourses are shown for the hemisphere used for microstimulation. **(A, D, G)** Monkey M2: This animal lacked an AF in the right hemisphere. **(B, E, H)** Monkey M3: This animal showed a full set of six discrete face patches in both hemispheres. **(C, F, I)** Monkey M4: This animal showed a full set of six discrete face patches in the left hemisphere. In the right hemisphere, PL and ML were confluent.

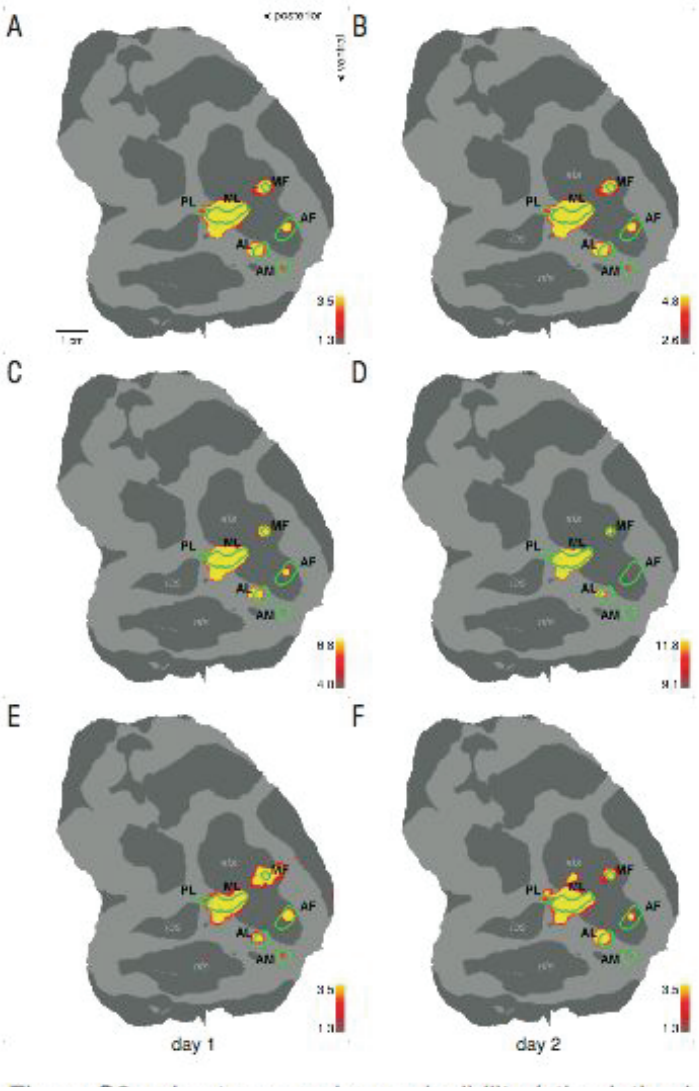

Fig. S2. Robustness of the activation pattern to stimulation in ML of monkey M1. Same conventions as Fig. 2C. **(A-D)** Areas activated by microstimulation versus no microstimulation, at four different significance thresholds. **(E, F)** Areas activated by microstimulation versus no microstimulation, for two separate scan sessions.

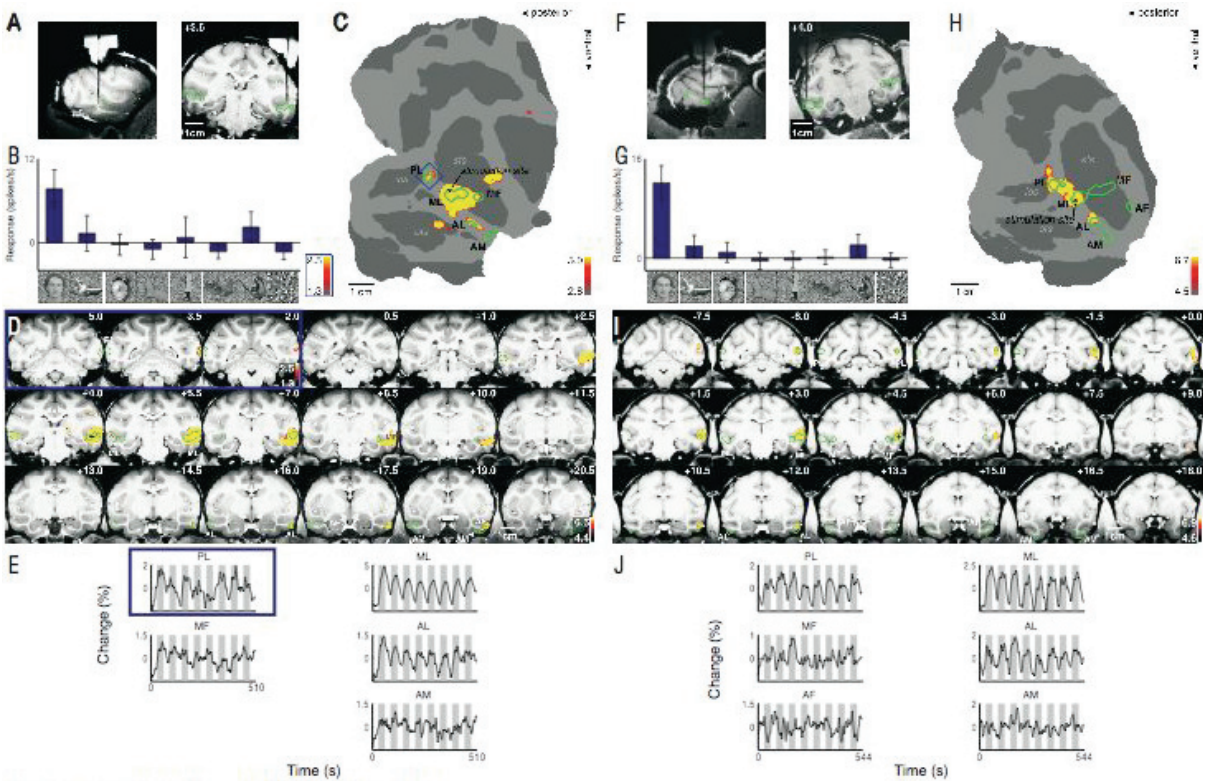

Fig. S3. Brain regions activated by microstimulation in the lateral middle face patch (ML) of monkeys M2 and M3. Same conventions as Fig. 2. **(A-E)** Monkey M2: Since the slice prescription for the initial experiments did not include PL, the experiment was repeated with a more posterior slice prescription. Results from this experiment are shown in the blue inset. Stimulation in ML of this animal produced activity in PL, MF, and AL. Judging from the slice data (D), the two patches of activation in the OTS and upper STS are likely due to blurring of activity at the stimulation site itself and therefore spurious. **(F-J)** Monkey M3: Stimulation produced activity in ML, PL, and AL.

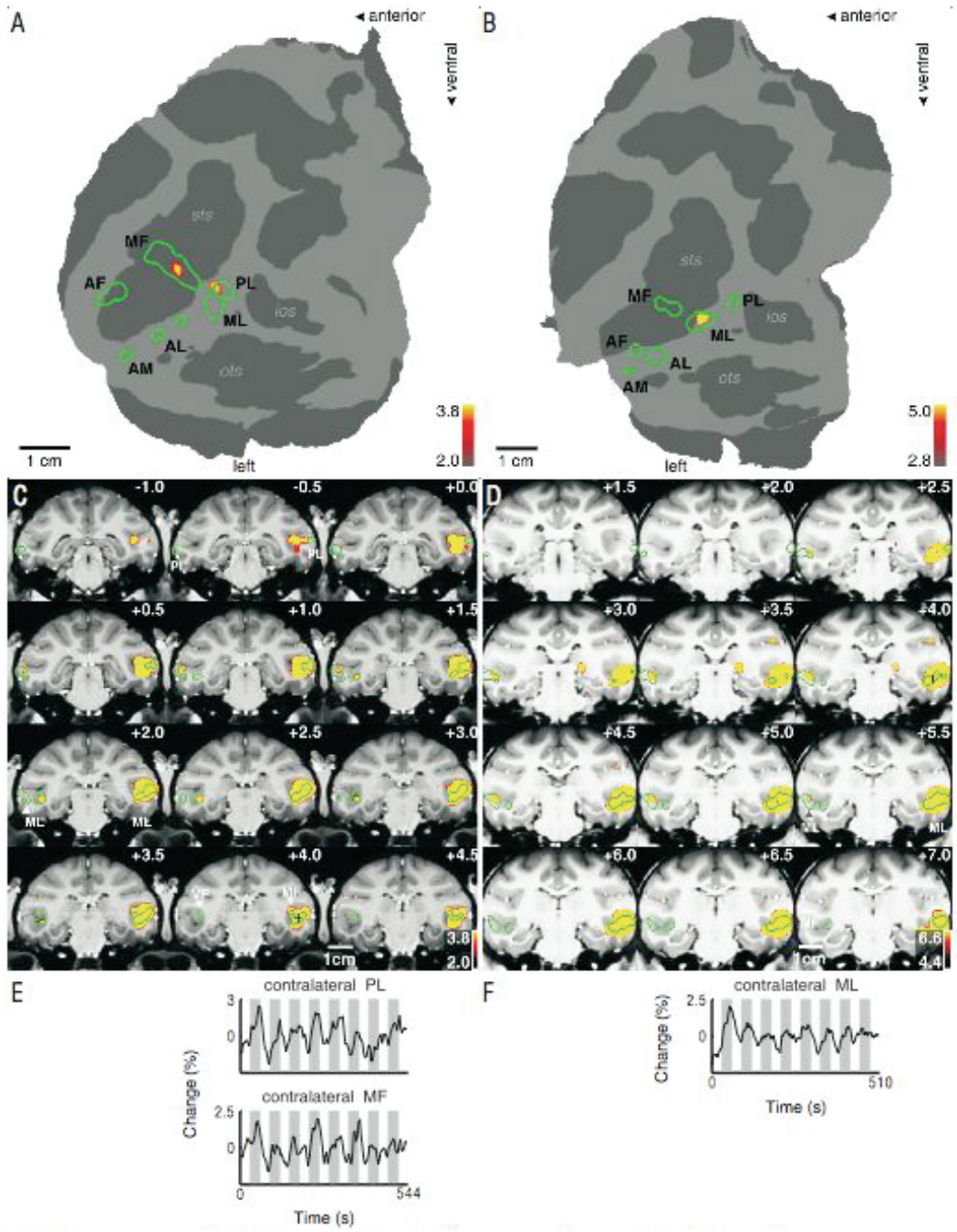

Fig. S4. Contralateral cortical activation elicited by microstimulation in the lateral middle face patches (ML) of monkeys M1 and M2. **(A)** In monkey M1, microstimulation in ML produced activation in two contralateral face patches, PL and MF. **(B)** In monkey M2, microstimulation in ML produced activation in contralateral ML (PL was not included in the slice prescription for this experiment). **(C, D)** The same contrast (microstimulation versus no microstimulation) shown on coronal slices (C, monkey M1; D, monkey M2). In both monkeys the ipsilateral effects of microstimulation were stronger and extended over longer distances than the contralateral effects. **(E, F)** Time courses from the contralateral face patches that were activated in monkey M1 (E) and M2 (F).

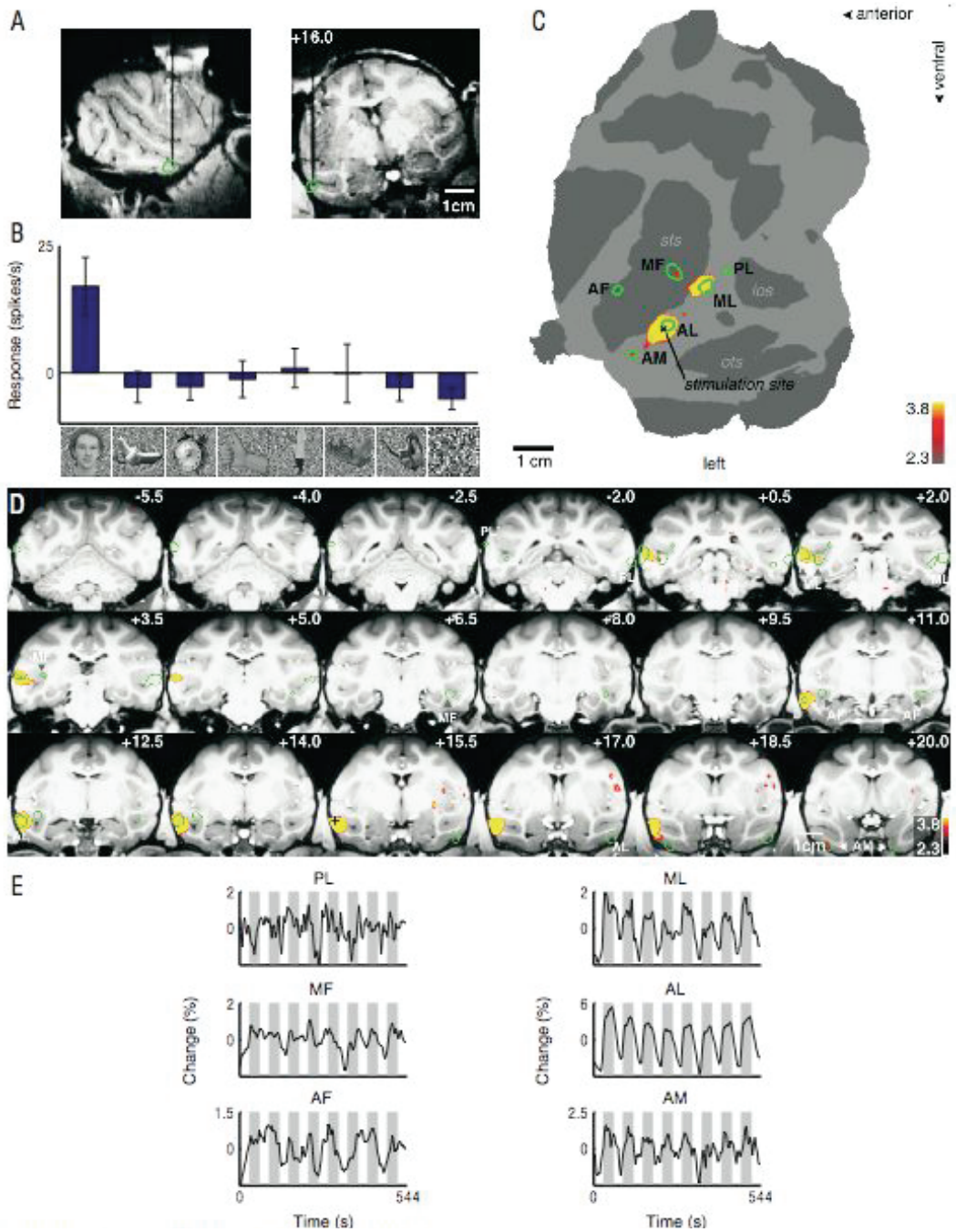

Fig. S5. Brain regions activated by microstimulation in the left hemisphere lateral anterior face patch (AL) of monkey M4. Same conventions as Fig. 2. Stimulation produced activity in ML, MF, AL, and AM.

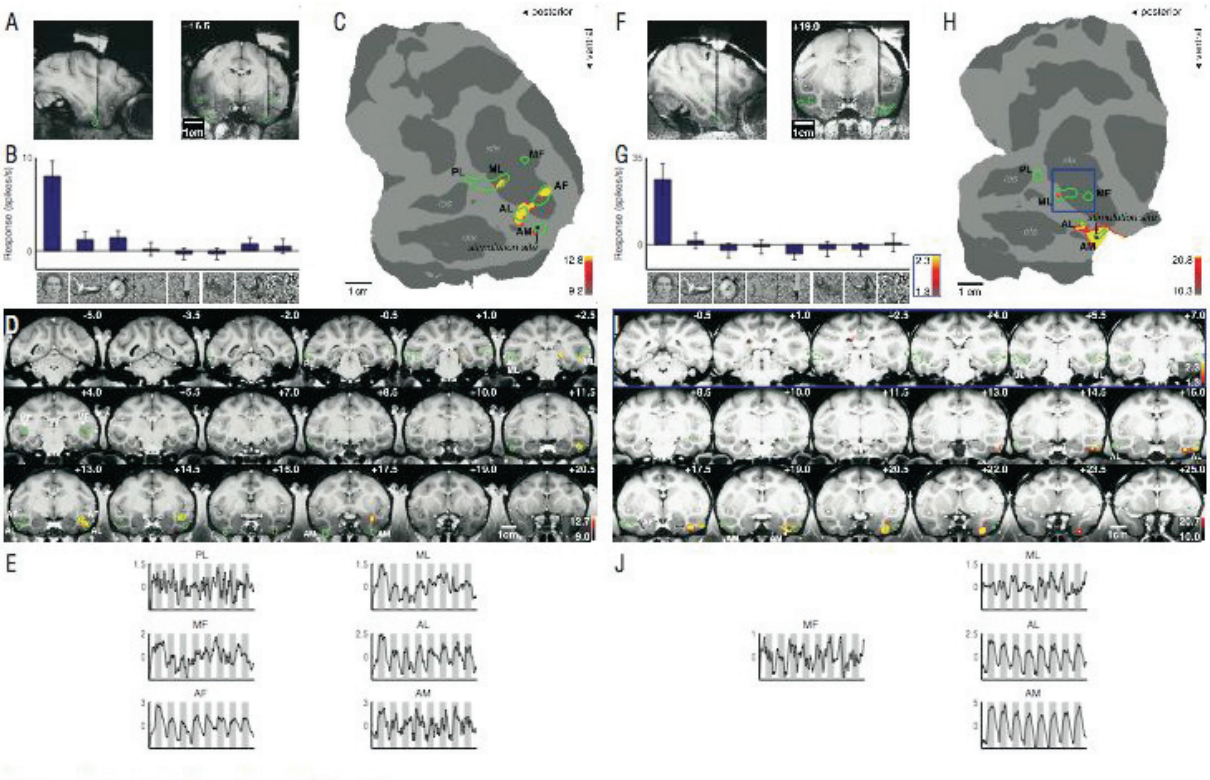

Fig. S6. Brain regions activated by microstimulation in the ventro-medial anterior face patch (AM) of monkeys M1 and M2. Same conventions as Fig. 2. **(A, F)** Electrode position in AM. **(B, G)** Examples of neuronal selectivity. **(C, H)** In M1, stimulation in AM produced specific activity in ML, AL, and AF. The small region of activation next to AM likely represents spread around the stimulation site that was displaced due to increased susceptibility artifacts from the electrode at this position. In M2, AM stimulation produced specific activity in AL and ML. The slice prescription for M2 excluded PL, so possible activation of this patch could not be observed. The blue inset shows data from the same experiment at lower threshold (the activation in ML was not visible at higher thresholds). **(D, I)** Activation overlaid on coronal slices. PL and MF were the only two face patches that did not show activity modulation by microstimulation. In M1, note activation in the pulvinar (AP position +2.5) and lateral amygdala and claustrum (AP position +17.5). **(E, J)** Time courses from face patches.

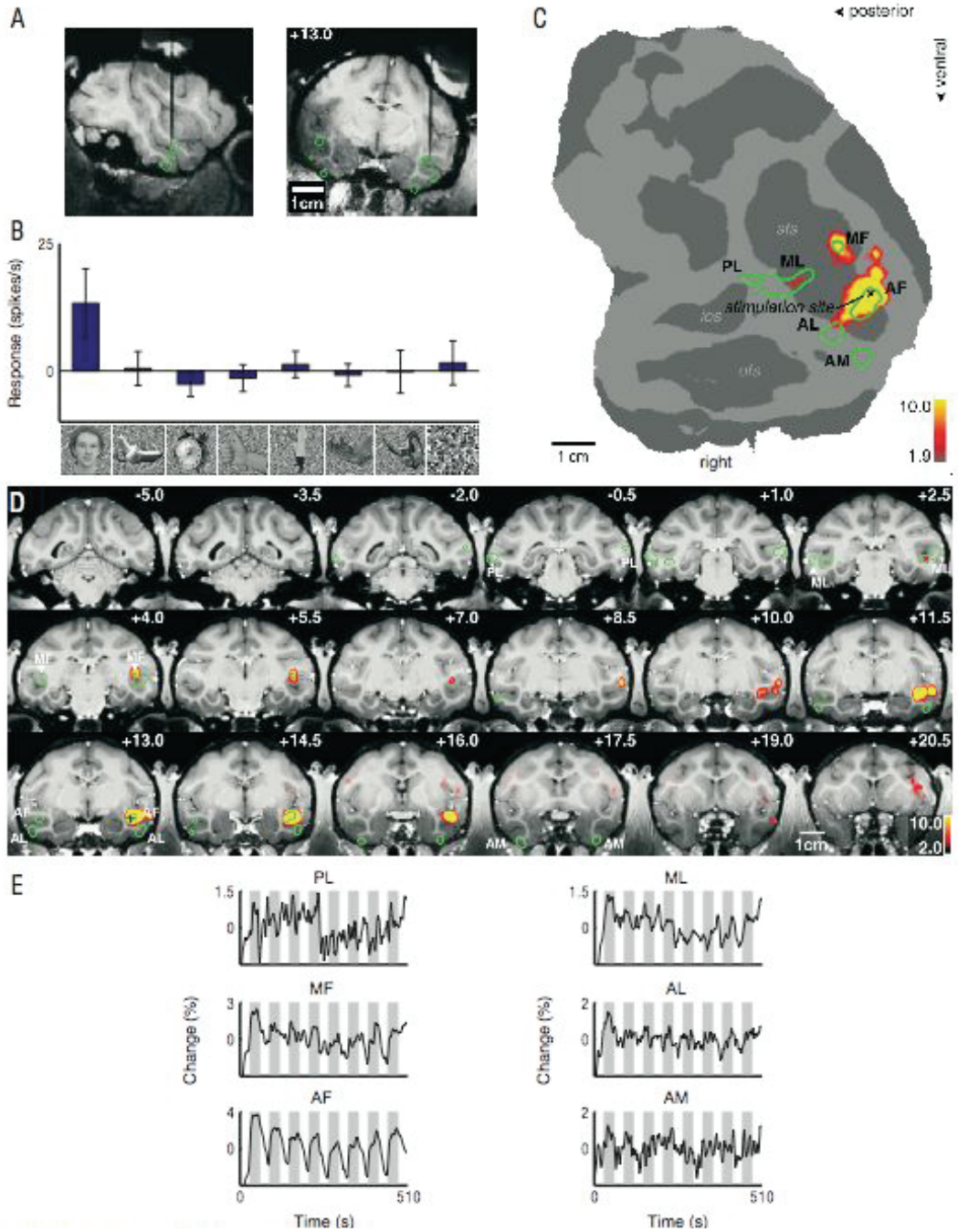

Fig. S7. Brain regions activated by microstimulation in the anterior face patch in the fundus of the STS (AF) in monkey M1. Same conventions as Fig. 2. **(A)** Electrode position in AF. **(B)** Example of neuronal selectivity. **(C)** Microstimulation in AF produced a spread of activation around the electrode tip, as well as strong activation of MF and weak activation of ML. **(D)** Activation map overlaid on coronal slices. **(E)** Time courses from the six face patches.

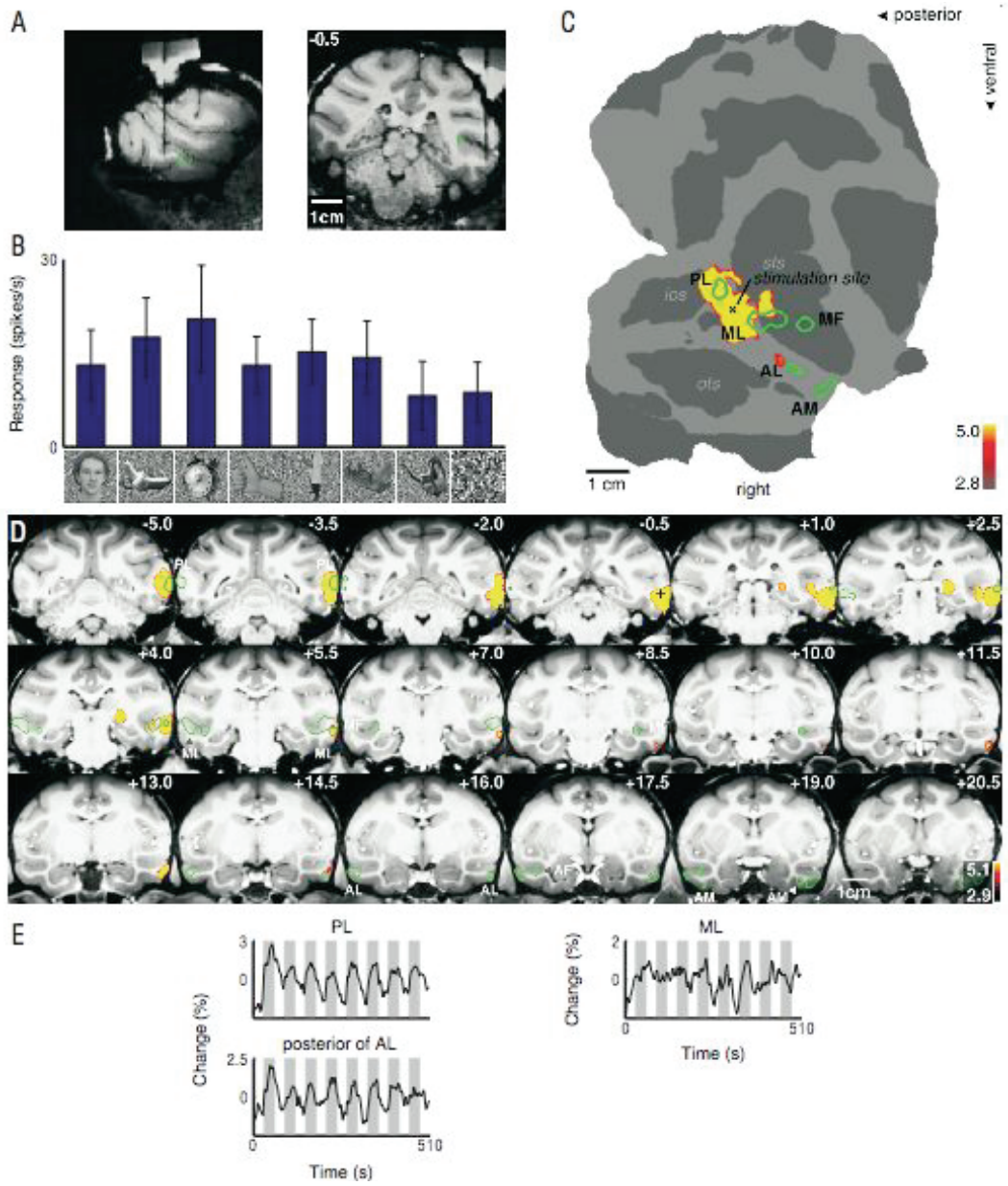

Fig. S8. Brain regions activated by microstimulation outside the lateral middle face patch (ML) of monkey M2. Same conventions as Fig. 2. **(A)** Electrode position posterior to ML. **(B)** Example of neuronal selectivity. Units recorded at the stimulation site had no clear preference for any of the eight image categories. **(C)** Microstimulation at this site produced a spread of activation around the electrode tip that included PL, but excluded all the other face patches. Note the discrete patch of activation anterior to ML and posterior to AL. **(D)** Activation map overlaid on coronal slices. **(E)** Time courses from PL, ML, and the patch anterior to ML.

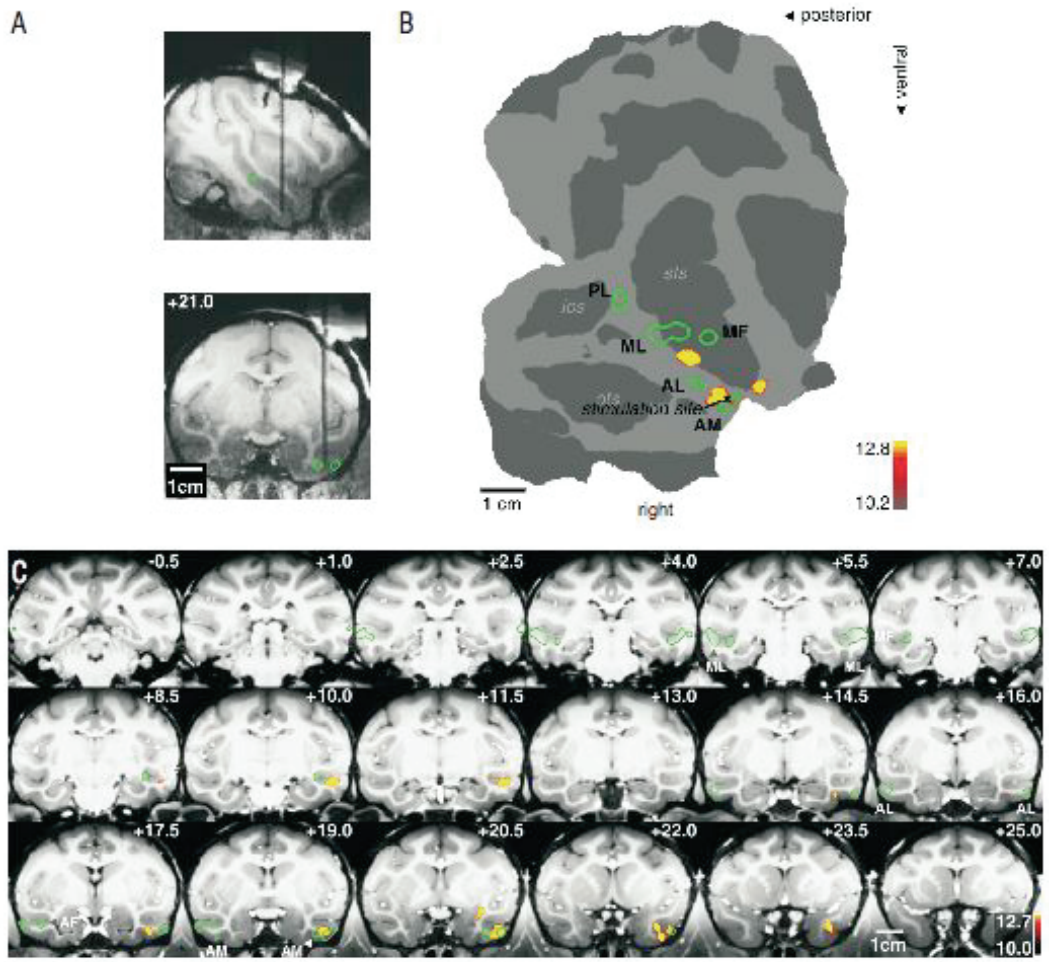

Fig. S9. Brain regions activated by microstimulation outside AM of monkey M2. Same conventions as Fig. 2. **(A)** Electrode position lateral to AM and medial to AL. **(B)** Microstimulation at this site produced activation around the electrode tip (which was likely shifted posterior due to increased susceptibility artifacts from the electrode at this position), as well as two discrete patches of additional activity. **(C)** Activation map overlaid on coronal slices.

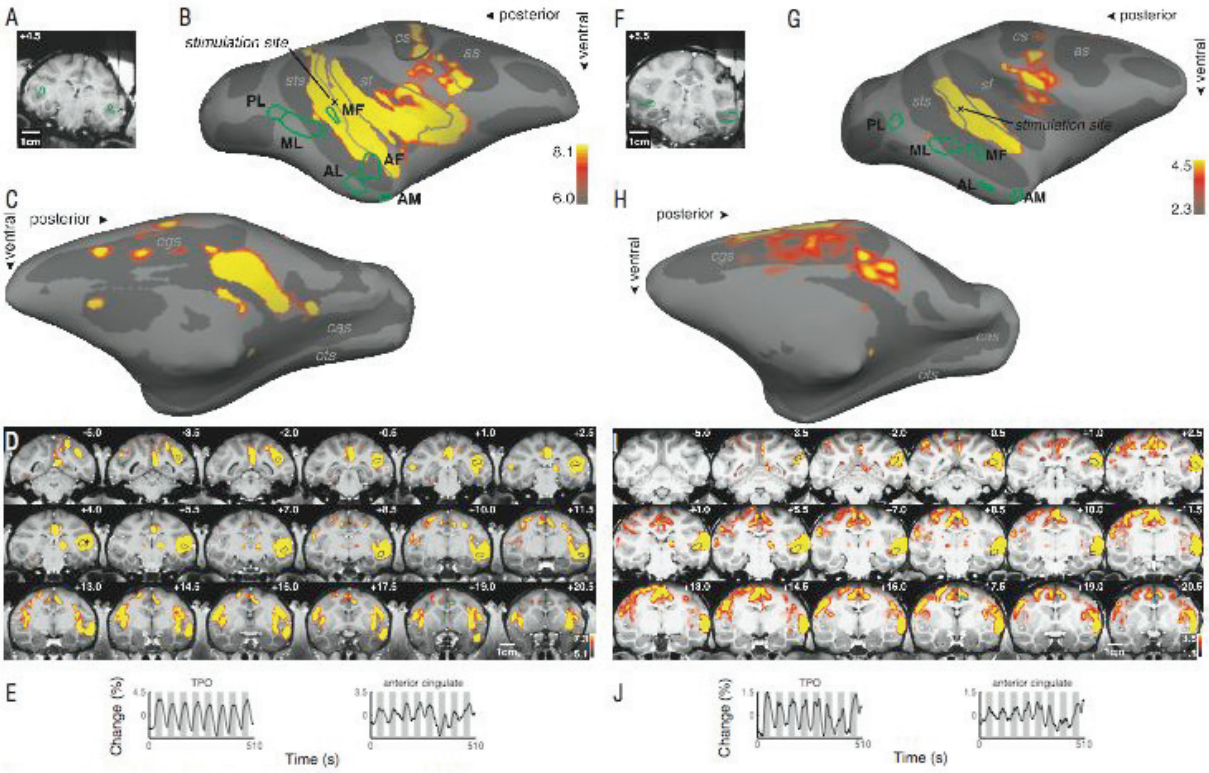

Fig. S10. A large swath of cortex is activated by microstimulation in the upper bank of the STS (monkeys M1 and M2). **(A, F)** Electrode position in the upper bank of the STS in area TPO. **(B, G)** Activation for the contrast microstimulation versus no microstimulation, overlaid on the inflated right hemisphere (outlines of the face patches in green). Anatomical labels: *sts:* superior temporal sulcus, *sf:* Sylvan fissure, *cs:* central sulcus, *as:* arcuate sulcus, *cgs:* cingulate sulcus, *cas:* calcarine sulcus, *ots:* occipitotemporal sulcus. **(C, H)** A medial view of the same data, revealing activation of cingulate cortex and adjacent somatosensory and supplementary motor areas. **(D, I)** The same activation overlaid on coronal slices. Posterior area TPO is indicated by black outlines; anterior cingulate cortex by cyan outlines for both monkeys. **(E, J)** Time courses from activated areas. Note the strong modulation in anterior cingulate cortex, despite its considerable distance from the stimulation site.

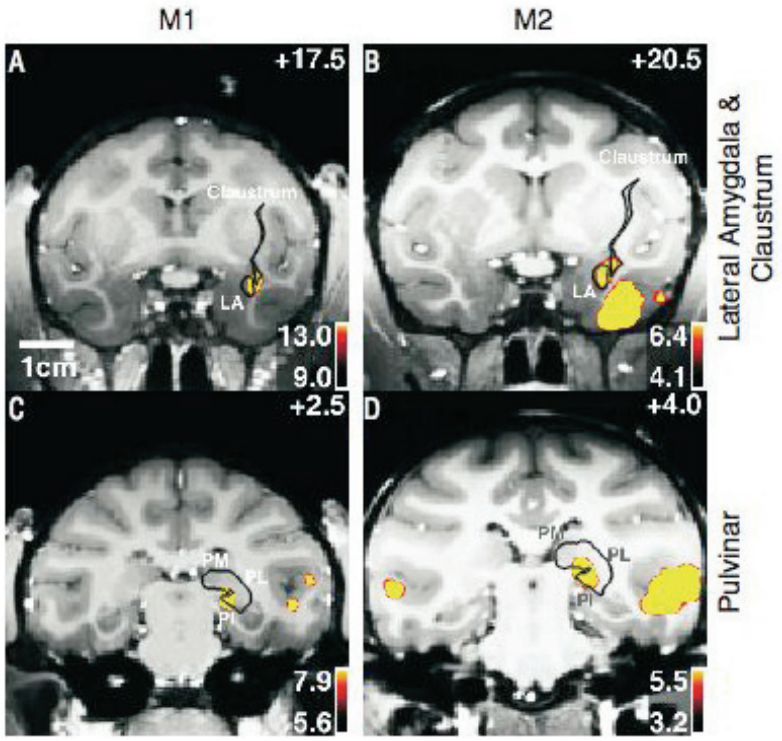

Fig. S11. Microstimulation of face patches activates the amygdala, claustrum, and pulvinar. **(A, B)** Microstimulation in AM of monkeys M1 and M2 produced activity in the ipsilateral lateral amygdala and adjacent claustrum. **(C)** Microstimulation of the lateral middle face patch (ML) in monkey M1 produced strong activity in the ipsilateral inferior pulvinar. **(D)** The inferior pulvinar was also activated by microstimulation in an anterior face patch (AL) in monkey M2. Anatomical labels: lateral amygdala (LA), inferior pulvinar (PI), lateral pulvinar (PL), medial pulvinar (PM). Subcortical area boundaries (black traces) adapted from Ref. 20; in the absence of histological confirmation, these should be regarded as tentative.

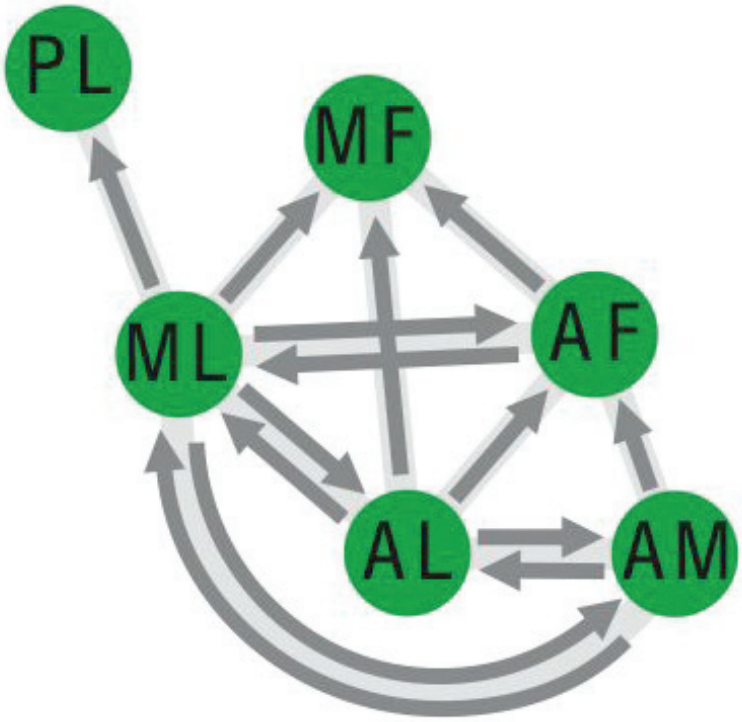

Fig. S12. The internal connectivity of the face patches. This schematic summarizes the results of all the experiments in the four monkeys (see also Table S2). For each of the four stimulated patches, arrows point to co-activated patches. Note that since MF and PL were not targeted for microstimulation, no arrows leave these patches.

Supplementary table 1. Summary of experiments

Experiment	Number of Runs Included in Analysis			
	M1	M2	M3	M4
face localizer	15	18	35	23
stimulation in ML	44	64	20	
stimulation in AL	22			13
stimulation in AM	22	27		
stimulation in AF	19			
stimulation outside ML	24	22		
stimulation outside AM		14		
stimulation in upper STS	19	27		
visual + microstimulation	29	30		

Table S1. Summary of experiments performed in monkeys M1 – M4. Each box indicates the total number of runs that were analyzed to generate the figure for that experiment.

Supplementary table 2. Summary of result

Stimulation site	Projection Site						
	ID	PL	ML	MF	AL	AF	AM
ML	M1	+++	+++	+++	+++	+++	++
	M2	++	+++	+++	+++	n. a.	-
	M3	+++	+++	-	+++	-	-
AL	M1	-	+++	++	+++	+++	+
	M4	-	+++	++	+++	-	+

AF	M1	-	+	+++	-	+++	-
AM	M1	-	++	-	+++	+++	+
	M2	-	+	-	+++	n. a.	+++

n. a.: face patch could not be localized in this monkey
-: no projection detected
+: weak projection detected
++: intermediate projection detected
+++: strong projection detected

Table S2. Summary of results from microstimulating the four face patches in monkeys M1 – M4.

References

1. D. Y. Tsao *et al.*, *Neuron* **39**, 555 (Jul 31, 2003).
2. D. Y. Tsao, W. A. Freiwald, T. A. Knutsen, J. B. Mandeville, R. B. Tootell, *Nat Neurosci* **6**, 989 (Sep, 2003).
3. D. Y. Tsao, W. A. Freiwald, R. B. H. Tootell, M. S. Livingstone, *Science* **311**, 670 (2006).
4. D. Wegener, W. A. Freiwald, A. K. Kreiter, *J Neurosci* **24**, 6106 (Jul 7, 2004).
5. K. Nelissen, W. Vanduffel, G. A. Orban, *J Neurosci* **26**, 5929 (May 31, 2006).
6. F. P. Leite *et al.*, *Neuroimage* **16**, 283 (Jun, 2002).
7. W. Vanduffel *et al.*, *Neuron* **32**, 565 (Nov 20, 2001).
8. R. Cusack, M. Brett, K. Osswald, *Neuroimage* **18**, 127 (Jan, 2003).
9. H. Zeng, R. T. Constable, *Magn Reson Med* **48**, 137 (Jul, 2002).
10. D. H. Brainard, *Spat Vis* **10**, 433 (1997).
11. R. W. Cox, J. S. Hyde, *NMR Biomed* **10**, 171 (Jun-Aug, 1997).

Comparing face patch systems in macaques and humans

(accepted for publication in PNAS 2008)

Doris Y. Tsao, Sebastian Moeller, and Winrich A. Freiwald

Institute for Brain Research and Center for Advanced Imaging, University of Bremen, P.O.B. 330440, D-28334 Bremen, FR Germany

Correspondence should be addressed to D.Y.T (doris@nmr.mgh.harvard.edu), W.A.F. (winrich.freiwald@googlemail.com)

Face recognition is of central importance for primate social behavior. In both humans and macaques, the visual analysis of faces is supported by a set of specialized face areas. The precise organization of these areas, and the correspondence between individual macaque and human face-selective areas, is debated. Here we examined the organization of face-selective regions across the temporal lobe in a large number of macaque and human subjects. Macaques showed six regions of face-selective cortex arranged in a stereotypical pattern along the temporal lobe. Human subjects showed, in addition to three previously reported face areas (the occipital, fusiform, and superior temporal sulcus face areas), a new face-selective area located anterior to the fusiform face area, in the anterior collateral sulcus. These results suggest a closer anatomical correspondence between macaque and human face processing systems than previously realized.

For primates as social animals, faces are immensely important stimuli, carrying a wealth of social information. Given the paramount importance of face recognition for primates, the underlying neural mechanisms must have been subject to the highest selective pressure through the course of evolution (1, 2). As a consequence, a common primate face-recognition system may exist, providing the basic scaffold around which species-specific specializations may have then evolved.

In humans, extensive behavioral and neurological evidence suggests that specialized mechanisms exist for processing faces (3, 4). This notion is supported by functional imaging experiments showing several face-selective areas in the temporal lobe, including the fusiform face area (FFA), the occipital face area (OFA), and a face area in the superior temporal sulcus (STS-FA) (5). Furthermore, evidence has been put forward that these areas have different functional specializations, suggesting that the OFA is involved in processing face parts (6), the STS-FA in processing changeable aspects such as gaze direction (7), and the FFA in processing identity (8, 9). Thus, the human face-processing system seems to be organized around three specialized face areas (10).

In macaque monkeys, the existence of face-selective cortical areas, so called “face patches”, was demonstrated by fMRI (11, 12). Tsao et al. reported three regions of face-selective cortex in inferotemporal cortex, organized along an anterior-posterior axis. This finding immediately raised the question of how macaque face patches relate to those of humans and, more generally, whether there is a common functional organization for face processing in primates. By computationally stretching the cortical surface of the macaque brain over the human cortical surface, the macaque middle face patch was found to lie quite close to the human FFA (11). The human FFA and macaque middle face patch were also the largest within each species.

While this spatial correspondence analysis is, of course, a far cry from demonstrating homology, it raises an important question about the functional organization of face-selective cortex. If the human FFA corresponds to the macaque middle face patch, then what does the macaque anterior face region correspond to? Since no face area anterior to the FFA has been reported in humans to date, an area corresponding to the anterior macaque face region seems to be missing. Therefore, the correspondence between macaque and human face areas remains unclear and it is an open question whether the two species whose last common ancestor dates back more than 20 million years (13) share a common functional architecture for face processing.

Here we used fMRI in macaques and humans to address two fundamental questions about the organization of the primate face processing system. First, what is the exact composition of the macaque face processing system? Is there a consistent and reproducible pattern of face-selective cortex across individuals? The numbers of face-selective regions reported in previous studies differ (three, (11); two, (12, 14)), but only small numbers of animals were used in these studies. Here, we identified face-selective regions across the temporal lobes of 10 macaques, allowing a true population perspective. Second, is there face-selective cortex anterior to the FFA in humans? Intracranial electrocorticograms show face-selective evoked potentials (15) anterior to the FFA, suggestive of an anterior temporal face region. But earlier fMRI studies did not cover the anterior portions of the human temporal lobe (5), and, therefore, could not address the existence of face-selective regions in the anterior temporal lobe. Here, we used a slice prescription that covered the entire human temporal lobe (as well as a large portion of the frontal lobe).

Results

Both monkeys and humans were scanned while awake and passively fixating. Stimuli consisted of human faces, macaque faces, hands, gadgets, fruits and vegetables, headless bodies, and scrambled patterns, presented in separate blocks. By using the same method (fMRI), the same stimulus material, and the same analysis procedures, we could directly compare the functional organization of face selectivity in these two species.

Face-selective regions in monkeys

We scanned ten macaques with the standard face localizer stimulus to identify face-selective regions. In one animal (M10), we did not find any face-selective regions despite repeated scans (Suppl. Table 3). Fig. 1 and Suppl. Figs. 1 and 2 present results from the nine remaining monkeys. Fig. 1a shows face-selective regions in the left and right hemispheres of monkey M1 on flattened maps of the posterior half of the brain; Suppl. Fig. 2a shows the same data on high resolution coronal slices. This animal had six discrete face patches in each hemisphere, distributed along the anterior-posterior axis of the temporal lobe. These patches were organized into: one posterior patch on the lateral surface of TEO (which we will refer to as “PL”, for posterior lateral), two middle face patches in posterior TE, one located in the fundus of the STS (“MF”, for middle fundus) and one on the lower lip of the STS (“ML”, for middle lateral), and three patches in anterior TE, one located near the fundus of the STS (“AF”, for anterior fundus), one on the lower lip of the STS and adjacent gyrus, in TEad (“AL”, for anterior lateral), and one more medially on the ventral surface, just lateral and anterior to the AMTS, in TEav (“AM”, for anterior medial).

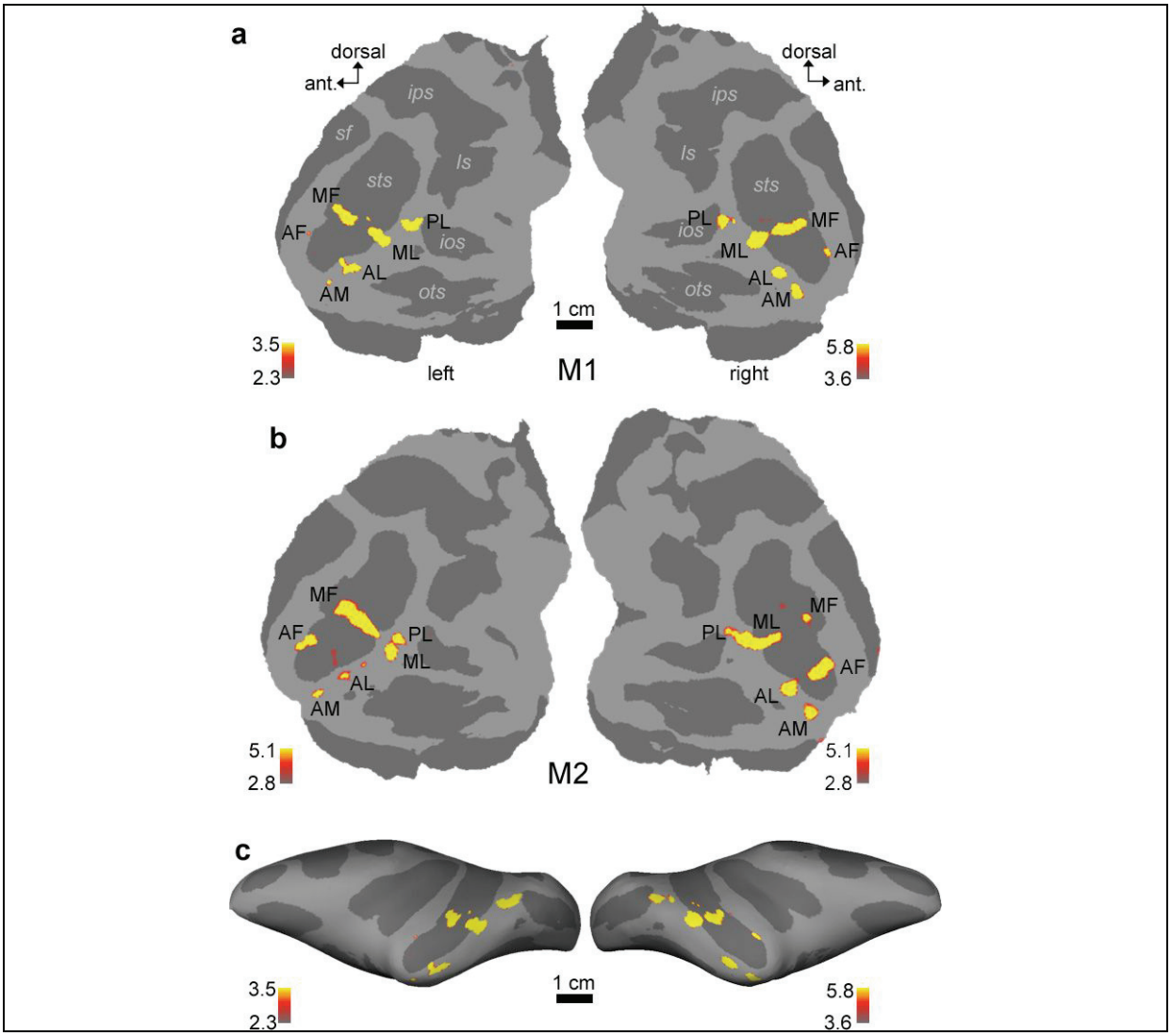

F 1. Face-selective regions in two macaque (a, b), superimposed on flattened cortical surfaces and a lateral view of the inflated hemispheres (c). Computational flattening involves distorting the spatial arrangement of the data, and under-estimates the size of the sulci (shown in dark grey). Color scale bars indicate the negative common logarithm of the probability of error. Area initials: posterior face patch (PL), middle face patch in the STS fundus (MF), middle face patch on the STS lip (ML), anterior face patch in the STS fundus (AF), anterior face patch on the STS lip (AL), and anterior face patch on the ventral surface of IT just lateral and anterior to the AMTS (AM). Sulcal abbreviations: lunate sulcus (ls), inferior occipital sulcus (ios), occipito-temporal sulcus (ots), superior temporal sulcus (sts), intraparietal sulcus (ips), Sylvan fissure (sf).

The set of face patches for monkey M1 (Fig. 1a, Suppl. Fig. 2a) represents the prototypical pattern. Face patches of eight additional animals (panels b-i in Suppl, Figs. 1 and 2) confirmed this pattern. Individual animals and hemispheres exhibited slight variations from this pattern. We observed four specific types of variation: 1) In four out of 18 hemispheres, PL and ML were confluent (right hemispheres of M2, M4, and M6; left hemisphere of M5). 2).

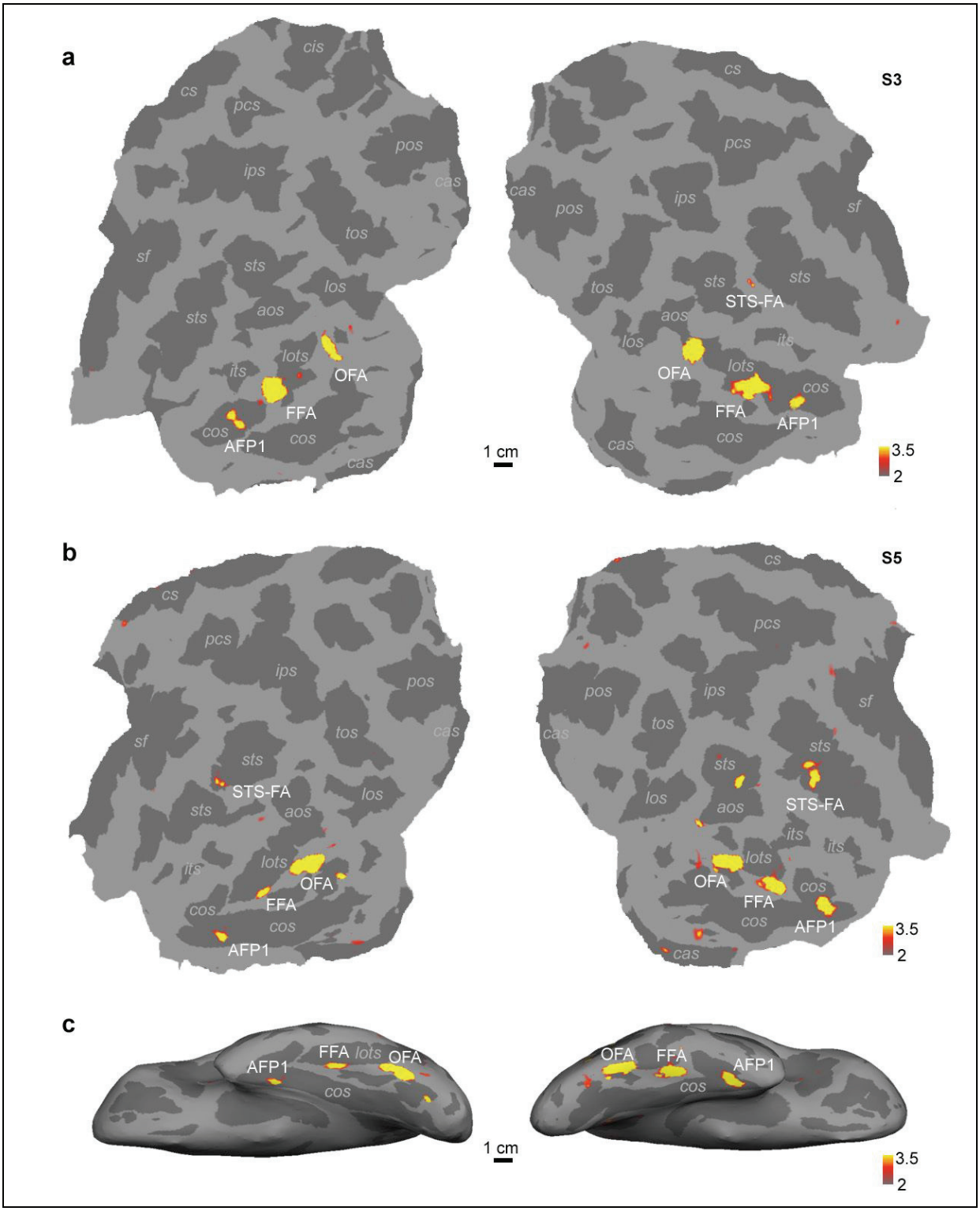

F 2. Face-selective regions in the left and right temporal lobes of two humans, superimposed on flattened cortical surfaces (a, b) and a ventral view of the inflated hemispheres (c). Face-region abbreviations: occipital face area (OFA), fusiform face area (FFA), superior temporal sulcus face area (STS-FA), anterior face patch 1 (AFP1). Sulcal abbreviations: anterior occipital (aos), lateral occipital (los), lateral occipito-temporal (lots), intraparietal (ips), inferior temporal (its), superior temporal (sts),

parieto-occipital (pos), calcarine (cas), collateral (cos), transoccipital (tos), precentral (pcs), and Sylvan fissure (sf).

In three hemispheres, ML and MF were confluent (left hemispheres of M5, M8 and M9). 3) In several animals, "extra" spots of face-selective activation beyond the prototypical six patches were observed; these were usually small and unilateral (e.g., left hemisphere of M2, just posterior to AL; right hemisphere of M3, just posterior to ML; right hemisphere of M9, posterior to MF in the fundus of the STS). In one case, we observed a sizeable, bilateral pair of face patches at an unexpected location (M7, posterior to PL, in both hemispheres). 4) Finally, in two hemispheres, one or more of the six patches were absent (AM and AF in the right hemisphere of M7; PL in the right hemisphere of M9). Overall, despite these variations, the robustness of the six patch pattern across the nine animals is striking.

In cases where two patches were confluent (always either PL and ML, or ML and MF), we could also, in theory, have concluded that one of the patches was missing. However, the size of agglomerate patches suggests that they do indeed represent confluent sub-components. For example, in monkey M6, PL was confluent with ML in the right hemisphere, but discrete from ML in the left hemisphere (Suppl. Fig. 1f). The size and location of the PL-ML agglomerate in the right hemisphere was similar to that of PL and ML combined in the left hemisphere.

All the patches shown in Figs. 1 and 2 were robust and reproducible across independent scan sessions (Suppl. Fig. 3, 4). Thresholds were chosen to allow all robust patches to be revealed, and the number of patches was not dependent on the particular threshold chosen. The pattern of temporal lobe patches was identical when all data is shown at a common threshold of $p = 10^{-3.1}$ (Suppl. Fig 4), with two exceptions: AM, the face patch on the ventral surface of IT that is most susceptible to signal extinction due to use of a surface coil, was not visible in two cases at this threshold (right hemisphere of M4 and left hemisphere of M7).

Suppl. Table 1 gives the sizes of the six face patches in each of the nine macaques. ML was the largest of the six patches, followed by AL, PL, MF, AM, and AF. For the seven cases of confluent patches, ROIs were drawn to conform as best as possible to the pattern in the opposite hemisphere (in which patches were discrete) (Suppl. Fig. 4).

Face-selective regions in humans

We scanned 13 human subjects using the same face localizer stimulus used for the monkeys. We took care to use a slice prescription covering the entire temporal lobe. In addition to previously reported face areas OFA, FFA, and STS-FA, in the majority of subjects (9/13) we identified one or two face-selective regions anterior to the FFA. We call these regions "AFP1" (anterior face patch 1) and "AFP2" (anterior face patch 2). Fig. 2 shows face-selective regions in the left and right temporal lobes of two human subjects, superimposed on flattened cortical surfaces (Fig. 2a, b) as well as a ventral view of the inflated brain (Fig. 2c). AFP1 can be seen to lie in the anterior collateral sulcus in both animals. Suppl. Fig. 5 shows face-selective regions in the left and right temporal lobes of all nine human subjects that had at least one anterior face patch, superimposed on coronal, horizontal, and sagittal MRI slices. Subjects 1 and 2 (Suppl. Fig. 5 a, b) had both AFP1 and AFP2, while the remaining subjects (Suppl. Fig. 5c-i) each had one anterior face patch (AFP1). AFP2 was also located in the collateral sulcus, at its anterior-most tip. All nine subjects had an FFA and OFA in both hemispheres, and 6/9 subjects had an STS-face area.

Suppl. Table 2 gives the sizes of the face-selective regions in each of the nine human subjects. The largest face-selective region was the FFA, followed by the OFA, STS-FA,

AFP1, and AFP2. Human temporal face-selective regions were larger over the right than the left hemisphere, whereas the monkey temporal face-selective regions were bilateral (Suppl. Table 1).

All of the human face-selective regions, including AFP1 and AFP2, were reproducible across independent scan sessions within the same subject. Suppl. Fig. 6 shows face-selective regions of four subjects (S1, S2, S4, S5) obtained in two independent scan sessions. Subjects S1 and S2 each had two anterior face patches that were reproducible across scan sessions (Suppl. Fig. 6a, b). Subjects S4 and S5 each had one anterior face patch (S4 only in the right hemisphere and S5 bilaterally), and the anterior patch in the right hemisphere was reproducible in both subjects.

Susceptibility artifacts created by the ear canals cause major signal loss in a significant portion of the temporal lobe in humans; the effects are much less in macaques due to the smaller voxels sizes (16-18). Suppl. Fig. 7 shows face patches displayed on raw EPI (echo planar imaging) slices; for each subject, the slice containing the anterior face patch is shown. In several cases, the anterior face patch can be seen to lie close to the ear canal artifact (e.g., Suppl. Fig. 7b, right; Suppl. Fig. 7d). This raises the possibility that AFP1/AFP2 are actually continuations of the FFA, and only appear discrete from it due to the chasm created by the ear canal susceptibility artifact. We doubt this for two reasons: 1) in all 9 subjects, non-face-selective grey matter lying outside the artifact could be found between the FFA and AFP1/AFP2, and 2) there was a wide separation between AFP1 and the FFA (typically more than 2 cm). It is entirely possible that additional face-selective regions could lie within the artifact zone, e.g., in the four subjects in which we did not find any anterior face-selective regions. Methodological improvements, including use of spin echo imaging (19) and high resolution scanning (18, 20), may uncover such regions.

Face-selective regions in prefrontal cortex

We recently reported the existence of three face-selective regions in macaque prefrontal cortex (21). These include a bilateral pair of face patches in orbitofrontal cortex (within the lateral orbitofrontal sulcus), a patch located in the inferior convexity below the principal sulcus that is lateralized to the right hemisphere, and a patch in the anterior bank of the lower arcuate sulcus (Fig. 3a). In 3/9 human subjects, we observed face-selective activation within prefrontal cortex (see also (22)). The location of this activation, in the inferior frontal sulcus (IFS) and lateralized to the right hemisphere, was consistent across the three subjects (Fig. 3b-d). In a few subjects we also observed face-selective activation in orbitofrontal cortex (Fig. 3e). The fact we observed these prefrontal face patches in only 3/9 subjects may be due to variability across subjects, or to their small size (in the latter case, higher resolution scanning may reveal prefrontal face-selective regions more consistently).

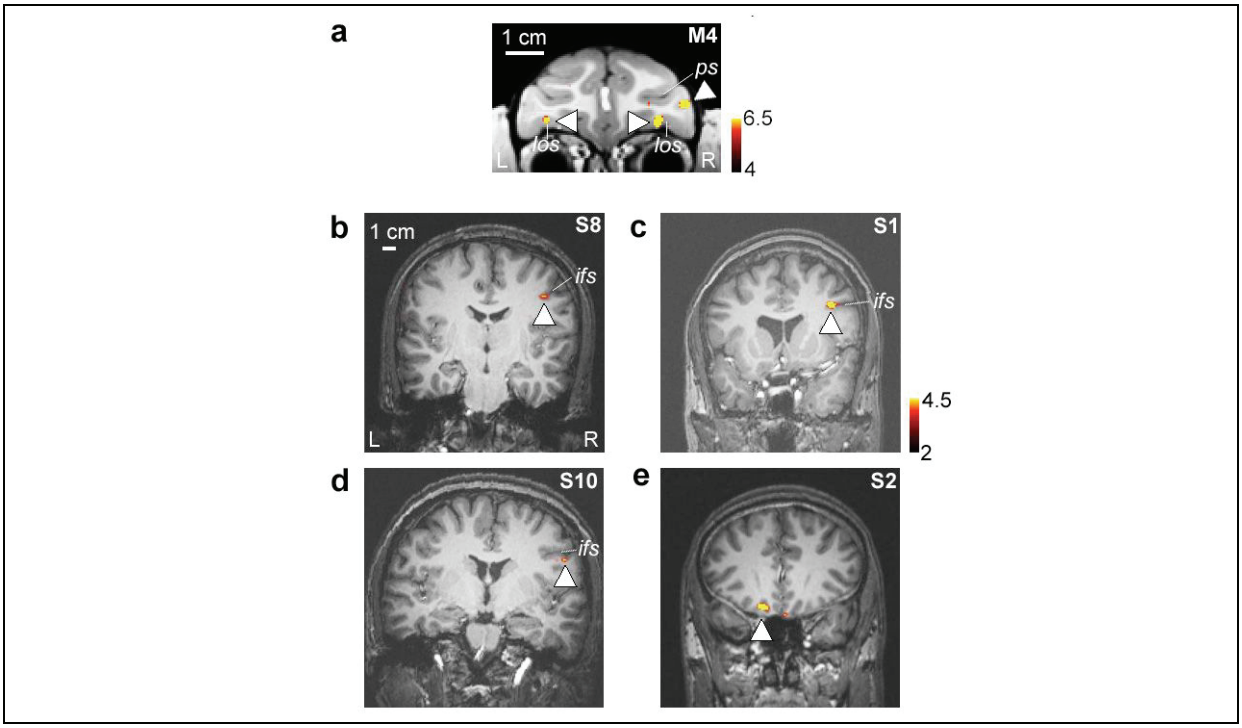

F 3. Prefrontal face-selective regions in macaque and humans. a) Prefrontal face patches from one macaque (M4), shown on a coronal slice. Taken from (21). The monkey had a face patch in the lateral orbitofrontal sulcus bilaterally, as well as one face patch in the inferior convexity, within the infraprincipal dimple, exclusively in the right hemisphere. Sulcal abbreviations: lateral orbitofrontal sulcus (los), principal sulcus (ps). b-d) Lateral prefrontal face-selective regions from three human subjects (S8, S1, and S10), shown on coronal slices. The location of the human lateral prefrontal face-selective region was consistent across subjects (within the inferior frontal sulcus, strongly lateralized to the right hemisphere). e) Face-selective region in orbitofrontal cortex of a human subject (S2).

Selectivity profiles of macaque and human face-selective regions

Average time courses (Suppl. Fig. 8a, b) and percent signal changes (Suppl. Fig. 8c, d) to faces and non-face objects confirm the strong face selectivity of each of the six macaque face patches (PL, ML, MF, AL, AF, AM), and six human face selective regions (OFA, FFA, STS-FA, AFP1, AFP2, and IFS) (analogous data for the macaque prefrontal face patches is given in (21)). To compute response profiles, we used half the data to define ROIs, and the other half to extract time courses and percent signal changes from the ROIs.

In humans, activation was significantly greater (at $p = 0.01$) to human faces than to macaque faces in AFP1 (but not in OFA, FFA, or STS-FS); this is consistent with anterior human temporal regions being more sensitive to familiar faces (23) (since human subjects are presumably more familiar with human than macaque faces). In macaques, ML and AL were the only two macaque regions that showed a significantly greater response to human than macaque faces.

None of the face-selective regions in either humans or macaques appeared to require viewing of familiar faces in order to be activated. The face stimuli used in the present study were familiar to a subset of the monkeys (M1, M2, M3, M4, M7) who had seen the stimuli

previously during training, but were completely novel (i.e., seen for the first time during the face localizer scan) to the remaining monkeys (M5, M6, M8, M9). The stimuli were completely novel to all human subjects except S2, S9, and S10. The pattern of face-selective regions was similar regardless of whether the stimuli were familiar or not; in particular, we identified anterior face regions in both human and macaque subjects for whom the face stimuli were completely novel.

The face localizer stimulus contained four categories of non-face objects (hands, gadgets, vegetables and fruits, and headless human bodies) presented in separate blocks. Therefore, we could compare the response to bodies with that to other non-face object categories within each face region. Consistent with previous reports of body areas neighboring face areas in both macaques (11, 12) and humans (20, 24), we observed a stronger response to bodies than to the other non-face object categories across the macaque and human face regions (Suppl. Fig. 8e, f); this difference reached significance in PL, ML, MF, AL, and AF in macaques, and in the FFA, AFP1, and IFS in humans. Whether these body responses arise from the face-selective regions themselves, or from nearby regions, will require ultra high-resolution fMRI and/or single-unit recordings to resolve. High resolution fMRI shows that the FFA does not respond to bodies (20), and targeted single-unit recordings show that the macaque middle face patch does not respond to bodies either (25). Importantly, however, the response to faces was significantly greater (at $p = 0.01$) than that to bodies in each of the six macaque face patches and in OFA, FFA, AFP, and AFP2 in humans (in human STS-FA and IFS, the response to faces was only marginally greater than that to bodies; $p = 0.026$ and $p = 0.059$, respectively).

Discussion

A stereotyped face-patch system in the macaque temporal lobe

Expanding earlier reports of face-responsive cortex (responding more to faces than scrambled pattern controls (14, 26)) and face-selective cortex (responding more to face than to non-face object controls (11, 12)) in the macaque temporal lobe, we show here that there is a stereotyped pattern of face-selective patches of cortex in the macaque temporal lobe. The spatial composition of this face-patch system was highly reproducible across individuals, and consisted of one posterior (PL), two middle (ML, MF), and three anterior (AL, AF, AM) face patches. The distance between PL and AM in the anterior posterior direction was more than 20 mm. The face-patch system thus presents us with a new kind of functional organization in TE, more macroscopic than feature columns of inferotemporal cortex (~0.5 mm in diameter, (27, 28)), yet more delicate than the coarse partitioning of IT into anatomically defined subregions (29-31). The components of the face patch system are compact (few mm in diameter), yet transgress area boundaries, with face patches located in posterior, middle and anterior portions of IT (31). Recordings from the two middle face patches (25) have shown that these consist almost entirely of face-selective neurons. It is possible that only a limited number of the patches show true preferential coding of faces. Others may have a more general function and show increased activation as a result of connectivity with the former. Alternatively, each of the face patches may constitute a domain-specific face module (32).

Anterior inferotemporal face areas in humans

In the human brain, multiple face-selective areas exist as well. In addition to the OFA, FFA, and STS-FA, we describe here the existence of up to two face-selective regions anterior to the FFA (see also Supplementary Figure 7, (18)). This finding extends earlier lines of evidence on the importance of anterior inferotemporal cortex for face recognition. Intracranial recordings of epicortical potentials in epileptic patients revealed a face-selective evoked potential (15, 33) originating from anterior IT. A positron emission tomography (PET) study found anterior IT activation specifically during performance of a face-identity task (34). fMRI reveals adaptation to face identity in anterior IT (8, 18). Finally, it has been shown that individuals with congenital prosopagnosia often show normal face- and object-related patterns of BOLD activity in the FFA, implying that the processing of face identity requires regions other than just the FFA (22). Subsequent anatomical analyses suggested defects in temporal lobe regions anterior to the FFA: Behrmann et al. found that congenital prosopagnosics have a smaller anterior fusiform gyrus than controls (35). Taken together, evidence from electrophysiology, functional and structural imaging, and behavioral investigations of prosopagnosia all point to an important role for anterior IT in face recognition. Our results suggest that these functions may be supported by dedicated face areas in this region.

These anterior face areas may have been missed by earlier studies using similar face localizers either because they did not cover the entire temporal lobe (5), or because they used group analysis to explore new regions (22). Group analysis may fail if the anatomical variance of a region is large or the region is only present in a subset of subjects because of low SNR caused by susceptibility.

A recent study demonstrates that multi-voxel response patterns in anterior human inferotemporal cortex can be used to distinguish between two different faces (18). Surprisingly, however, the same voxel sets, dubbed “face-exemplar regions”, could not distinguish a face from a house; thus they must be distinct from the human anterior face patches identified in the present paper. It remains to be determined whether the human anterior face patches are able to distinguish different face identities.

A possible homology between macaque and human face areas

Both macaque and human temporal lobes host multiple face-selective regions. In the macaque we consistently found six; in individual hemispheres with less than six patches, the lower count could be explained by fusion of patches. In humans the number of face areas varied between three and five. We consistently found the three previously described areas, OFA, STS-FA, and FFA. In addition we found one or two anterior face regions. Thus the overall numbers of macaque und human face-selective regions are comparable.

The spatial patterning of macaque and human face-processing systems exhibits both a striking similarity and a striking difference. The striking similarity is the arrangement of areas along the occipito-temporal axis (compare Figs. 1 and 2), the striking difference is their location along the dorso-ventral axis within the temporal lobe. While the macaque face patches are mostly located inside or close to the superior temporal sulcus, all the human face-selective regions, with the exception of the STS-FA, are located further ventral, primarily along or inside the collateral sulcus. A claim of homology between these areas, then, would imply a major shift of face area location in the course of primate evolution following the split of catarrhine primates into hominoids and old world monkeys.

It is counter-intuitive that humans have a smaller number of face-selective patches compared to macaques, whereas humans are presumably better in face perception. This could be due to a technical artifact (the use of smaller voxels sizes in macaques leads to decreased interaural suscpetibility artifacts, and the use of Sinerem contrast agent leads to a factor of 3 increase in signal/noise ratio at 3T (36)). Alternatively, a subset of human anterior face areas may have coalesced during evolution, or acquired new functions making them more general purpose and less face-selective.

Future directions

Our findings present steps along the way to establishing whether a common primate face-processing system exists. Establishing homologies between cortical areas and other brain structures is notoriously difficult and requires the combination of multiple criteria (37-40). It may be argued that the search for homologies between functionally defined high-level cortical areas is in vain, since these are developmentally malleable and because functional similarities could represent convergent solutions to the same computational problem. Yet, the intra-species consistency of the spatial pattern of the face-processing system across macaques and across humans indicates that the development of face selectivity is not arbitrary within the expanse of inferotemporal cortex but rather uses a fixed scaffold. Furthermore, the high social importance of faces for primates provides a rationale for why a specialized face-processing system may have evolved early during primate evolution. Clearly, many more and, ideally, diverse criteria need to be used to test areal homologies between man and macaque. Should these homologies be established for the face-processing system, then face areas could serve as landmarks that can be used to understand the evolution of the large expanse of temporal lobe between them (40).

Among the many criteria necessary to establish homology between cortical areas across species are functional similarities and links to behavior (38). Different functional properties for the different human face areas have indeed been found (6-9), and similarly for face cells in different parts of inferotemporal cortex (32, 41-43). Electrophysiological recordings targeted to the macaque face patches will be a powerful way to determine the functional specializations of these areas. Similarly, electrical stimulation (44) targeted to the different face patches should reveal their involvement in face-recognition behaviors. These experiments may suggest future functional testing that can be conducted in both macaques and human subjects using the same imaging modality to allow for direct comparisons of functional specializations across species.

Methods

All animal procedures complied with the NIH Guide for Care and Use of Laboratory Animals, regulations for the welfare of experimental animals issued by the Federal Government of Germany, and stipulations of Bremen authorities. Informed consent was obtained from all human subjects.

Surgery. The implantation of the MR-compatible headpost (Ultem, General Electric Plastics) followed standard anesthetic, aseptic, and postoperative treatment protocols which have been described in detail elsewhere (45). MR-compatible ceramic screws (Thomas Recording) and acrylic cement (Grip Cement, Caulk, Dentsply International) were used to secure the headpost to the skull.

Monkey fMRI. All scanning was performed on a 3T MR scanner (Allegra, Siemens). For each monkey we acquired 10 anatomical volumes at high spatial resolution (0.5 mm isometric). We used a T1 weighted inversion recovery sequence (MPRAGE). These scans were performed under anesthesia (Ketamin / Medetomidine, 8 mg/kg / 0.04 mg/kg) to reduce motion artifacts.

For all functional imaging, a contrast agent, ferumoxtran-10 (Sinerem, Guerbet, France; concentration: 21 mg Fe/ml in saline; dosage: 8 mg Fe/kg) was injected into the femoral vein prior to each scan session. Sinerem is the same compound as MION, produced under a different name (46). Sinerem/MION increases signal-to-noise and gives finer spatial localization than BOLD (36, 46-48). Sinerem results in a signal reduction at activated voxels; for all functional data we inverted the signal to facilitate comparison with BOLD data.

All functional data was acquired in coronal slices, using a multi-echo sequence (EPI, TR 3 or 4 s, TE 30 or 25 ms, 64 by 64 matrix) and a single-loop surface coil. In combination with a concomitantly acquired fieldmap, this allowed high fidelity reconstruction by undistorting most of the B0-field inhomogeneities (49, 50).

In these localizer experiments we acquired 136 volumes per run (28 or 42 slices, spatial resolution 1.25 mm and 1.5 mm isometric). The slice volume was adjusted for each monkey to cover the entire temporal lobe. Suppl. Table 3 summarizes the experiments performed in each monkey for this study.

Human fMRI. Human functional data was acquired in horizontal slices, tilted slightly upwards in the front and downwards in the back, covering all of the temporal lobe and most of the frontal lobe. We used a standard EPI sequence (EPI, TR 2.5 s, TE 32, 64 by 64 matrix, 2.5 mm x 2.5 mm in-plane resolution, 2 mm slice thickness, flip angle 90°) and a circularly polarized birdcage coil. At the end of ach scan session, we obtained a high resolution anatomical volume of the entire brain (MPRAGE, 1 mm isometric). Suppl. Table 3 summarizes the experiments performed in each human subject for this study.

Visual stimulation. The face patch localizer stimulus followed a block design. Blocks lasted 32 seconds, and included the following image categories: human faces (F), monkey faces (M), human hands (H), gadgets (G), fruits and vegetables (V), and headless bodies (B). There were 16 different images in each category. Each image block was preceded by a block consisting of scrambled versions of the same images (S), resulting in the following sequence: S F S H S M S G S F S V S M S B R (the final block consisted of a gray random dot pattern). Each image subtended 12° visual angle (10.4 cm diameter at 49 cm distance), and was presented for 0.5 s.

Visual stimulation was performed using custom code utilizing the Psychophysics Toolbox (51). Stimuli were displayed at 60 Hz with a resolution of 1280 by 1024 pixels, using a video beamer (JVC DLA -G15E) and a back projection screen.

fMRI data analysis. We used FreeSurfer and FSFAST (http://surfer.nmr.mgh.harvard.edu) to reconstruct cortical surfaces and perform functional data analysis, following procedures detailed in (11). To define face-selective areas we calculated the contrast faces versus all other objects (without scrambled images). Color scale bars show the significance of the contrast maps as negative common logarithm of the probability of error.

The stereotaxic coordinates of the slices were obtained as follows: each brain was rotated to align the anterior and posterior commisures. Then the slice most closely matching AP 0 in Red's Atlas (52) was assigned to AP 0. Sulcal identities in humans (Fig. 2) were determined using the automated sulcus annotation feature of Freesurfer.

A t-test was used to determine the significance of the difference in activation to faces vs. objects, and to bodies vs. other non-face objects (Suppl. Fig. 8c-f), with voxels pooled across all monkeys for each patch.

Macaque data (Figs. 1, 2; Suppl. Figs. 2, 5) represent averages of all runs across multiple sessions. Human data (Figs. 3,5; Suppl. Figs. 4, 5) was computed from a single representative scan session in cases where more than one data session was available.

Acknowledgements: We are grateful to Nicole Schweers, Katrin Thoss, and Ramazani Hakizimana for technical support, and to Guerbet for providing Sinerem. This work was supported by a Sofia Kovalevskaya Award from the Alexander von Humboldt Foundation, by the German Science Foundation (DFG FR1437/3-1), and by the German Ministry of Science (Grant 01GO0506, Bremen Center for Advanced Imaging).

References

1. Darwin C (1872) *The expression of the emotions in man and animals* (John Murray, London).
2. Nelson CA (2001) The development and neural bases of face recognition. *Infant and child development* 10:3-18.
3. Moscovitch M, Winocur G, & Behrmann M (1997) What is special about face recognition? Nineteen experiments on a person with visual object agnosia and dyslexia but normal face recognition. *Journal of Cognitive Neuroscience* 9:555-604.
4. Yin R (1969) Looking at upside-down faces. *J. Exp. Psychol.* 81:141-145.
5. Kanwisher N, McDermott J, & Chun M (1997) The fusiform face area: A module in human extrastriate cortex specialized for face perception. *J. Neurosci.* 17:4302-4311.
6. Pitcher D, Walsh V, Yovel G, & Duchaine B (2007) TMS evidence for the involvement of the right occipital face area in early face processing. *Curr Biol* 17(18):1568-1573.
7. Hoffman EA & Haxby JV (2000) Distinct representations of eye gaze and identity in the distributed human neural system for face perception. *Nat Neurosci* 3(1):80-84.
8. Rotshtein P, Henson RN, Treves A, Driver J, & Dolan RJ (2005) Morphing Marilyn into Maggie dissociates physical and identity face representations in the brain. *Nat Neurosci* 8(1):107-113.
9. Yovel G & Kanwisher N (2005) The neural basis of the behavioral face-inversion effect. *Curr Biol* 15(24):2256-2262.
10. Haxby JV, Hoffman EA, & Gobbini MI (2000) The distributed human neural system for face perception. *Trends Cogn Sci* 4(6):223-233.
11. Tsao DY, Freiwald WA, Knutsen TA, Mandeville JB, & Tootell RB (2003) Faces and objects in macaque cerebral cortex. *Nat Neurosci* 6(9):989-995.
12. Pinsk MA, DeSimone K, Moore T, Gross CG, & Kastner S (2005) Representations of faces and body parts in macaque temporal cortex: a functional MRI study. *Proc Natl Acad Sci U S A* 102(19):6996-7001.
13. Stewart CB & Disotell TR (1998) Primate evolution - in and out of Africa. *Curr Biol* 8(16):R582-588.
14. Hadj-Bouziane F, Bell AH, Knusten TA, Ungerleider LG, & Tootell RB (2008) Perception of emotional expressions is independent of face selectivity in monkey inferior temporal cortex. *Proc Natl Acad Sci U S A* 105(14):5591-5596.
15. Allison T, McCarthy G, Nobre A, Puce A, & Belger A (1994) Human extrastriate visual cortex and the perception of faces, words, numbers, and colors. *Cereb Cortex* 4(5):544-554.

16. Merboldt KD, Finsterbusch J, & Frahm J (2000) Reducing inhomogeneity artifacts in functional MRI of human brain activation-thin sections vs gradient compensation. *J Magn Reson* 145(2):184-191.
17. Devlin JT*, et al.* (2000) Susceptibility-induced loss of signal: comparing PET and fMRI on a semantic task. *Neuroimage* 11(6 Pt 1):589-600.
18. Kriegeskorte N, Formisano E, Sorger B, & Goebel R (2007) Individual faces elicit distinct response patterns in human anterior temporal cortex. *Proc Natl Acad Sci U S A* 104(51):20600-20605.
19. Goense JB, Ku SP, Merkle H, Tolias AS, & Logothetis NK (2008) fMRI of the temporal lobe of the awake monkey at 7 T. *Neuroimage* 39(3):1081-1093.
20. Schwarzlose RF, Baker CI, & Kanwisher N (2005) Separate face and body selectivity on the fusiform gyrus. *J Neurosci* 25(47):11055-11059.
21. Tsao DY, Moeller SM, & Freiwald WA (2008) Patches of face-selective cortex in the macaque frontal lobe. *Nat Neurosci* under review.
22. Avidan G, Hasson U, Malach R, & Behrmann M (2005) Detailed exploration of face-related processing in congenital prosopagnosia: 2. Functional neuroimaging findings. *J Cogn Neurosci* 17(7):1150-1167.
23. Sugiura M*, et al.* (2001) Activation reduction in anterior temporal cortices during repeated recognition of faces of personal acquaintances. *Neuroimage* 13(5):877-890.
24. Peelen MV & Downing PE (2005) Selectivity for the human body in the fusiform gyrus. *J Neurophysiol* 93(1):603-608.
25. Tsao DY, Freiwald WA, Tootell RBH, & Livingstone MS (2006) A cortical region consisting entirely of face-selective cells. *Science* 311:670-674.
26. Logothetis NK, Guggenberger H, Peled S, & Pauls J (1999) Functional imaging of the monkey brain. *Nat Neurosci* 2(6):555-562.
27. Wang G, Tanaka K, & Tanifuji M (1996) Optical imaging of functional organization in the monkey inferotemporal cortex. *Science* 272(5268):1665-1668.
28. Tanaka K (2003) Columns for complex visual object features in the inferotemporal cortex: clustering of cells with similar but slightly different stimulus selectivities. *Cereb Cortex* 13(1):90-99.
29. Von Bonin G & Bailey P (1947) *The Neocortex of Mucoca Mulutru* (Univ. Ill. Press, Urbana, IL).
30. Seltzer B & Pandya DN (1994) Parietal, temporal, and occipital projections to cortex of the superior temporal sulcus in the rhesus monkey: a retrograde tracer study. *J Comp Neurol* 343(3):445-463.
31. Felleman DJ & Van Essen DC (1991) Distributed hierarchical processing in the primate cerebral cortex. *Cereb Cortex* 1(1):1-47.
32. Freiwald WA & Tsao DY (2007) Face representations in three fMRI-identified macaque face patches. *Society for Neuroscience Annual Meeting.*
33. Allison T, Puce A, Spencer DD, & McCarthy G (1999) Electrophysiological studies of human face perception. I: Potentials generated in occipitotemporal cortex by face and non-face stimuli. *Cereb Cortex* 9(5):415-430.
34. Sergent J, Ohta S, & MacDonald B (1992) Functional neuroanatomy of face and object processing. A positron emission tomography study. *Brain* 115 Pt 1:15-36.
35. Behrmann M, Avidan G, Gao F, & Black S (2007) Structural imaging reveals anatomical alterations in inferotemporal cortex in congenital prosopagnosia. *Cereb Cortex* 17(10):2354-2363.
36. Vanduffel W*, et al.* (2001) Visual motion processing investigated using contrast agent-enhanced fMRI in awake behaving monkeys. *Neuron* 32(4):565-577.

37. Striedter GF & Northcutt RG (1991) Biological hierarchies and the concept of homology. *Brain Behav Evol* 38(4-5):177-189.
38. Pritz MB (2005) Comparisons and homology in adult and developing vertebrate central nervous systems. *Brain Behav Evol* 66(4):222-233.
39. Payne BR (1993) Evidence for visual cortical area homologs in cat and macaque. *Cereb Cortex* 3:1-25.
40. Orban GA, Van Essen D, & Vanduffel W (2004) Comparative mapping of higher visual areas in monkeys and humans. *Trends Cogn Sci* 8(7):315-324.
41. Perrett DI, Mistlin AJ, & Chitty AJ (1987) Visual neurones responsive to faces. *Trends in Neurosciences* 10:358-364.
42. Eifuku S, De Souza WC, Tamura R, Nishijo H, & Ono T (2004) Neuronal correlates of face identification in the monkey anterior temporal cortical areas. *J Neurophysiol* 91(1):358-371.
43. De Souza WC, Eifuku S, Tamura R, Nishijo H, & Ono T (2005) Differential characteristics of face neuron responses within the anterior superior temporal sulcus of macaques. *J Neurophysiol* 94(2):1252-1266.
44. Afraz SR, Kiani R, & Esteky H (2006) Microstimulation of inferotemporal cortex influences face categorization. *Nature* 442(7103):692-695.
45. Wegener D, Freiwald WA, & Kreiter AK (2004) The influence of sustained selective attention on stimulus selectivity in macaque visual area MT. *J Neurosci* 24(27):6106-6114.
46. Nelissen K, Luppino G, Vanduffel W, Rizzolatti G, & Orban GA (2005) Observing others: multiple action representation in the frontal lobe. *Science* 310(5746):332-336.
47. Zhao F, Wang P, Hendrich K, Ugurbil K, & Kim SG (2006) Cortical layer-dependent BOLD and CBV responses measured by spin-echo and gradient-echo fMRI: Insights into hemidynamic regulation. *Neuroimage* 30:1149.
48. Leite FP*, et al.* (2002) Repeated fMRI using iron oxide contrast agent in awake, behaving macaques at 3 Tesla. *Neuroimage* 16(2):283-294.
49. Zeng H & Constable RT (2002) Image distortion correction in EPI: comparison of field mapping with point spread function mapping. *Magn Reson Med* 48(1):137-146.
50. Cusack R, Brett M, & Osswald K (2003) An evaluation of the use of magnetic field maps to undistort echo-planar images. *Neuroimage* 18(1):127-142.
51. Brainard DH (1997) The Psychophysics Toolbox. *Spat Vis* 10(4):433-436.
52. Ungerleider LG (*Red's atlas* (Laboratory of Neuropsychology, NIMH Department of Health and Human Services.).

Supplementary material

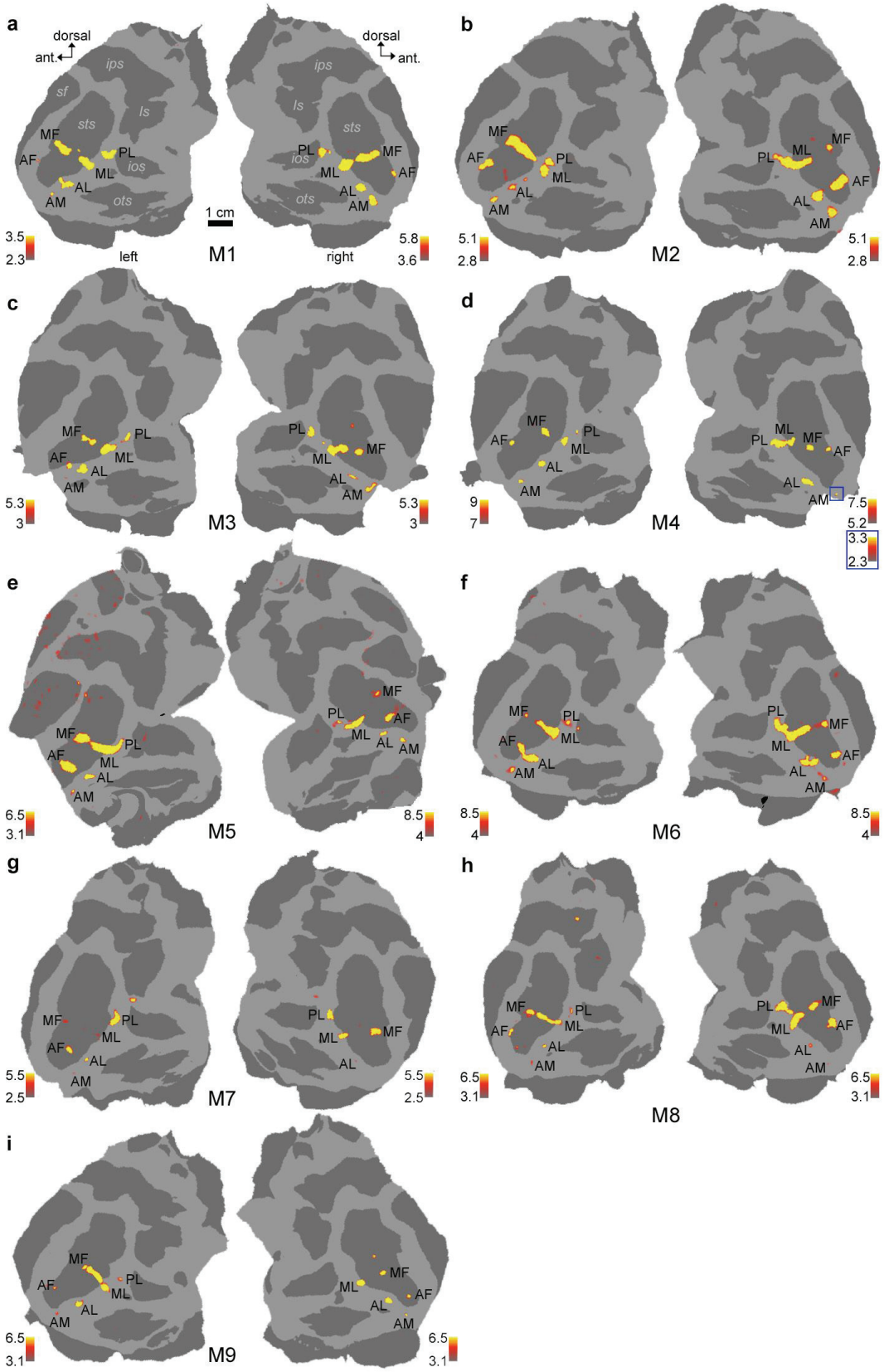

Supplementary Figure 1. Face-selective regions in nine macaque (**a-i**), superimposed on flattened cortical surfaces. Conventions as in Figure 1. The blue inset in (d) shows data from the same experiment at lower threshold.

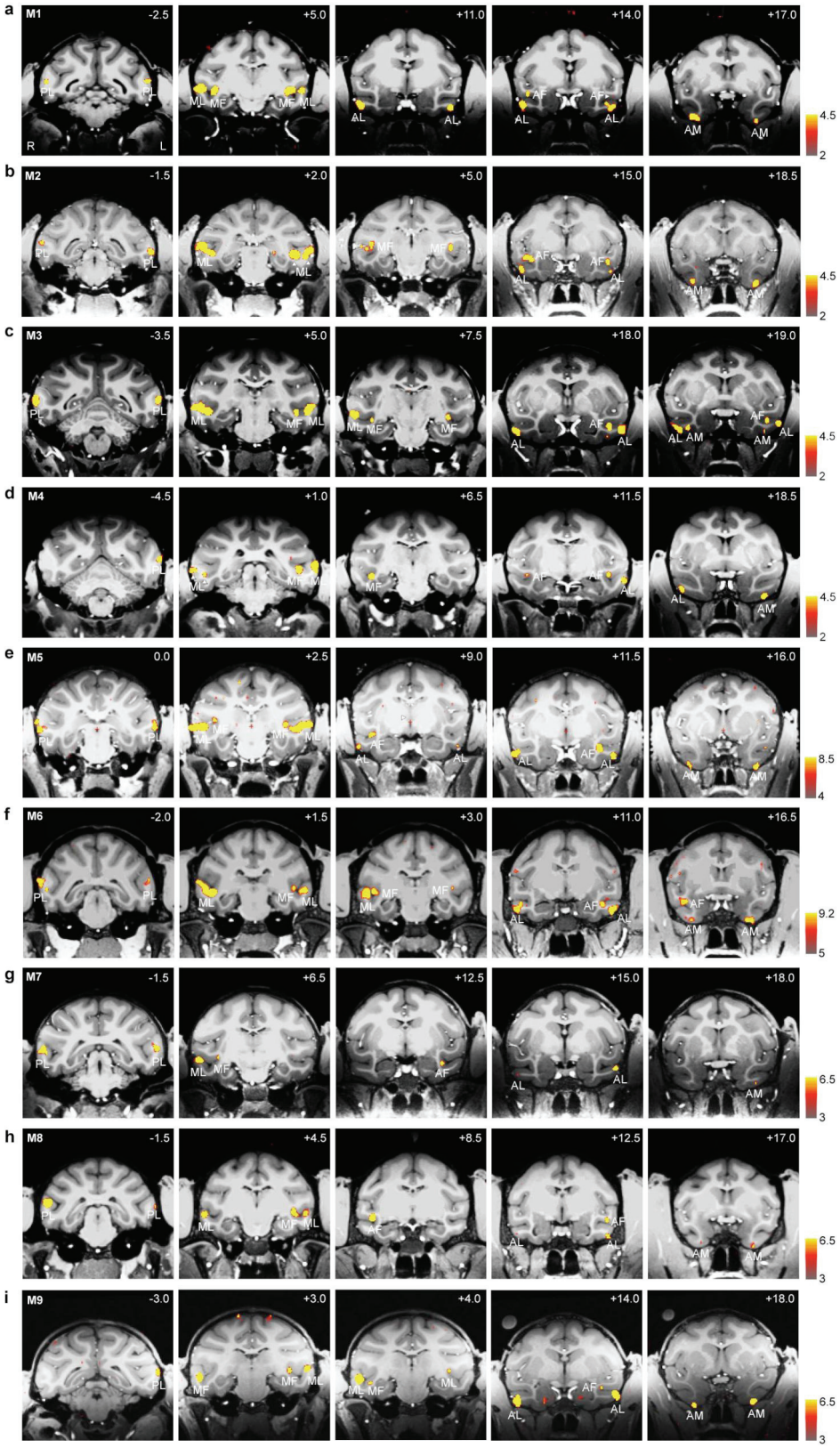

Supplementary Figure 2. Face-selective patches in the left and right temporal lobes of nine macaques (**a-i**), shown on coronal slices (mm relative to the interaural line indicated by numbers at top right corner). Face-patch abbreviations as in Fig. 1.

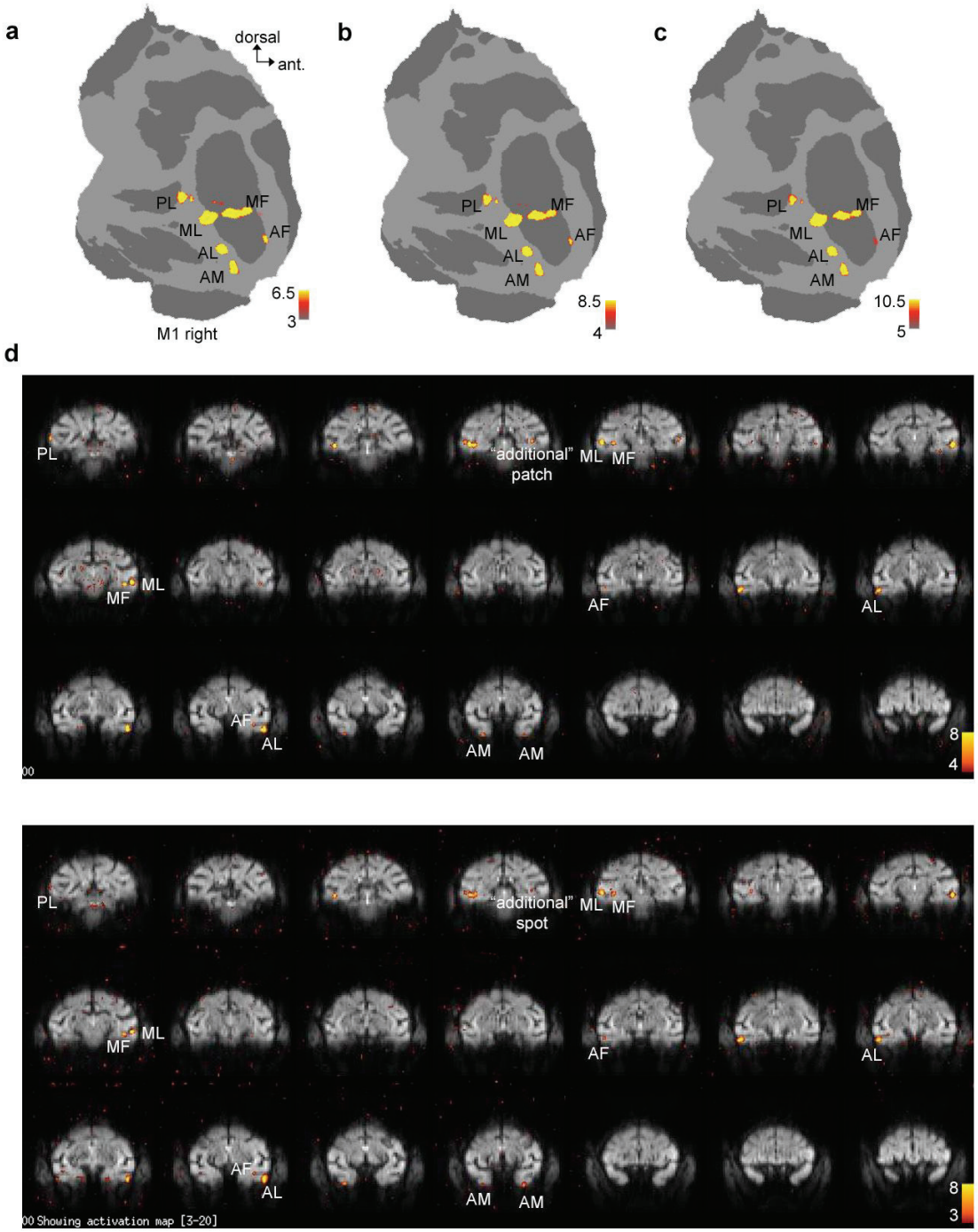

Supplementary Figure 3. Robustness of macaque face-selective regions. **(a-c)** Face-selective regions in the right hemisphere of monkey M1 at three different thresholds; the six face patches were robust across all three thresholds. **(d)** Reproducibility of face patches in monkey M9 across two independent sets of scans. Both the six primary patches as well as an additional patch in the fundus of STS posterior to MF in the right hemisphere were reproducible. Activation overlaid on raw EPI slices.

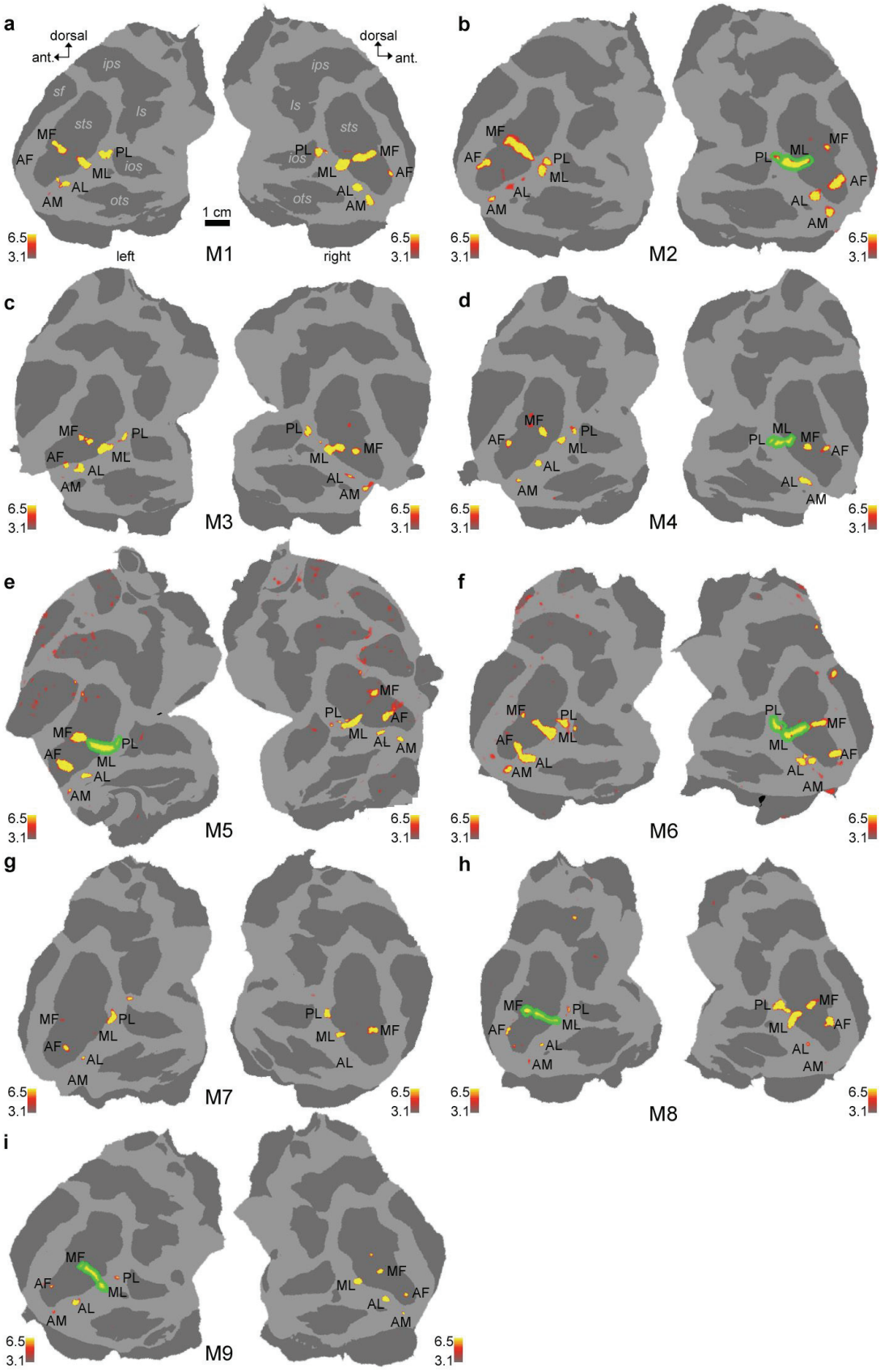

Supplementary Figure 4. Macaque face patches shown at a common threshold of $p = 10^{-3.1}$. Same conventions as Figure 1. The green outlines indicate the subdivision of confluent patches used for the analyses of Suppl. Fig. 5 and Suppl. Table 1.

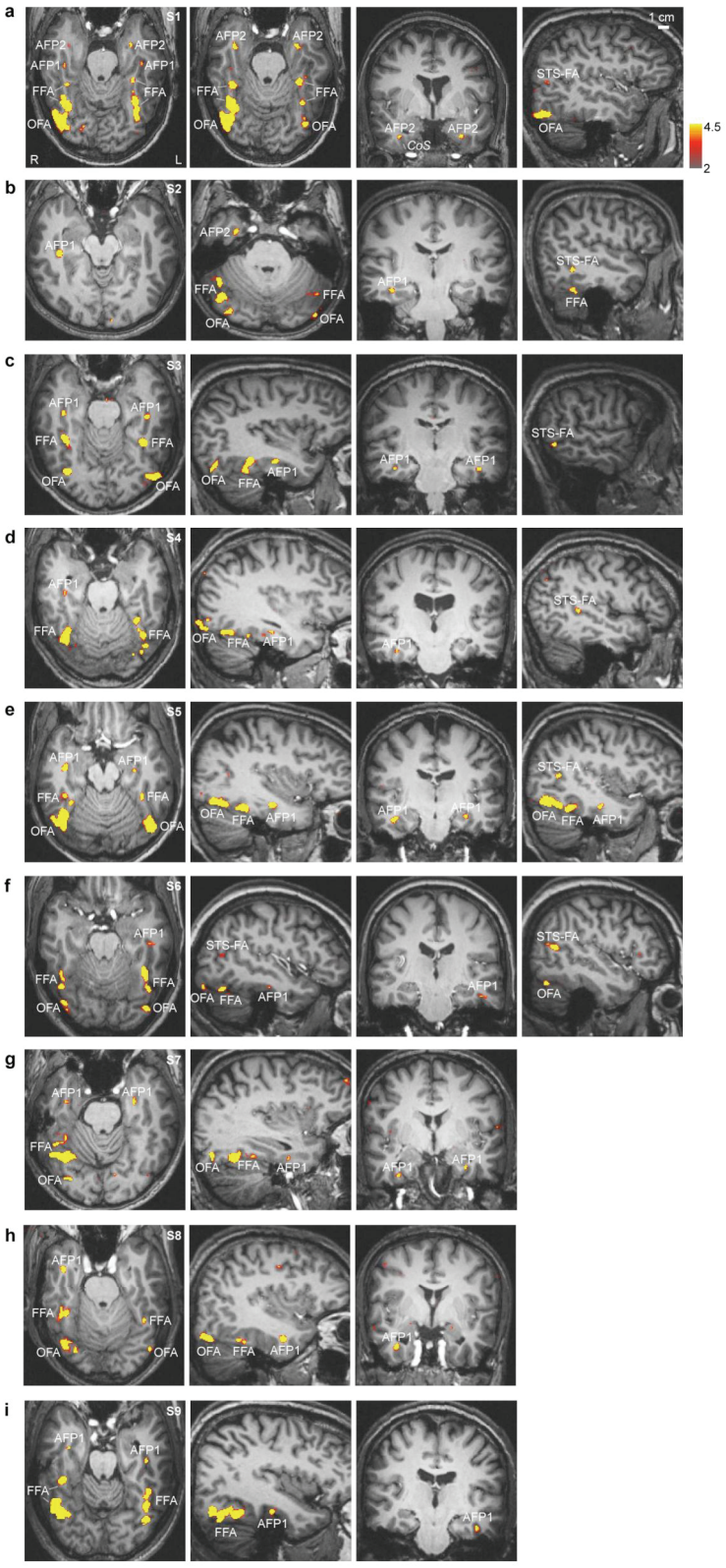

Supplementary Figure 5. Face-selective regions in the left and right temporal lobes of nine human subjects (**a-i**), shown on coronal, horizontal, and sagittal MRI slices. Face-region abbreviations as in Fig. 2. The different apparent size of face-selective regions across subjects is partly due to the choice of slice. Subjects 1 and 2 (**a, b**) had two anterior face patches (AFP1, AFP2), while the remaining subjects (**c-i**) each had one anterior face patch (AFP1).

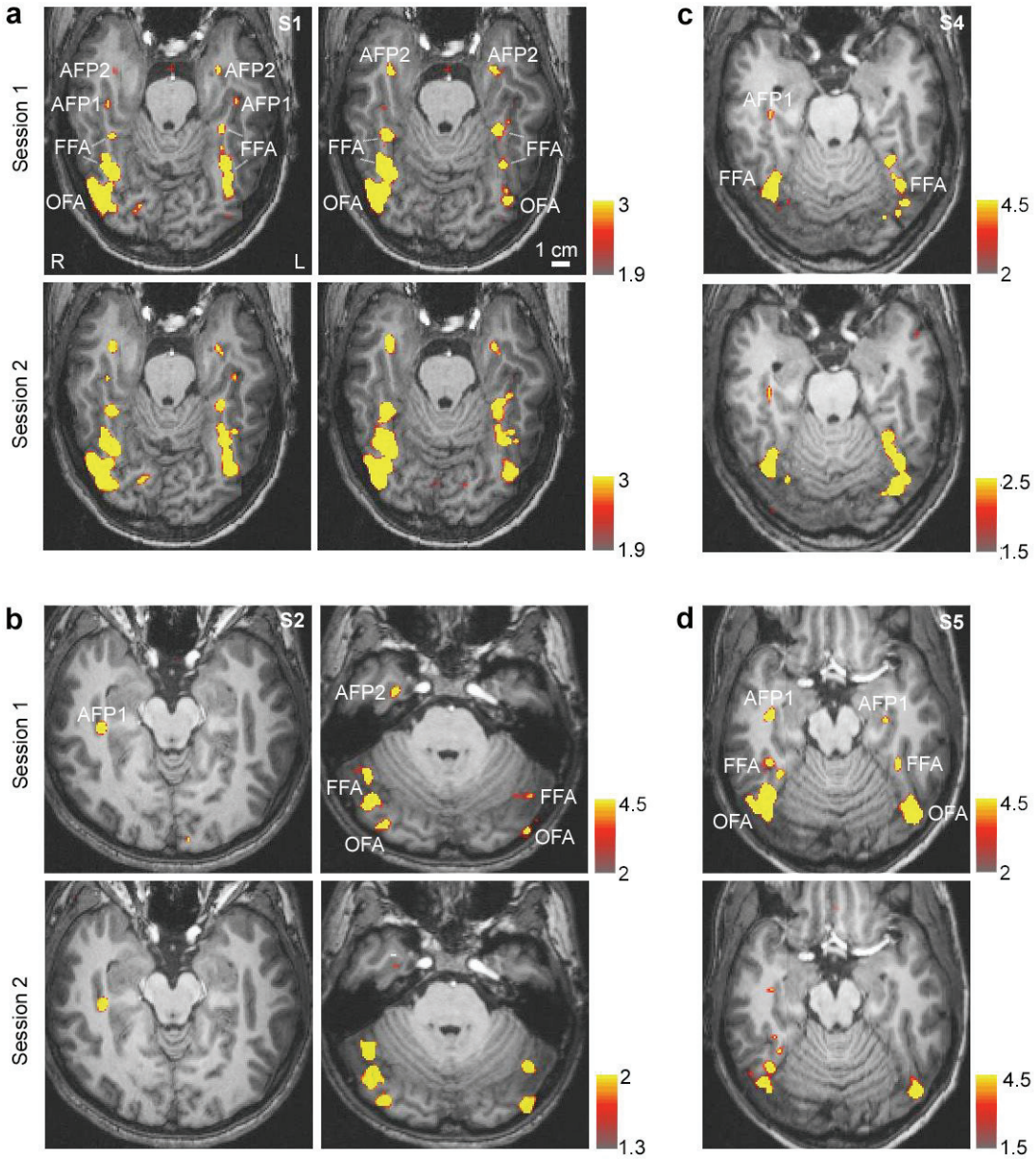

Supplementary Figure 6. Reproducibility of the human face-selective regions. **(a-d)** Face-selective regions obtained in two independent scan sessions for four subjects (S1, S2, S4, S5). Comparison of the top (Session 1) and bottom (Sessions 2) rows for each subject shows that face-selective regions, including AFP1 and AFP2, were reproducible (with the exception of subject S5; right hemisphere AFP1 and FFA were not activated in Session 2 in this subject). Face-region abbreviations as in Fig. 3. The two scan sessions were separated by 98, 7, 7, and 14 days, respectively, for subjects S1, S2, S4, and S5.

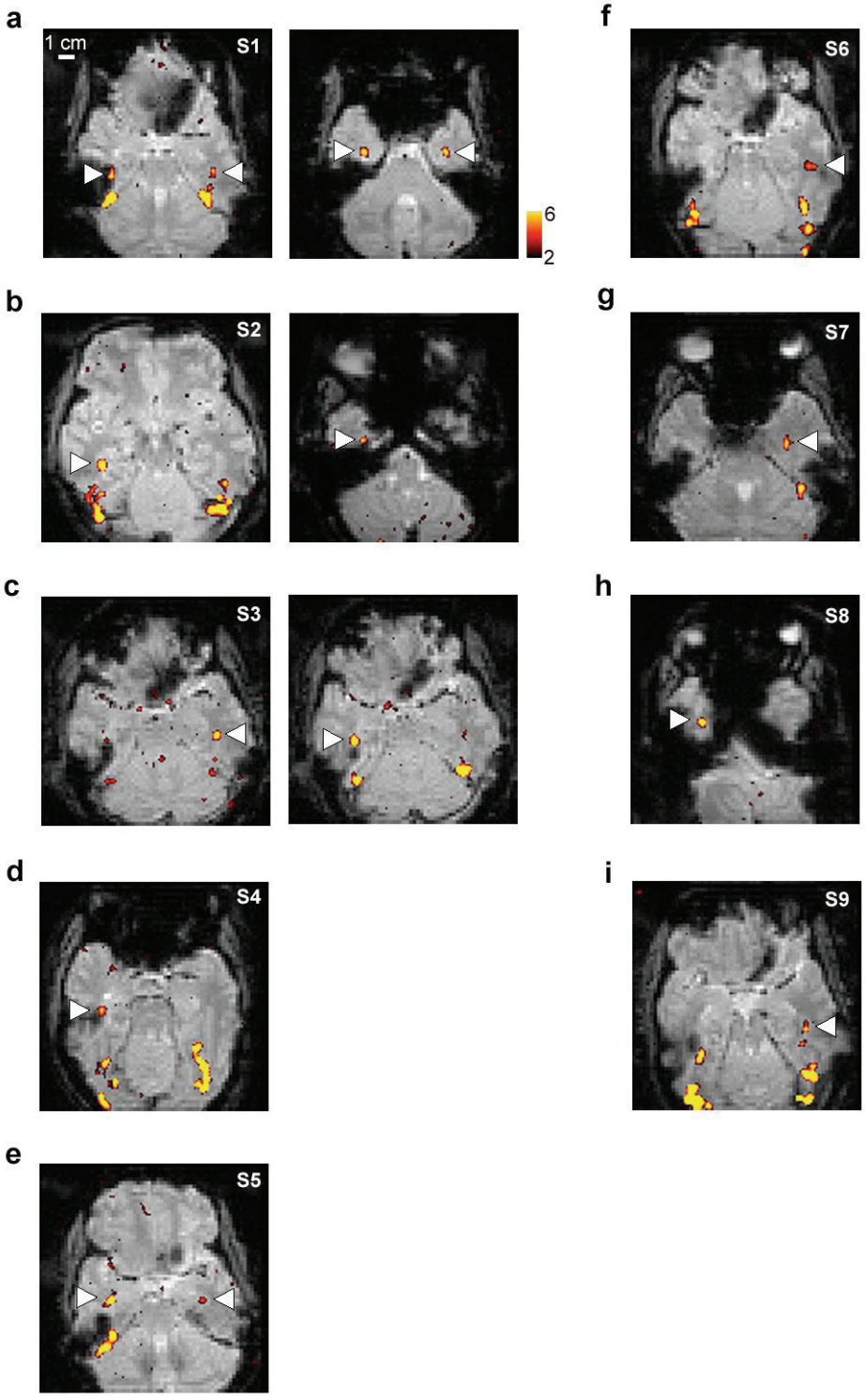

Supplementary Figure 7. Human anterior face regions for nine subjects shown on raw EPI slices (**a-i**). The anterior face patches, indicated by arrows, were often located close to the susceptibility artifact induced by the ear canals. This artifact is stronger on one side of the brain than the other (for readout direction from right to left, as in all our scans, the artifact is stronger on the right).

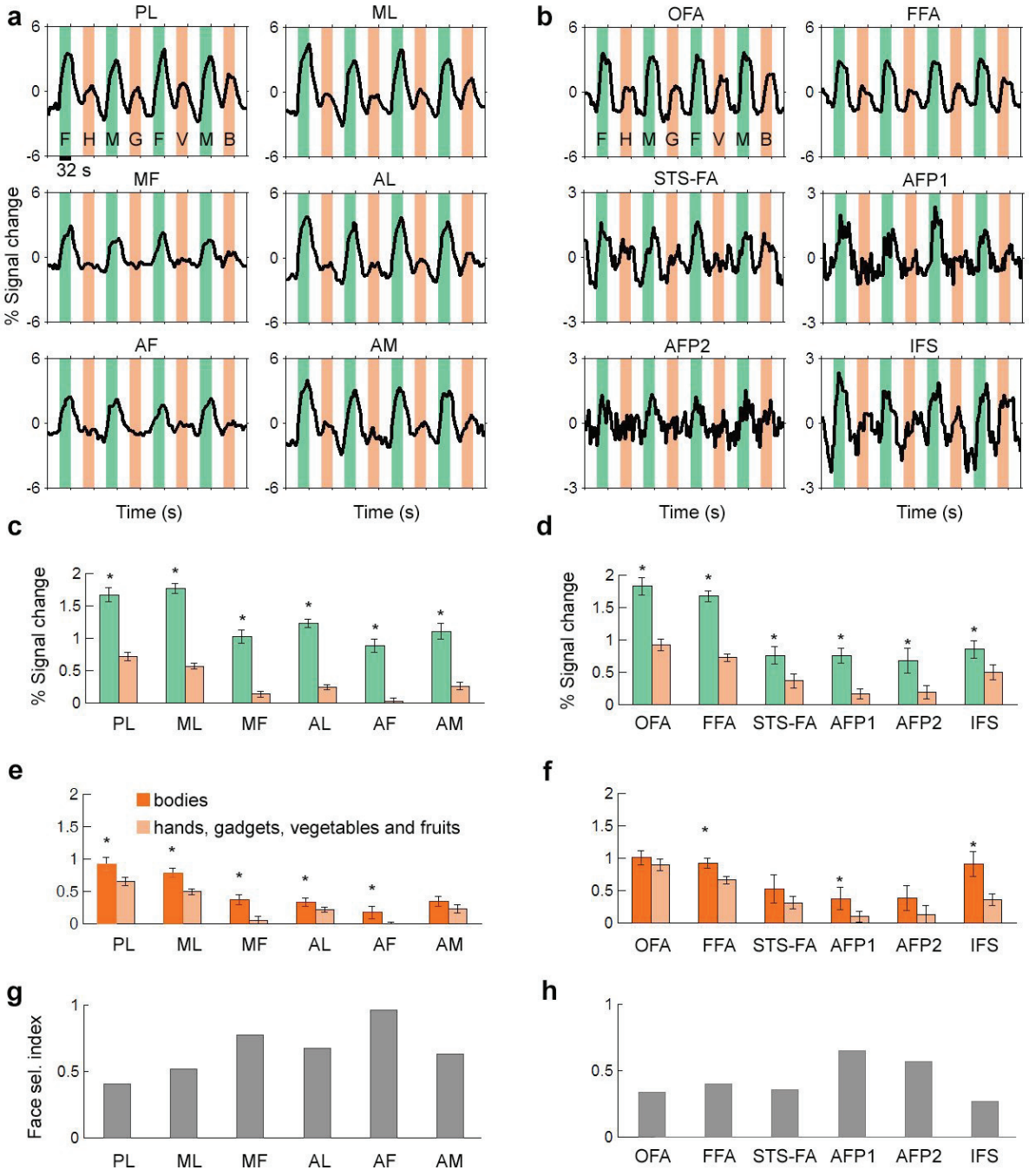

Supplementary Figure 8. Response profiles from macaque and human face patches. **a)** Mean time courses extracted from the macaque face patches, averaged across nine animals (shown in Figs. 1, 2) and across hemispheres. Three different visual stimulation conditions were presented: faces (green epochs; F: human faces, M: monkey faces), non-face objects (orange epochs; H: hands, G: gadgets, V: vegetables and fruits, B: headless bodies), and scrambled versions of the same images (white epochs). Face-region abbreviations are given in Fig. 1 for the macaque and Fig. 3 for the human; IFS, inferior frontal sulcus. In parts (a-d), even runs were used to define ROIs and odd runs to extract time courses and percent signal changes from the ROIs. **b)** Mean time courses extracted from human face areas, averaged across nine human subjects (shown in Figs. 3, 4). Conventions as in (a). For OFA, FFA, STS-

FA, and AFP1, data were averaged across both hemispheres of all nine human subjects that showed an AFP1. For AFP2, data were averaged across the two subjects that showed an AFP2. For IFS, data were averaged across the three subjects that showed a prefrontal face-selective region in the inferior frontal sulcus. **c)** Bar graphs showing % fMRI signal change to faces (green bars) and to non-face objects (orange bars) in the six macaque face regions. Error bars indicate 95% confidence intervals. In (c-f), asterisks mark a significant difference at p <= 0.01. T-tests confirmed that the response to faces was significantly greater than that to non-face objects at $p = 10^{-4}$ in all six macaque face patches. Data averaged across both hemispheres of all nine macaques. **d)** Bar graphs showing % fMRI signal change to faces non-face objects in the six human face regions. T-tests confirmed that the response to faces was significantly greater than that to non-face objects at $p = 10^{-4}$ in all six human face regions. Data were averaged as in (b). **e, f**) Bar graphs showing % fMRI signal change to bodies (dark orange bars) and to three other non-face object categories (hands, gadgets, vegetables and fruits, light orange bars) in the six macaque (e) and six human (f) face patches. The response to bodies was significantly greater than that to the other three non-face categories in all macaque face patches at p = 0.001 except for in AM (p = 0.02). In humans, the p-values for the comparison of bodies to other non-face objects were as follows: 0.1 (OFA), 1e-8 (FFA), 0.07 (STS-FA), 0.003 (AFP1), 0.03 (AFP2), 1.6e-6 (IFS). **g, h)** Bar graphs showing the face selectivity index = $(Response_{face} - Response_{nonface}) / (Response_{face} + Response_{nonface})$ for each macaque and human face-selective area.). In both species, the posterior-most face patch (PL in macaques and OFA in humans) was the least selective.

	PL		ML		MF		AL		AF		AM	
ID	**L**	**R**	**L**	**R**	**L**	**R**	**L**	**R**	**L**	**R**	**L**	**R**
M1	56.6	43.0	50.8	84.0	35.2	37.1	46.9	50.8	5.9	7.8	11.7	46.9
M2	56.6	46.9	68.4	70.3	5.9	3.9	62.5	60.5	17.6	23.4	35.2	21.5
M3	23.4	35.2	74.2	111.3	27.3	15.6	82.0	62.5	19.5	5.9	7.8	21.5
M4	21.5	31.3	56.6	41.0	31.3	15.6	44.9	44.9	15.6	9.8	25.4	3.9
M5	21.5	27.3	107.4	76.2	31.3	15.6	33.2	54.7	29.3	31.3	17.6	21.5
M6	23.6	64.1	74.3	40.5	33.8	54.0	74.3	37.1	23.6	47.3	30.4	23.6
M7	60.5	29.3	13.7	50.8	13.7	23.4	17.6	15.6	15.6	2.0	7.8	5.9
M8	37.1	60.8	43.9	77.6	13.5	13.5	16.9	13.5	10.1	20.3	6.8	6.8
M9	77.6	16.9	141.8	77.6	40.5	23.6	87.8	74.3	20.3	13.5	33.8	23.6
avg	42.1	39.4	70.1	69.9	25.8	22.5	51.8	46.0	17.5	17.9	19.6	19.5
std	21.2	15.7	37.1	22.7	11.9	14.9	26.5	20.7	6.9	14.4	11.7	13.2

Supplementary Table 1. Volumes [mm^3] of the different macaque face patches

Supplementary Table 1. The size (in mm^3) of the six temporal face patches in left and right hemispheres of nine macaques, at p < 0.001.

	STS-FA		FFA		OFA		AFP1		AFP2		IFS	
ID	L	**R**	**L**	**R**	**L**	**R**	**L**	**R**	**L**	**R**	**L**	**R**
S1	150.0	87.5	975.0	875.0	362.5	787.5	37.5	112.5	75.0	62.5	200.0	362.5
S2	0.0	187.5	925.0	1037.5	275.0	275.0	0.0	75.0	0.0	12.5	0.0	0.0
S3	0.0	87.5	375.0	525.0	337.5	300.0	37.5	62.5	0.0	0.0	0.0	0.0

S4	62.5	325.0	475.0	375.0	87.5	250.0	0.0	50.0	0.0	0.0	0.0	0.0
S5	0.0	137.5	262.5	725.0	425.0	687.5	12.5	100.0	0.0	0.0	0.0	0.0
S6	50.0	150.0	375.0	262.5	225.0	237.5	112.5	0.0	0.0	0.0	0.0	0.0
S7	0.0	0.0	762.5	912.5	12.5	112.5	87.5	12.5	0.0	0.0	0.0	0.0
S8	0.0	0.0	175.0	175.0	337.5	312.5	0.0	112.5	0.0	0.0	0.0	125.0
S9	0.0	0.0	562.5	975.0	212.5	100.0	50.0	25.0	0.0	0.0	0.0	0.0
avg	29.2	108.3	543.1	651.4	252.8	340.3	37.5	61.1	8.3	8.3	22.2	54.2
std	51.5	107.2	286.4	325.6	134.2	238.6	40.5	42.6	25.0	20.7	66.7	122.8

Supplementary Table 2. Volumes [mm^3] of the different human face patches

Supplementary Table 2. The size (in mm^3) of the six temporal face regions in left and right hemispheres of nine human subjects, at $p < 0.001$.

ID	sessions	runs	n_slices	resolution	slice thickness
M1	3	35	28	1.25 x 1.25	1.25
M2	2	15	28	1.25 x 1.25	1.25
M3	3	18	28	1.25 x 1.25	1.25
M4	3	23	28	1.25 x 1.25	1.25
M5	3	19	28	1.25 x 1.25	1.25
M6	1	12	28	1.5 x 1.5	1.50
M7	3	44	28	1.25 x 1.25	1.25
M8	1	12	42	1.5 x 1.5	1.50
M9	3	29	28	1.5 x 1.5	1.50
M10	14	99	28	1.25 x 1.25	1.25
S1	3	38	44	2.5 x 2.5	2.00
S2	2	21	44	2.5 x 2.5	2.00
S3	1	10	44	2.5 x 2.5	2.00
S4	2	21	44	2.5 x 2.5	2.00
S5	2	21	44	2.5 x 2.5	2.00
S6	1	10	44	2.5 x 2.5	2.00
S7	2	18	44	2.5 x 2.5	2.00
S8	2	25	44	2.5 x 2.5	2.00
S9	1	10	44	2.5 x 2.5	2.00
S10	2	26	44	2.5 x 2.5	2.00
S11	1	11	44	2.5 x 2.5	2.00
S12	2	25	44	2.5 x 2.5	2.00
S13	2	27	44	2.5 x 2.5	2.00

Supplementary Table 3. Summary of Experiments

Supplementary Table 3. Summary of experiments. The table lists the number of independent scan sessions, the number of runs within each session, and the scan parameters for each session (number of slices, in-plane resolution, and slice thickness) for the 10 macaque subjects and 13 human subjects used in this study.

Patches of face-selective cortex in the macaque frontal lobe

(Nature Neuroscience 11: 877-879)

Doris Y. Tsao, Nicole Schweers, Sebastian Moeller, Winrich A. Freiwald

Institute for Brain Research and Center for Advanced Imaging, University of Bremen, P.O.B. 330440, D-28334 Bremen, FR Germany

In primates, specialized occipital-temporal face areas support the visual analysis of faces, but it is unclear whether similarly specialized areas exist in the frontal lobe. Here, using fMRI in alert macaques, we identified three discrete regions of highly face-selective cortex in ventral prefrontal cortex, one of which was strongly lateralized to the right hemisphere. These prefrontal face patches may constitute dedicated modules for retrieving and responding to facial information.

Faces are perhaps the most behaviorally significant class of visual forms processed by the primate brain. The perception of a face reveals information about identity, age, gender, mood, gaze direction, and intention, and each of these pieces of information can powerfully influence behavior. Faces activate a wide network of brain areas including the inferior occipital gyrus, fusiform gyrus, superior temporal sulcus, hippocampus, amygdala, inferior frontal gyrus, and orbitofrontal cortex [1-5]. A subset of these areas, all within the ventral pathway dedicated to visual form analysis, has been found to be *face selective* [3,4,6]: these areas respond significantly more to faces than to various non-face object categories. In one such face area, the macaque middle face patch, almost all visually responsive cells are face selective [7].

Since face perception has such a powerful and unique influence on behavior, we wondered whether face-selective modules exist outside the ventral visual pathway for translating face information into behavior. Clusters of face-selective cells have previously been found in prefrontal cortex, in the inferior prefrontal convexity [8] and in orbitofrontal cortex [9], but the existence of face areas in prefrontal cortex could not be inferred from these studies due to the low penetration density and the small number of face cells recorded.

We scanned four macaque monkeys using a slice prescription that included all of the frontal lobe. To our knowledge, this is the first attempt to search for face-selective areas in prefrontal cortex of any primate without active task requirements. Previous fMRI studies of face processing either did not systematically cover the frontal lobe [4,5,7], did not test for face selectivity [1,2,5], or required performance of cognitive tasks on faces and objects [10].

Monkeys were scanned while awake and passively fixating. Stimuli consisted of human faces, macaque faces, hands, gadgets, fruits and vegetables, headless bodies, and scrambled patterns, presented in separate blocks. Comparing activation to faces with activation to non-face objects revealed three discrete face-selective patches in prefrontal cortex.

In all four monkeys, we observed a bilateral pair of face patches within the lateral orbital sulcus (Fig. 1a, left column). We term this area PO for “prefrontal orbital”. Fig. 1c shows coronal, horizontal, and sagittal slices through the right hemisphere PO of monkey M4.

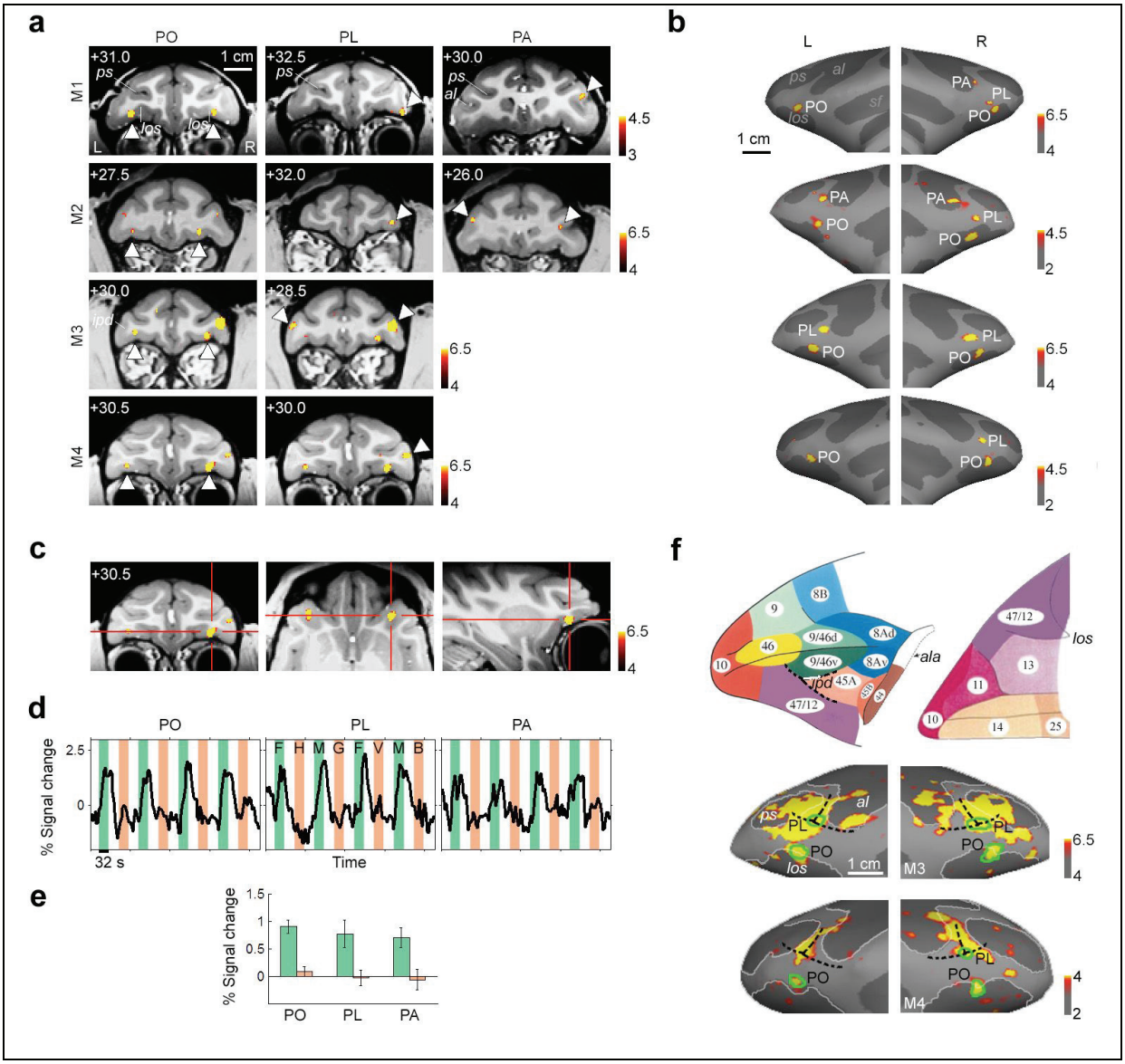

Fig. 1. Face-selective patches in prefrontal cortex of four macaques. a) Face-selective patches from four macaques superimposed on coronal anatomical slices. Activated regions showed a significantly greater response to faces than to four categories of non-face objects. The first column shows the orbital face patch (PO), the second column shows the ventrolateral face patch (PL), and the third column shows the face patch at the ventral tip of the anterior bank of the inferior arcuate sulcus (PA); patches are indicated by white arrows. The AP position of each slice is indicated at the top left corner of each slice (in mm relative to the interaural canal). Sulcal labels for (a) and (b): *ps:* principle sulcus, *al:* lower ramus of arcuate sulcus, *sf:* Sylvan fissure, *los:* lateral orbital sulcus, *ipd:* infraprincipal dimple. b) Prefrontal face patches overlaid on reconstructed inflated left and right frontal lobes of the four monkeys. Order of monkeys from top to bottom same as in (a). c) Coronal, horizontal, and sagittal slices through the right hemisphere PO of monkey M4. d) Mean time courses extracted from the face patches shown in (a), averaged across monkeys and across hemispheres for patches that were bilateral. To generate the data shown here and in (e) below, even runs were used to define ROI's for the face patches in each monkey, and odd runs were used to extract the time courses and activation values. Three different visual stimulation

conditions were presented: faces (light grey epochs; F: human faces, M: monkey faces), non-face objects (dark grey epochs; H: hands, G: gadgets, V: vegetables and fruits, B: headless bodies), and scrambled versions of the same images (white epochs). e) Bar graph showing % fMRI signal change to faces (light grey bars) and to non-face objects (dark grey bars) in the three prefrontal face patches. Error bars indicate 95% confidence intervals. f) Top: atlas of macaque prefrontal cortex, adapted from Petrides and Pandya [15]. Lateral view on the left, ventral view on the right. The junction between areas 9/46v, 45A, and 47/12 coincides with the anterior end of the infraprincipal dimple (*ipd*). *ala*: anterior bank of lower ramus of arcuate sulcus. Bottom: Activation to faces and non-face objects (hands, gadgets, vegetables and fruits, and bodies) versus grid-scrambled patterns. The prefrontal face patches are indicated by green outlines. In both of these monkeys (M3 and M4), the infraprinciple dimple could be seen in the anatomical MR images, and PL was located partially within this dimple. See Supplementary Text 1 for discussion of area assignments for the three prefrontal face patches.

We observed a second face-selective patch of cortex on the inferior convexity in all four monkeys (Fig. 1a, middle column). We term this area PL for "prefrontal lateral". A striking feature of PL common to all four monkeys was a strong bias for the right hemisphere. In three animals (M1, M2, M4), PL was found only in the right hemisphere; in the fourth (M3), PL was 2.5 times larger in the right hemisphere than in the left (Supplementary Table 1 gives the size of the face patches in each monkey and hemisphere). PL was located at the base of the inferior convexity in monkeys M1 and M2, and more dorsally, within the fundus of the infraprincipal dimple, in monkeys M3 and M4. This difference in location across animals raises the possibility that PL may actually constitute two functionally distinct regions that are expressed exclusively of each other.

In two animals (M1 and M2), we found a third prefrontal face patch more posteriorly, within the anterior bank of the lower ramus of the arcuate sulcus (Fig. 1a, right column). We term this face-selective region PA for "prefrontal arcuate".

The match between the locations of PL and PO and the previously reported locations of face cell clusters is striking. Scalaidhe et al. [8] found the largest cluster of face cells in a region within the infraprincipal dimple, precisely where PL was located in monkeys M3 and M4. Rolls et al. [9] reported a concentration of face cells within the lateral orbitofrontal sulcus, matching the location of PO in all four monkeys. Moreover, the fact that we were able to find these prefrontal face patches in passively fixating animals is consistent with the finding that most prefrontal face cells respond to faces under passive fixation conditions [8].

In all four monkeys, the existence and location of the face patches was robust across independent scan sessions (as an example, Supplementary Fig. 1a shows the reproducibility of both PO and PL in monkey M4 across two sessions). The overall layout of the three prefrontal face patches was similar across animals (Fig. 1b). Mean time courses (Fig. 1d) and percent signal changes (Fig. 1e) to faces and non-face objects confirm the strong face selectivity of each of the three patches.

Areas PO, PL, and PA represent a small subset of the larger object-responsive territory in macaque prefrontal cortex. Fig. 1f shows the activation to faces and non-face objects versus scrambled patterns in two monkeys (M3 and M4). This activation pattern is largely consistent with previous monkey fMRI studies describing activation to objects versus scrambled patterns in a large swath of ventral prefrontal cortex [3,11]. However, activation in orbitofrontal cortex was not reported in a previous monkey fMRI study employing images consisting only of non-face objects [11].

Orbitofrontal cortex has been implicated in the control of mood, processing of emotions, and social reinforcement [12], raising the possibility that it may be selective for facial expressions. Thus in a second experiment, we measured responses to neutral and expressive macaque faces (Fig. 2a) and to non-face objects. All three patches responded more strongly to expressive than to neutral faces (Fig. 2b, c). The difference was highly significant in PO ($p = 1.9*10^{-7}$), but not PL ($p = 0.10$) or PA ($p = 0.21$). In monkey M1, left and right PO were the only two brain regions activated by the contrast (expressive > neutral) at a threshold of $p = 0.001$ (Fig. 2d). Temporal lobe face patches, by comparison, were only weakly modulated by facial expression (Supplementary Fig. 2a-c). Thus the increased activity to expressive faces in PO and PA was likely not caused by a general increase in attention or arousal; rather, these areas appear to play a specific role in responding to the emotional content of faces.

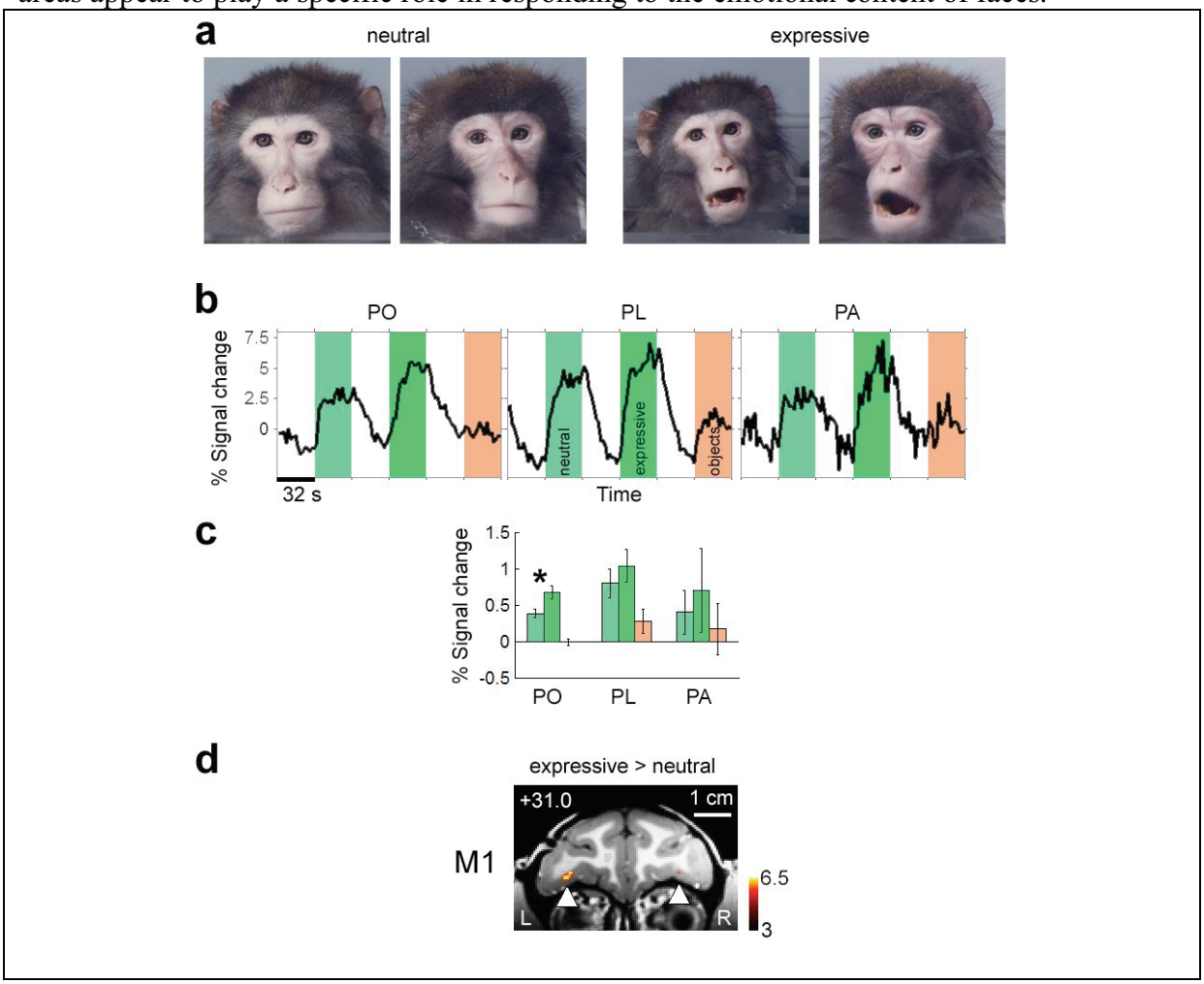

Fig. 2. Sensitivity of prefrontal and temporal face patches to facial expression. a) Example images of neutral and expressive macaque faces used to test selectivity of prefrontal face patches for expressive versus neutral faces. b) Average time course from PO, PL, and PA to neutral faces (medium grey), expressive faces (light grey), and non-face objects (dark grey). Data averaged across three monkeys (M1, M3, M4). c) Bar graph showing % fMRI signal change to neutral faces (medium grey), expressive faces (light grey), and non-face objects (dark grey). Data averaged across three monkeys (M1, M3, M4). Error bars indicate 95% confidence intervals. d) Coronal slice showing activation to expressive versus neutral faces in monkey M1. PO was the only region activated by this contrast at p = 0.001.

Goldman-Rakic and colleagues found face cells with selective delay activity in working memory tasks [8] near the infraprinciple dimple, where PL was located in two animals. Thus PL may contribute to face-related working memory, attention to faces, face categorization, and perhaps even social reasoning about faces. The most posterior prefrontal face patch, PA, lies at the border between areas 44 and 45B. Area 44 is involved in fine control of facial musculature and may be the macaque homolog of Broca's area [13]. The location of PA near area 44 may facilitate interaction between face perception and control of facial musculature, e.g., in mimicking behavior. PA is also located near area 45B, which is involved in more general cognitive operations including active memory retrieval and set shifting [14].

The selective fMRI response to faces in PO, PL, and PA could have been due to specific visual features in faces, to specific internal states elicited by faces (e.g., emotional arousal), or to specific physical behaviors triggered by faces (e.g., lip smacking or eye movements). With the possible exception of PA, it is unlikely that activation of the macaque face patches was due to face-induced physical behaviors, since we did not observe face-selective activations in somatomotor cortex or frontal eye fields. Furthermore, analysis of eye movement traces in the four monkeys did not reveal a significant difference across stimulus conditions (scrambled, faces, objects) for any of five different eye movement parameters analyzed (Supplementary Fig. 3), ruling out differential eye movements as a possible source for the face-selective activation.

Previous work in humans on the material specificity of prefrontal cortex during memory tasks suggests a broad specialization for verbalizable content (e.g., words) in the left and for non-verbalizable content (e.g., faces and abstract patterns) in the right posterior inferior frontal cortex [10]. The strong right lateralization of PL raises the possibility that it may constitute the macaque homolog of the region in human right prefrontal cortex activated during remembrance of faces. It is then tempting to ask what is being coded by the corresponding left hemisphere region in the macaque -- the answer may reveal a precursor of language.

The variety of cognitive tasks that involve faces is endless. However, the visual component of each of these tasks may only require communication between prefrontal cortex and face-selective areas of inferotemporal cortex. Therefore, PO, PL, and PA could receive visual inputs primarily from face modules in IT cortex, and at the same time receive diverse inputs from other sensory sources, and send outputs to a widespread region of cortex, as necessary for effecting a rich repertoire of face-related behavioral responses. Our finding of a regional specialization for faces supports the notion put forward by Goldman-Rakic that information domain is a powerful organizing principle in prefrontal cortex [8].

Acknowledgements: We are grateful to Katrin Thoss and Ramazani Hakizimana for technical support, to Michael Borisov for help with data analysis, to Hidehiko Komatsu for providing pictures of macaque faces, and to Guerbet for providing Sinerem. This work was supported by a Sofia Kovalevskaya Award from the Alexander von Humboldt Foundation, by the German Science Foundation (DFG FR1437/3-1), and by the German Ministry of Science (Grant 01GO0506, Bremen Center for Advanced Imaging).

References

1. Haxby, J.V., Hoffman, E.A. & Gobbini, M.I. The distributed human neural system for face perception. *Trends Cogn Sci* **4**, 223-233 (2000).
2. Ishai, A., Schmidt, C.F. & Boesiger, P. Face perception is mediated by a distributed cortical network. *Brain Res Bull* **67**, 87-93 (2005).

3. Tsao, D.Y., Freiwald, W.A., Knutsen, T.A., Mandeville, J.B. & Tootell, R.B. Faces and objects in macaque cerebral cortex. *Nat Neurosci* **6**, 989-95 (2003).
4. Pinsk, M.A., DeSimone, K., Moore, T., Gross, C.G. & Kastner, S. Representations of faces and body parts in macaque temporal cortex: a functional MRI study. *Proc Natl Acad Sci U S A* **102**, 6996-7001 (2005).
5. Hoffman, K.L., Gothard, K.M., Schmid, M.C. & Logothetis, N.K. Facial-expression and gaze-selective responses in the monkey amygdala. *Curr Biol* **17**, 766-72 (2007).
6. Kanwisher, N., McDermott, J. & Chun, M. The fusiform face area: A module in human extrastriate cortex specialized for face perception. *Journal of Neuroscience* **17**, 4302-4311 (1997).
7. Tsao, D.Y., Freiwald, W.A., Tootell, R.B.H. & Livingstone, M.S. A cortical region consisting entirely of face-selective cells. *Science* **311**, 670-674 (2006).
8. Scalaidhe, S.P., Wilson, F.A. & Goldman-Rakic, P.S. Face-selective neurons during passive viewing and working memory performance of rhesus monkeys: evidence for intrinsic specialization of neuronal coding. *Cereb Cortex* **9**, 459-75 (1999).
9. Rolls, E.T., Critchley, H.D., Browning, A.S. & Inoue, K. Face-selective and auditory neurons in the primate orbitofrontal cortex. *Exp Brain Res* **170**, 74-87 (2006).
10. Kelley, W.M. et al. Hemispheric specialization in human dorsal frontal cortex and medial temporal lobe for verbal and nonverbal memory encoding. *Neuron* **20**, 927-36 (1998).
11. Denys, K. et al. Visual activation in prefrontal cortex is stronger in monkeys than in humans. *J Cogn Neurosci* **16**, 1505-16 (2004).
12. Rolls, E.T. *The brain and emotion*, (Oxford University Press, Oxford, 1999).
13. Petrides, M., Cadoret, G. & Mackey, S. Orofacial somatomotor responses in the macaque monkey homologue of Broca's area. *Nature* **435**, 1235-8 (2005).
14. Nakahara, K., Hayashi, T., Konishi, S. & Miyashita, Y. Functional MRI of macaque monkeys performing a cognitive set-shifting task. *Science* **295**, 1532-6 (2002).
15. Petrides, M. & Pandya, D.N. Comparative cytoarchitectonic analysis of the human and the macaque ventrolateral prefrontal cortex and corticocortical connection patterns in the monkey. *Eur J Neurosci* **16**, 291-310 (2001).

Supplementary material

Surgery. The implantation of the MR-compatible headpost (Ultem, General Electric Plastics) followed standard anesthetic, aseptic, and postoperative treatment protocols which have been described in detail elsewhere [1]. MR-compatible ceramic screws (Thomas Recording) and acrylic cement (Grip Cement, Caulk, Dentsply International) were used to secure the headpost to the skull.

Monkey fMRI. All scanning was performed in a 3T MR scanner (Allegra, Siemens). For each monkey we acquired 10 anatomical volumes at high spatial resolution (0.5 mm isometric). We used a T1 weighted inversion recovery sequence (MPRAGE). These scans were performed under anesthesia (Ketamin / Medetomidine, 8 mg/kg / 0.04 mg/kg) to reduce motion artifacts.

For all functional imaging, a contrast agent, ferumoxtran-10 (Sinerem, Guerbet, France; concentration: 21 mg Fe/ml in saline; dosage: 8 mg Fe/kg) was injected into the femoral vein prior to each scan session. Sinerem is the same compound as MION, produced under a different name [2]. Sinerem/MION increases signal-to-noise and gives finer spatial localization than BOLD [3-5]. Sinerem results in a signal reduction at activated voxels; for all functional data we inverted the signal to facilitate comparison with BOLD data.

All functional data was acquired in coronal slices. For data presented in Fig. 1a (M1, M2, and M4), we used a multi echo sequence (EPI, TR 4 s, TE 30 or 25 ms, 64 by 64 matrix). In combination with a concomitantly acquired fieldmap, this allowed high fidelity reconstruction by undistorting most of the B0-field inhomogeneities [6,7]. For data presented in Fig. 1a (M3) we used a standard single-shot EPI sequence (TR 2 s, TE 24 s, 64 by 64 matrix); this sequence generally produces larger activations because it does not correct for motion-induced distortions (the signal dropoff in the fieldmap due to the large muscles of monkey M3 prevented us from using the multi-echo sequence with undistortion as for the other three monkeys).

The data for each animal shown in Fig. 1 was acquired over two scan sessions (M1: 24 runs in 2 sessions, M2: 23 runs in 2 sessions, M3: 17 runs in 2 sessions, M4: 27 runs in 2 sessions). In these localizer experiments we acquired 136 volumes per run (28 slices, spatial resolution 1.25 mm isometric). The slice volume was adjusted for each monkey to cover the entire frontal lobe. The data for Fig. 2 was acquired over one scan session in monkeys M1 and M4 (M1: 12 runs, M4: 13 runs), and two scan sessions in monkey M3 (24 runs).

Visual stimulation. The face patch localizer stimulus followed a block design. Blocks lasted 32 seconds, and included the following image categories: human faces (F), monkey faces (M), human hands (H), gadgets (G), fruits and vegetables (V), and headless bodies (B). There were 16 different images in each category. Each image block was preceded by a block consisting of scrambled versions of the same images (S), resulting in the following sequence: S F S H S M S G S F S V S M S B R (the final block consisted of a gray random dot pattern). Each image subtended 12° visual angle (10.4 cm diameter at 49 cm distance), and was presented for 0.5 s.

The expression stimulus also followed a block design. Blocks lasted 32 seconds, and included the following image categories: neutral macaque faces (N), expressive macaque faces (E), and mixed non-face objects (O). There were 16 images in the two face categories, and 32 images in the object category. Each image block was preceded by a block of mean gray (G), resulting in the following sequence: G N G E G O G N G E G O G.

Visual stimulation was performed using custom code utilizing the Psychophysics Toolbox [8]. The stimuli were displayed at 60 Hz with a resolution of 1280 by 1024 pixels, using a video beamer (JVC DLA -G15E) and a back projection screen.

fMRI data analysis. We used FreeSurfer and FSFAST (http://surfer.nmr.mgh.harvard.edu) to reconstruct cortical surfaces and perform functional data analysis, following procedures detailed in [9]. To define face-selective areas we calculated the contrast faces versus all other objects (without scrambled images). Color scale bars show the significance of the contrast maps as negative common logarithm of the probability of error.

The stereotaxic coordinates of the slices were obtained as follows: each brain was rotated to align the anterior and posterior commissures. Then the slice most closely matching AP 0 in Red's Atlas [10] was assigned to AP 0.

A t-test was used to determine the significance of the difference in activation to expressive vs. neutral faces (Fig. 2c, Supplementary Fig. 2c), with voxels pooled across all monkeys for each patch. A two-way ANOVA with monkey identity and visual stimulus condition as factors was used to determine the significance of differences in the five eye movements parameters (horizontal eye position standard deviation, vertical eye position standard deviation, mean saccade frequency, mean saccade amplitude, and mean saccade duration) across visual stimulus conditions (Supplementary Fig. 3b).

Eye movement analysis. Blinks were removed from the eye trace prior to analysis. Saccades were detected by the methods described in [11]. The threshold for a saccade velocity was set to 20°/s to account for the reduced sampling frequency and increased noise level of our eye measurements compared to [11]. Saccade amplitude was computed by subtracting the end saccade position from initial saccade position. It was assumed that between saccades there was a linear slow drift. Supplementary Fig. 3b shows an example raw eye movement trace together with the fitted estimator, a straight line which only has breaks at saccade start and endpoints. Plots of peak velocity v versus movement amplitude d in log-log scale fell along the "main sequence" reported for primates [11-13] (Supplementary Fig. 3c, left column), providing evidence that our saccade detection algorithm worked.

Supplementary Text 1: Assigning areas to prefrontal face patches

Macaque prefrontal cortex has been parceled into multiple subregions based on cytoarchitectonic and connectional data. Fig. 1f (top) shows a map of these areas, adapted from Petrides [14]. On the orbital surface, area 47/12 includes all of the cortex within the lateral orbital sulcus. PO lies in the lateral orbital sulcus, within area 47/12. PL was located close to the infraprincipal dimple. The anterior end of the infraprinciple dimple provides a useful landmark for the junction between areas 9/46v, 47/12, and 45A; PL could thus contain parts of any of these three areas. PA was located in the rostral bank of the inferior ramus of the arcuate sulcus, close to the border between areas 44 and 45B.

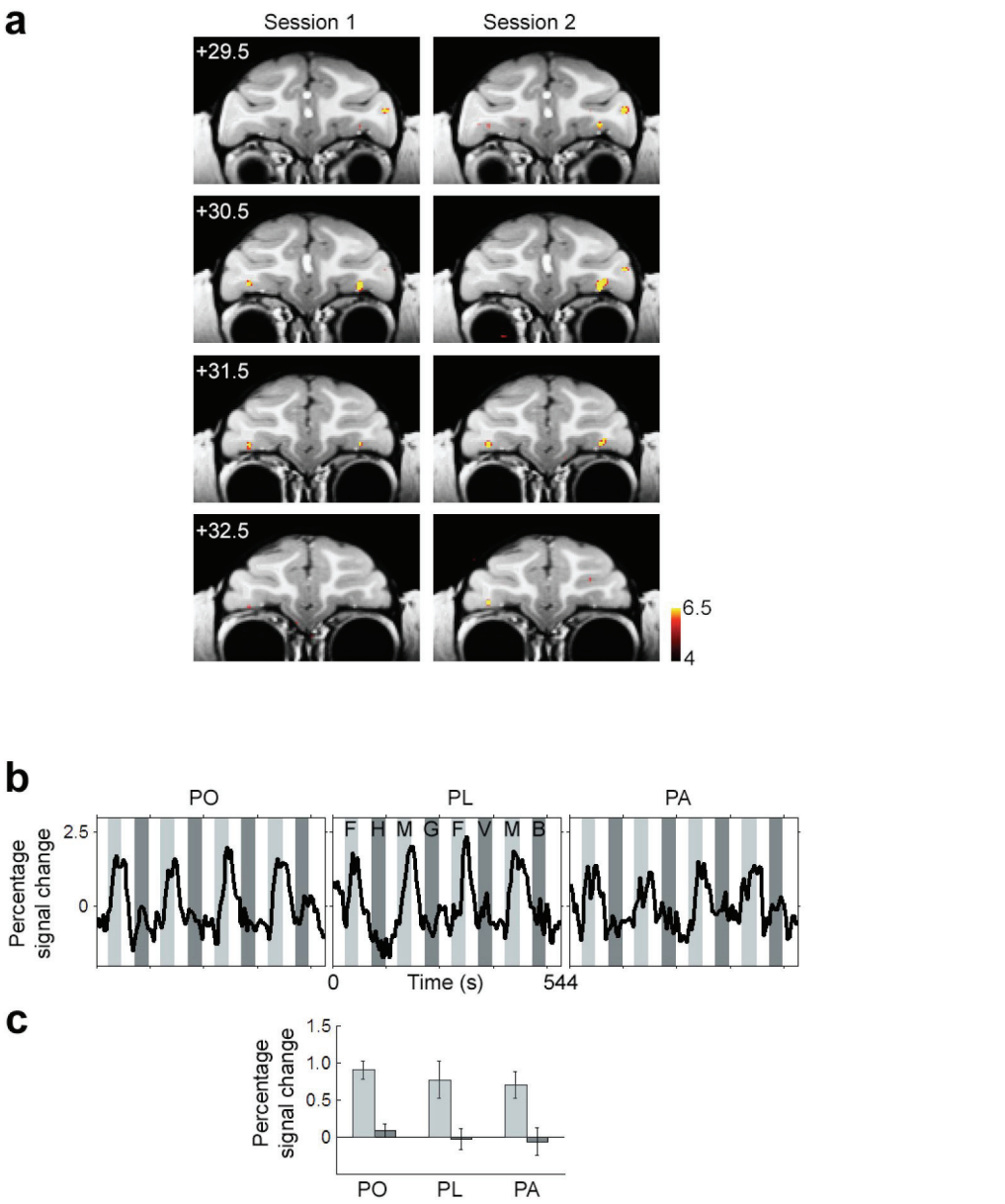

Supplementary Fig. 1. Robustness of the macaque prefrontal face patches. **a)** Prefrontal face patches in monkey M4 obtained in two independent scan sessions of 12 runs each. **b)** Mean time courses from the three prefrontal face patches, averaged across monkeys and across hemispheres for patches that were bilateral. To generate the data shown here and in (c) below, even runs were used to define ROI's for the face patches in each monkey, and odd runs were used to extract the time courses and activation values. Conventions as in Fig. 1d. **c)** Bar graph showing % fMRI signal change to faces (green bars) and to non-face objects (orange bars). Asterisk indicates significant difference between activation to expressive versus neutral faces at p = 0.01.

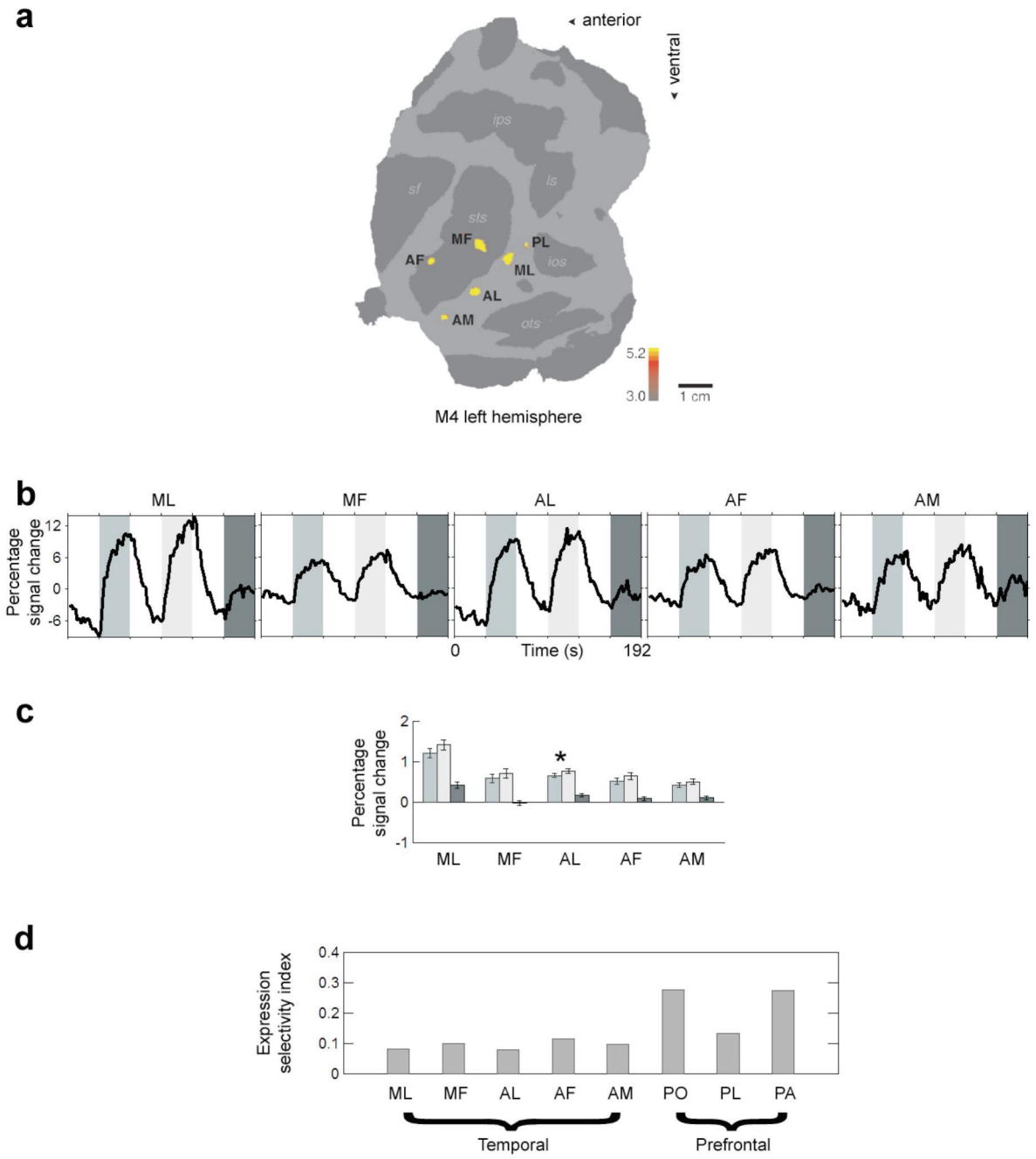

Supplementary Fig. 2. Sensitivity of temporal lobe face patches to facial expression. **a)** Six face-selective patches in the left hemisphere of monkey M4 (representative of most monkeys). The flattened cortical surface shows temporal lobe regions significantly more activated by faces than by other objects. Sulci are shown in dark grey. Area initials: posterior face patch (PL), middle face patch in the STS fundus (MF), middle face patch on the STS lip (ML), anterior face patch in the STS fundus (AF), anterior face patch on the STS lip (AL), and anterior face patch on the ventral surface of IT just lateral and anterior to the AMTS (AM). Anatomical labels: *sts:* superior temporal sulcus, *sf:* sylvian fissure, *ips:* intraparietal sulcus, *ls:* lunate sulcus, *ios:* inferior occipital sulcus, *ots:* occipitotemporal sulcus**. b)** Average time course from ML, MF, AL, AF, and AM to neutral faces (light green),

expressive faces (dark green), and non-face objects (orange). Data averaged across three monkeys (M1, M3, M4) and both hemispheres. The data were extracted from same experiment and using same methods as that shown in Fig. 2. The slice prescription did not include ML and MF for monkey M4, thus time courses for ML and MF were averaged only over monkeys M1 and M3. The posterior face patch (PL) was not included in the slice prescription for any of the monkeys. **c)** Bar graph showing % fMRI signal change to neutral faces (light green), expressive faces (dark green), and non-face objects (orange). Data averaged across three monkeys (M1, M3, M4). Error bars indicate 95% confidence intervals. Results of t-test comparing activation to expressive versus neutral faces: ML, $p = 0.02$; MF, $p = 0.13$; AL, $p = 0.004$; AF, $p = 0.03$; AM, $p = 0.04$). **d)** Bar graph of Expression Selectivity Index across temporal and prefrontal face patches.

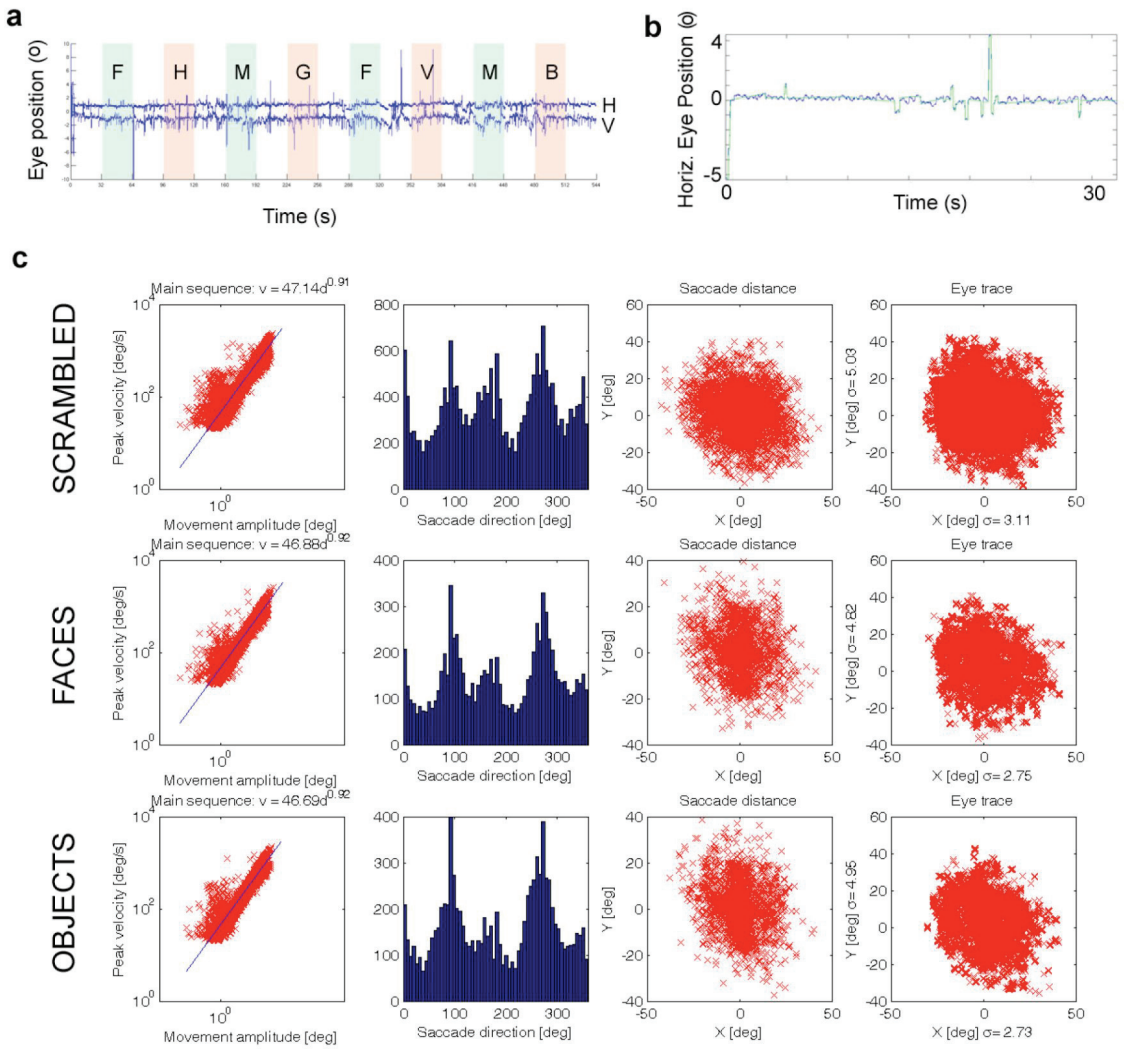
a
Eye position (°)
F
H
M
G
F
V
M
B
H
V
Time (s)
b
Horiz. Eye Position (°)
4
0
-5
0
Time (s)
30
c
SCRAMBLED
FACES
OBJECTS
Main sequence: v = 47.14d^0.91
Main sequence: v = 46.88d^0.92
Main sequence: v = 46.69d^0.92
Peak velocity [deg/s]
Movement amplitude [deg]
Saccade direction [deg]
Saccade distance
Eye trace
Y [deg]
X [deg]
Y [deg] σ= 5.03
X [deg] σ= 3.11
Y [deg] σ= 4.82
X [deg] σ= 2.75
Y [deg] σ= 4.96
X [deg] σ= 2.73
d
Horizontal Eye Position STD (°)
Vertical Eye Position STD (°)
M1
M2
M3
M4
Scrambled
Faces
Objects
Saccades/s
Mean Saccade Amplitude (°)
Mean Saccade Duration (ms)

Supplementary Fig. 3. Comparison of eye movements across different visual stimulus conditions. **a)** An example eye movement trace (from monkey M3) showing the horizontal (H) and vertical (V) eye position during one run; eye blinks have been removed. Epoch identities are as in Fig. 1d (green epochs: faces, orange epochs: objects). For presentation purposes, the horizontal trace was shifted by 1° up, and the vertical trace by 1° down. **b)** An example horizontal eye movement trace (blue trace, from monkey M3) together with fitted predictor (green trace) showing detected saccades, drifts, and periods of steady fixation (see Supplementary Methods for details). **c)** Eye movement parameters across stimulus conditions for monkey M3 (other three monkeys showed similar results). Top row: Scrambled, middle row: Faces, bottom row: Objects. First column: plots of peak velocity versus movement amplitude; in all four monkeys and all three conditions, this plot approximated the "main sequence" relationship of v = 70d reported by [12]. Second column: saccade direction distributions; all four monkeys showed a preference for vertical and horizontal over other saccade directions. Third column: scatter plots of saccade displacement vectors. Fourth column: scatter plots of vertical (y) versus horizontal (x) eye positions. **c)** Bar graphs showing the standard deviation of the horizontal and vertical eye positions, the saccade frequency, the mean saccade amplitude, and the mean saccade direction, computed separately for each monkey and each stimulus condition (scrambled patterns, faces, objects). For each monkey and condition, data was pooled across analyzed runs and blocks of the same condition within a run. ANOVA revealed no significant difference across the three visual stimulus conditions for any of these five eye movement parameters.

	PO		**PL**		**PA**	
	L	**R**	**L**	**R**	**L**	**R**
M1	5.6	7.8	0	5.9	0	5.9
M2	13.7	13.7	0	5.9	13.7	13.7
M3	17.6	23.4	15.6	39.1	0	0
M4	17.6	21.5	0	11.7	0	0
Mean	16.1	16.6	3.9	15.6	3.4	4.9
Std	1.6	6.2	6.8	13.7	5.9	5.6

Supplementary Table 1. The size (in mm^3) of the three macaque prefrontal face patches in left and right hemispheres of four macaques tested, at $p < 0.001$. Note that in monkey M3, we used a different MR sequence than in the other monkeys, which may account in part for the larger size of the patches in this monkey (see Supplementary Methods for details).

References

1. Wegener, D., Freiwald, W.A. & Kreiter, A.K. The influence of sustained selective attention on stimulus selectivity in macaque visual area MT. *J Neurosci* 24, 6106-14 (2004).
2. Nelissen, K., Luppino, G., Vanduffel, W., Rizzolatti, G. & Orban, G.A. Observing others: multiple action representation in the frontal lobe. *Science* 310, 332-6 (2005).
3. Leite, F.P. et al. Repeated fMRI using iron oxide contrast agent in awake, behaving macaques at 3 Tesla. *Neuroimage* 16, 283-94 (2002).
4. Vanduffel, W. et al. Visual motion processing investigated using contrast agent-enhanced fMRI in awake behaving monkeys. *Neuron* 32, 565-77 (2001).
5. Zhao, F., Wang, P., Hendrich, K., Ugurbil, K. & Kim, S.G. Coritcal layer-dependent BOLD and CBV responses measured by spin-echo and gradient-echo fMRI: Insights into hemidynamic regulation. *Neuroimage* 30, 1149 (2006).
6. Cusack, R., Brett, M. & Osswald, K. An evaluation of the use of magnetic field maps to undistort echo-planar images. *Neuroimage* 18, 127-42 (2003).
7. Zeng, H. & Constable, R.T. Image distortion correction in EPI: comparison of field mapping with point spread function mapping. *Magn Reson Med* 48, 137-46 (2002).
8. Brainard, D.H. The Psychophysics Toolbox. *Spat Vis* 10, 433-6 (1997).
9. Tsao, D.Y., Freiwald, W.A., Knutsen, T.A., Mandeville, J.B. & Tootell, R.B. Faces and objects in macaque cerebral cortex. *Nat Neurosci* 6, 989-95 (2003).
10. Ungerleider, L.G. *Red's atlas*, (Laboratory of Neuropsychology, NIMH Department of Health and Human Services.).
11. Bair, W. & O'Keefe, L.P. The influence of fixational eye movements on the response of neurons in area MT of the macaque. *Vis Neurosci* 15, 779-86 (1998).
12. Bahill, A.T., Clark, M.R. & Stark, L. The main sequence, a tool for studying human eye movements. *Mathematical Biosciences* 24, 191-204 (1975).
13. Mitchell, J.F., Sundberg, K.A. & Reynolds, J.H. Differential attention-dependent response modulation across cell classes in macaque visual area V4. *Neuron* 55, 131-41 (2007).
14. Petrides, M. Lateral prefrontal cortex: architectonic and functional organization. *Philos Trans R Soc Lond B Biol Sci* 360, 781-95 (2005).

Conclusion

My combined fMRI and microstimulation experiments show that in macaques faces are processed by a separate system of patches that are strongly and specifically inter-connected. These patches do not send major projections into non-face cortex. Furthermore, my results suggest that non-face objects are also processed by connected systems of discrete patches. Thus it seems that the organization of IT cortex in macaques is modular in nature and probably hierarchical. In the following paragraphs I would like to discuss some of the remaining challenges for understanding the face patch system.

Functional organization of IT modules. What is the precise nature of the connections between the face patches? The microstimulation experiments tell us that the face patches are connected. However, to differentiate feed-forward from feedback projections, we need to know *layer-specific* projection patterns, requiring spatial resolution beyond what is possible with fMRI. Once anatomical tracer studies reveal the connections of the face patches at high resolution then we can understand their hierarchy and formulate better hypotheses about the flow of information required for processing a face.

What is the contribution of each individual face patch to the recognition and processing of a face? Addressing this will require systematic electrophysiological experiments to characterize in detail each patch's selectivity for different face-related features and modulation by face-related behaviors. Furthermore, what is the functional organization for face processing within a patch? Is each patch 'homogenous' in its representation or are there specific sub-modules within a patch? Also, what is being coded in the transition zone between face patches and surrounding cortex?

The finding that cortex outside the face patches is also organized into systems of connected patches (see Fig 4, page 45) raises the question: what defines these non-face patches? Are there common object properties that 'bind' and unify groups of feature columns into larger patches, bringing high-level organization into what currently looks like a random distribution of feature columns?

Evolution and development of the face patch system. How did the face patch system evolve? So far, physiological evidence for a distinct cortical face processing system exists for humans and Old World monkeys. It is not yet known whether New World monkeys, which separated some 40 million years ago from Old World monkeys (Goodman et al. (2005)), also possess a similar dedicated system for faces.

Humans and macaques both possess a face processing system that spans the whole temporal lobe (see F 1 page 72, and F 2, page 73). How homologous are the two systems? Is there a human face module for each macaque face module, and how similar is the organization of object vision in general between the two species?

A recent study by Sugita (2008) showed that monkeys raised without ever seeing a face nevertheless preferred to look at faces compared to other objects. In addition, these animals showed a remarkable ability to discriminate between already seen and new faces based on subtle changes in facial features or spacing. Finally, the monkeys permanently preferred the species' faces they saw for a month after the deprivation period. These results show that the face patch system has both a genetic 'nature' component (as even deprived monkeys preferred faces over other objects) and a plastic 'nurture' component (as the preferred template, macaque or human, was shaped by the faces encountered first).

Interactions between the face patch system and other brain systems. How does the temporal lobe face patch system interact with other parts of the brain? We know that the anterior temporal face patches are connected with the amygdala (see Fig. S11). What

information is being passed through this connection? The amygdala's involvement in emotion suggests that it may help to parse emotional content from faces.

We found that the macaque frontal lobe also contains face-selective regions (see Fig. 1, page 95). Preliminary data (Moeller et al. (2008)) shows that microstimulation of one of the anterior temporal face patches, namely AM, selectively activates the prefrontal face patches. What processing takes place inside these prefrontal face patches? Are other modalities (e.g., auditory, olfactory) or higher level cognitive information (like rank of group members) integrated with the visual representation of faces in the prefrontal face patches?

The anterior temporal face patches are located close to perirhinal cortex and the hippocampus, structures known to be necessary for memory consolidation and memory readout. This proximity makes the anterior temporal face patches prime candidates for being involved in the storage of memory of faces.

Outlook. In the last ten years the precise localization of face-selective modules in humans and monkeys pushed the neuronal mechanisms of face recognition into the focus of many research groups. The most important step, in my humble opinion, was transferring human fMRI methods and paradigms to monkeys, as this opened up the face processing system for targeted experiments on the single neuron level. And to truly understand the function of any brain processing capabilities, we really have to understand the contributions of the smallest building blocks, the neurons. Thus in the face-patch system, we now have access to an exemplary object processing system that will allow us to further scrutinize how face perception is implemented in macaque and in human cortex. Hopefully this will help elucidate how the ventral visual pathway performs what abstractly is called object vision.

Zusammenfassung

Die zentrale Frage meiner Doktorarbeit ist: Was ist der neurale Schaltkreis fuer die Verarbeitung von Gesichtern bei Rhesusaffen? Bisherige Untersuchungen wie Gesichts- und Objektwahrnehmung im ventralen visuellen Pfad organisiert ist, haben zu drei unterschiedlichen Hypthesen gefuehrt. Es gibt Evidenz fuer eine verteilte und ueberlappende Objektrepraesentation durch die gleichzeitige Aktivitaet im gesamten visuellen Temporallappen (‚Objekt-Form-Topographie', Haxby et al. (2001)); ebenso gibt es Indizien fuer weniger globale Objektrepraesentation, bei der unterschiedliche Gruppen von Eigenschaft-Kolumnen rekrutiert werden, die zusammen das praesentierte Objekt beschreiben, das ‚Kombinations-Kodierungs-Schema' (Tanaka et al. (1991), Wang et al. (1996), Tsunoda et al. (2001)); zuletzt gibt es Evidenz fuer eine modulare ‚domaenen-spezifische' Organisation fuer Gesichter und Koerper, in der spezifische kortikale Module ausschliesslich Objekte einer einzigen Kategorie repraesentieren (Kanwisher et al. (1997), Tsao et al. (2003)). Die gesichtsselektiven Eigenschaftskolumnen, die Wang et al. (1996) gefunden haben, neben Kolumnen, die selektiv fuer einfachere Objektformen waren, zeigen, dass selbst in einem kombinatorischen Kodierungsschema einige komplexe Stimuli hoeher integriert verarbeitet werden. Es ist unklar, wo in dem Kontimuum von voll verteilt bis rein modularisiert Gesichts- und Objekt-Wahrnehmung tatsaechlich organisiert sind.

Eine Vorhersage einer verteilten Organisation ist, dass jede Stelle des Objektkortex mit (fast) allen anderen Stellen verbunden ist, entweder vollstaendig oder raeumlich gewichtet, mit staerkeren Verbindungen zu nahem Kortex. Die Vorhersage eines modular-hierarchischen Systems hingegen ist, das jeder ‚Patch' nur mit wenigen anderen Stellen verbunden ist, basierend auf gemeinsamen funktionellen Eigenschaften. Nach welchem dieser beiden Prinzipien ist der visuelle Objektkortex organisiert? Um diese Frage zu beantworten, ist es notwendig, die anatomischen Projektionen von Orten mit bekannten funktionellen Eigenschaften (z.B. einzelne ‚Face-Patche') zu identifizieren, und dann die funktionellen Eigenschaften an den Projektionsorten zu bestimmen. Klassische neuroanatomische Tracer-Methoden bieten eine hohe raeumliche Aufloesung, und Tracer koennen an elektrophysiologisch charakterisierten Orten appliziert werden; die funktionelle Charakterisierung an den Projektionsorten ist mit ihnen jedoch unmoeglich, da die Projektionsorte nur post-mortem identifiziert werden koennen.

Tolias et al. (2005) haben eine neue, elegante Methode fuer in-vivo Traktidentifizierung durch Kombination von elektrischer Microstimulation mit funktioneller Magnet-Resonanz-Tomographie (fMRT) vorgestellt. Die elektrische Stimulation dient hierbei dazu den Kortex am Ort der Elektrode zu aktivieren, fMRT dient dazu, die daraus resultierende Aktivitaet zu messen. Da Stimulationselektroden auch zur elektrophysiologischen Charakterisierung verwendet werden koennen, kann mit dieser Methode auch die Stimulus-Praeferenz am Stimulationsort bestimmt werden. Mittels fMRT kann leicht das gesamte Gehirn abgedeckt werden, was es erlaubt auch weitentfernte Projektionsorte zu identifizieren. Und da die Projektionsorte in vivo bestimmt werden, koennen sie als neues Ziel fuer elektro-physiologische Charakterisierung verwendet werden, sie koennen sogar als neue Stimulationsorte verwendet werden.

Das Leitmotiv meiner Doktorarbeit war die Bearbeitung folgender Frage: Wie sind die gesichtsselektiven Module, die ‚Face-Patches', bei Rhesusaffen organisiert? Das Gesichts-verarbeitungssystem des Rhesusaffen stellt ein ideales Modelsystem dar, um die funktionelle Architektur der Objektwahrnehmung zu untersuchen, da fast alle Tiere mehrere gesichtsselektive Regionen besitzen, die sich leicht mittels fMRT lokalisieren lassen und sich damit sehr gut als Zielgebiete fuer elektrophysiologische und anatomische Experimente

eignen (mit Methodik nach Tsao et al. (2003b) und (2006)). Ich habe Microstimulation kombiniert mit fMRT benutzt um die Frage zu beantworten, ob die ‚Face-Patche' in eine verteilte Objektrepraesentation integriert sind, oder ob sie ein separates Modulsystem darstellen. Die erste Alternative sagt voraus, dass die Stimulation in jedem einzelnen Patch, weit verteilte Aktivitaet im Inferotemporalkortex verursachen sollte; die zweite Alternative sagt voraus, dass die Stimulation in einem einzelnen Patch nur andere Face-Patche aktivieren sollte.

Das Resultat meiner Experimente weist deutlich auf die zweite Alternative, dass die Face-Patche im Temporalkortex des Rhesusaffen ein eng gekoppeltes modulares System darstellen. Jeder Patch ist mit anderen Face-Patchen stark verbunden, nicht jedoch mit dem umliegenden nicht-gesichtsselektivem Kortex; darueber hinaus existieren Verbindungen von den Face-Patchen zu subkortikalen Structuren wie der Amygdala. Um jede Microstimulationsstelle fand sich bei allen Experimenten ein aktivierter Bereich der groesser war als der Zielpatch, verursacht entweder durch passive Ausbreitung des Stimulationsstromes im Gewebe oder durch laterale Verbindungen von jedem Patch in seinen direkt umgebenden Kortex. Interessanterweise fuehrte Microstimulation ausserhalb der Face-Patche ebenfalls zu aehnlich spezifisch verteilten Projektionsmustern. Dies deutet darauf hin, dass moeglicherweise eine gewisse modulare Struktur im gesamten Objektkortex zu finden ist, auch wenn die funktionellen Eigenschaften, die diese ‚Non-Face-Patches' zusammenbinden, noch unbekannt sind.

Das zweite Ziel meines Promotionsprojekts war es, die Organisation der gesichtsselektiven Module bei Menschen und Rhesusaffen zu vergleichen. Rhesusaffen zeigen meist ein typisches, robustes Muster von sechs distinkten Face-Patchen, die ueber die ganze Laenge des Temporallappens verteilt sind; bei Menschen liegt lediglich das anteriorste gesichtsselektive Modul, die Fusiform Face Area (FFA), in der Mitte des Temporallapens. Daraus ergibt sich die Froge, ob die Nutzung des anterioren Temporalkortex eine besondere Entwicklung der Rhesusaffen darstellt. Und da das Gesichtverarbeitungssystem in erster Naeherung als Beispielsystem fuer die hierarchische Organisation der Objektwahrnehmung angesehen werden kann, ergibt sich daraus die Frage, wie aehnlich beide Arten in der Organisation des ventralen visuellen Pfades sind.

Es existieren zwei Unterschiede zwischen den ueblichen Protokollen fuer fMRT-Experimenten zwischen Mensch und Rhesusaffe, die eine erneute Ueberpruefung der anterior-temporalen gesichtsselektiven Module relevant erscheinen lassen. Einerseits, werden Rhesusaffenversuche normalerweise mit funktionellen Kontrastmitteln durchgefuehrt, die das fMRT-Signal drei- bis fuenf-fach verstaerken, und es werden viele Wiederholungen derselben visuellen Stimulation durchgefuehrt, um die Signifikanz der resultierenden Aktivitaetskarten zu erhoehen. Anderseits ist der anterio-temporale Kortex bei Menschen fuer fMRT-Messungen aufgrund der Signalausloeschung durch die Suszeptibilitaetsartefakte der luftgefuellten Ohrkanaele ausnehmend schwer zugaenglich; und Humanexperimente werden ueblicherweise mit sowenigen Stimulations-Wiederholungen wie moeglich durchgefuehrt. Um diese beiden Unterschiede auszugleichen, haben wir die fMRT-Messparameter (Voxelgroesse und Schichtposition) optimiert und denselben visuellen Stimulus in jeder Versuchsperson sehr haeufig wiederholt.

Unsere Studie zeigte, dass die meisten Versuchspersonen ein oder zwei zusaetzliche gesichtsselektive Module besitzen, die im Temporalkortex anterior von FFA liegen und moeglicherweise mit den anterio-temporalen Modulen der Rhesusaffen korrelieren. Aus diesem Grund scheint die Grob-Organistation des Gesichtsverarbeitungsapparates in Menschen und Rhesusaffen konserviert, auch wenn die genaue Anzahl der Module unterschiedlich sein duerfte.

Das dritte und letzte Ziel meiner Dissertation war herauszufinden, ob das ‚Face-Patch'-System der Rhesusaffen auf den Temporalkortex beschraenkt ist. Ó Scalaidhe et al. (1997) konnten zeigen, dass der Praefrontalkortex gesichtsselektive Neurone enthaelt. Sind diese Neurone in distinkte ‚Patche' organisiert wie im Temporalkortex? Unser Ziel war es, die Organisation der Gesichtselektivitaet im Praefrontalkortex mit derselben Methode zu kartieren, die im Temporalkortex bereits erfolgreich war.

Wir fanden, dass Rhesusaffen typischerweise drei diskrete ‚Face-Patche' im Praefrontalkortex besitzen. Dabei reagieren diese praefrontalen Face-Patche staerker auf den emotionalen Ausdruck praesentierter Gesichter als die temporalen Face-Patche. Dieses Ergebnis passt zu der Rolle der Praefrontalkortex fuer soziales Verhalten, wofuer es essentiell ist, den emotionalen Zustand anderer Individuen erkennen zu koennen.

References

Bartels, A., Zeki, S.M. (2000): The architecture of the colour centre in the human visual brain: new results ad a review. European Journal of Neuroscience 12: 172-193, 2000.

Bonhoeffer, T., Grinvald, A. (1991): Iso-orientation domains in cat visual cortex are arranged in pinwheel-like patterns. Nature 353: 429-431, 1991.

Born, R.T., Bradley, D.C. (2005): Structure and Function of Visual Area MT. Annual Reviews Neuroscience 28: 157-189, 2005.

Bruce, C., Desimone, R., Gross, C.G. (1981): Visual Properties of Neurons in a Polysensory Area in Superior Temporal Sulcus of the Macaque. Journal of Neurophysiology 46: 369-384, 1981.

Casagrande, V.A., Yazar, F., Jones, K.D., Ding, Y. (2007): The Morphology of the Koniocellular Axon Pathway in the Macaque Monkey. Cerebral Cortex 17: 2334-2345, 2007.

Chen, G., Lu, H.D., Roe, A.W. (2008): A Map for Horizontal Disparity in Monkey V2. Neuron 58,:442-450, 2008

Conway, B.R., Tsao, D.Y. (2006): Color Architecture in Alert Macaque Cortex Revealed by fMRI. Cerebral Cortex 16: 1604-1613, 2006.

Dacey, D.M. (2000): Parallel Pathways for Spectral Coding in Primate Retina. Annual Reviews Neuroscience 23: 743-775, 2000.

DeAngelis, G.C., Newsome, W.T. (1999): Organization of Disparity-Selective Neurons in Macaque Area MT. The Journal of Neuroscience 19: 1398–1415, 1999.

Denys, K., Vanduffel, W., Fize, D., Nelissen, K., Peuskens, H., Van Essen, D.C., Orban, G.A. (2004): The Processing of Visual Shape in the Cerebral Cortex of Human and Nonhuman Primates: A Functional Magnetic Resonance Imaging Study. The Journal of Neuroscience 24: 2551-2565, 2004.

Desimone, R., Albright, T.D., Gross, C.G., Bruce, C. (1984): Stimulus-selective Properties of Inferior Temporal Neurons in the Macaque. The Journal of Neuroscience 4: 2051-2062, 1984.

Downing, P.E., Jiang, Y., Shuman, M., Kanwisher, N. (2001): A Cortical Area Selective for Visual Processing of the Human Body. Science 293: 2470-2473, 2001.

Felleman, D.J., Van Essen, D.C. (1991): Distributed Hierarchical Processing in the Primate Cerebral Cortex. Cerebral Cortex 1: 1-47, 1991.

Fujita, I., Tanaka, K., Ito, M., Cheng, K. (1992): Columns for visual features of objects in monkey inferotemporal cortex. Nature 360: 343-346, 1992.

Fujita, I., Fujita, T. (1996): Intrinsic Connections in the Macaque Inferior Temporal Cortex. The Journal of Comparative Neurology 368: 467-486, 1996.

Glickstein, M. (1969): Organization of the Visual Pathways. Science 164: 917-926, 1969.

Goodman, M., Grossman, L.I., Wildman, D.E. (2005): Moving primate genomics beyond the chimpanzee genome. Trends in Genomics 21: 511-517, 2005.

Gross, G.C. (1994): How Inferior Temporal Cortex Became a Visual Area. Cerebral Cortex 4: 455-469, 1994.

Hadjikhani, N., Liu, A.K., Dale, A.M., Cavanagh, P., Tootell, R.B.H. (1998): Retinotopy and color sensitivity in human visual cortical area V8. Nature Neuroscience 1: 235-241, 1998.

Haxby, J.V., Grady, C.L., Horwitz, B., Ungerleider, L.G., Mishkin, M., Carson, R.E., Herscovitch, P., Schapiro, M.B., Rapoport, S.I. (1991): Dissociation of Object and Spatial Visual Processing Pathways in Human Extrastriate Cortex, Proceedings of the National Academy of Sience 88: 1621-1625, 1991.

Haxby, J.V., Gobbini, M.I., Furey, M.L, Ishai, A., Schouten, J.L., Pietrini, P. (2001): Distributed and Overlapping Representations of Faces and Objects in Ventral Temporal Cortex. Science 293: 2425-2430, 2001.

Horton, J.C., Hubel, D.H. (1981): Regular patchy distribution of cytochrome oxidase staining in primary visual cortex of macaque monkey. Nature 292: 762-764, 1981.

Hubel, D.H., Wiesel, T.N. (1959): Receptive Fields of Single Neurons n the Cat's Striate Cortex. Journal of Physiology 148: 574-591, 1959.

Hubel, D.H., Wiesel, T.N. (1977): Ferrier Lecture: Functional Architecture of Macaque Monkey Visual Cortex. Proceedings of the Royal Society of London. Series B, Biological Siences 198: 1-59, 1977.

Hubel, D.H., Livingstone, M.S. (1987): Segregation of Form, Color, and Stereopsis in Primate Area 18. Journal of Neuroscience 7: 3378-3415, 1987.

Kanwisher, N., McDermott, J., Chun, M.M. (1997): The Fusiform Face Area: A Module in Human Extrastriate Cortex Specialized for Face Perception. The Journal of Neuroscience 17: 4302-4311, 1997.

Kanwisher, N., Yovel, G. (2006): The fusiform face area: a cortical region specialized for the perception of faces. Philosophical Transactions of the Royal Society Series B 361: 2109-2128, 2006.

Kwong, K.K., Belliveau, J.W., Chesler, D.A., Goldberg, I.E., Weisskoff, R.M., Poncelet, B.P., Kennedy, D.N., Hoppel, B.E., Cohen, M.S., Turner, R., Cheng, H.M., Brady, T.J., Rosen, B.R. (1992): Dynamic Magnetic Resonance Imaging of Human Brain Activity during Primary Sensory Stimulation. Proceedings of the National Academy of Science 89: 5675-5679, 1991.

LeVay, S., Hubel, D.H., Wiesel, T.N. (1975): The pattern of ocular dominance columns in macaqie visual cortex revealed by a reduced silver stain. Journal of Comparative Neurology 159: 559-576, 1975.

Livingstone, M.S., Hubel, D.H. (1984): Anatomy and physiology of a color system in the primate visual cortex. Journal of Neuroscience 4: 309-356, 1984.

Livingstone, M.S., Hubel, D.H. (1987): Psychophysical Evidence for Separate Channels for the Perception of Form, Color, Movement, and Depth. Journal of Neuroscience 7: 3416-3468, 1987.

Livingstone, M.S., Hubel, D.H. (1988): Segregation of Form, Color, Movement, and Depth: Aatomy, Physiology, and Perception. Science 240: 740-749, 1988.

Macko, K.A., Jarvis, C.D., Kennedy, C., Miyaoka, M., Shinohara, M., Sokoloff, L., Mishkin, M. (1982): Mapping the Primate Visual System with [2-^{14}C]Deoxyglucose. Science 218: 394-397, 1982.

Maunsell, J.H.R., Newsome, W.T. (1987): Visual Processing in Monkey Extrastriate Cortex. Annual Reviews Neuroscience 10: 363-401, 1987.

Mishkin, M., Ungerleider, L.G., Macko, K.A. (1983): Object Vision and Spatial Vision: two Cortical Pathways. Trends in Neurosciences 6: 414-417, 1983.

Moeller, S., Freiwald, W.A., Tsao D.Y. (2008): A direct link between face-selective regions in temporal and prefrontal cortex. Program No. 261.5. in Society for Neuroscience Annual Meeting. 2008.

Nakamura, H., Gattass, R., Desimone, R., Ungerleider, L.G. (1993): The modular organization of projections from areas V1 and V2 to areas V4 and TEO in macaques. The Journal of Neuroscience 13: 3681-3691, 1993.

Ó Scalaidhe, S.P., Wilson, F.A.W., Goldman-Rakic, P.S. (1997): Areal segregation of face processing neurons in prefrontal cortex. Science 278: 1135–1138, 1997.

Ogawa, S., Lee, T.M., Kay, A.R., Tank, D.W. (1990): Brain Magnetic Resonance Imaging with Contrast Dependent on Blood Oxgenation. Proceedings of the National Academy of Science 87: 9868-9872, 1990.

Ohki, K., Chung, S., Kara, P., Huebner, M., Bonhoeffer, T., Reid, C. (2006): Highly ordered arrangement of single neurons in orientation pinwheels. Nature 442: 925-928, 2006.

Orban, G.A., Van Essen, D.C., Vanduffel, W. (2004): Comparative Mapping of Higher Visual Areas in Monkeys and Humans. TRENDS in Cognitive Sciences 8: 315-324, 2004.

Orban, G.A. (2008): Higher Order Visual Processing in Macaque Extrastriate Cortex. Physiological Review 88: 59-89, 2008.

Perrett, D.I., Rolls, E.T., Caan, W. (1982): Visual Neurones Responsive to Faces in the Monkey Temporal Cortex. Experimental Brain Research 47: 329-342, 1982.

Pinsk, M.A., DeSimone, K., Moore, T., Gross, C.G., Kastner, S. (2005): Representations of faces and body parts in macaque temporal cortex: A functional MRI study. Proceedings of the National Academy of Science 102: 6996-7001.

Ponce, C.R., Lomber, S.G., Born, R.T. (2008): Integrating motion and depth via parallel pathways. Nature Neuroscience 11: 216-223, 2008.
Repérant, J., Ward, R., Miceli, D., Rio, J.P., Médina, M., Kenigfest, N.B., Vesselkin, N.P. (2006): The Centrifugal Visual System of Vertebrates: A Comparative Analysis if its Functional Anatomical Organisation. Brain Research Reviews 52: 1-57, 2006.
Roe, A.W., Parker, A.J., Born, R.T., DeAngelis, G.C. (2007): Disparity Channels in Early Vision. The Journal of Neuroscience 27: 11820-11831, 2007.
Saleem, K.S., Tanaka, K., Rockland, K.S. (1993): Specific and Columnar Projection from Area TEO to TE in the Macaque Inferotemporal Cortex. Cerebral Cortex 3: 454-464, 1993.
Schwarzlose, R.F., Baker, C.I., Kanwisher, N. (2005): Separate Face and Body Selectivity on the Fusiform Gyrus. The Journal of Neuroscience 25: 11055-11059, 2005.
Shipp, S., Zeki, S.M. (1985): Segregation of pathways leading from area V2 to areas V4 and V5 of macaque monkey visual cortex. Nature 315: 322-325, 1985.
Shipp, S., Zeki, S. (2002): The functional organization of area V2, II: the impact of stripes on visual topography. Visual Neuroscience 19: 211–231, 2002.
Sincich, L.C., Horton, J.C. (2002): Pale Cytochrome Oxidase Stripes in V2 Receive the Richest Projection From Macaque Striate Cortex. Journal of Comparative Neurology 447: 18-33, 2002.
Sincich, L.C., Park, K.F., Wohlgemuth, M.J., Horton, J.C. (2004): Bypassing V1: a direct geniculate input to area MT. Nature Neuroscience 7: 1123-1128, 2004.
Sincich, L.C., Horton, J.C. (2005): The Circuitry of V1 and V2: Integration of Color, Form, and Motion. Annual Reviews Neuroscience 28: 303-326, 2005.
Sincich, L.C., Jocson, C.M., Horton, J.C. (2007): Neurons in V1 Patch Columns Project to V2 Thin Stripes. Cerebral Cortex 17: 935-941. 2007.
Stoerig, P., Cowey, A. (1997): Blindsight in man and monkey. Brain 120: 535–559, 1997.
Sugita, Y. (2008): Face perception in monkeys reared with no exposure to faces. Proceedings of the National Academy of Science 105: 394-398, 2008.
Tanaka, K., Saito, H., Fukada, Y., Miriya, M. (1991): Coding Visual Images of Objects in the Inferotemporal Cortex of the Macaque Monkey. Ournal of Neurphysiology 66: 170-189, 1991.
Tolias, A.S., Sultan, F., Augath, M., Oeltermann, A., Tehovnik, E.J., Schiller, P.H., Logothetis, N.K. (2005): Mapping Cortical Activity Elicited with Electrical Microstimulation Using fMRI in the Macaque. Neuron 48: 901-911, 2005.
Tsao, D.Y., Vanduffel, W., Sasaki, Y., Fize, D., Knutsen, T.A., Mandeville, J.B., Wald, L.L., Dale, A.M., Rosen, B.R., Van Essen, D.C., Livingstone, M.S., Orban, G.A., Tootell, R.B.H. (2003a): Stereopsis Activates V3A and Caudal Intraparietal Areas in Macaques and Humans. Neuron 39: 555-568, 2003.
Tsao, D.Y., Freiwald, W.A., Knutsen, T.A., Mandeville, J.B., Tootell, R.B.H. (2003b): Faces and Objects in Macaque Cerebral Cortex. Nature Neuroscience 6: 989-995, 2003.
Tsao, D.Y., Freiwald, W.A., Tootell, R.B.H., Livingstone, M.S. (2006): A Cortical Region Consisting Entirely of Face-Selective Cells. Science 311: 670-674, 2006.
Tsunoda, K., Yamane, Y., Nishizaki, M., Tanifiji, M. (2001): Complex objects are represented in macaque inferotemporal cortex by the combination of feature columns. Nature Neuroscience 4: 832-838, 2001.
Ungerleider, L.G., Mishkin, M. (1982): Two Cortical Visual Systems. In: Ingle, D.J., Goodale, M.A., Mansfield, R.J.W. (Eds.) (1982): Analysis of Visual Behaviour. MIT Press, Cambridge, MA, 549-586, 1982.
Ungerleider, L.G., Haxby, J.V. (1994): 'What' and 'Where' in the Human Brain. Current Opinion in Neurobiology 4: 157-156, 1994.
Van Essen, D.C., Anderson, C.H., Felleman, D.J. (1992)): Information Processing in the Primate Visual System: An Integrated Systems Perspective. Science 255: 419-423, 1992.
Van Essen, D.C., Lewis J.W., Drury, H.A., Hadjikhani, N., Tootell, R.B.H., Bakiricioglu, M., Miller, M.I. (2001): Mapping Visual Cortex in Monkeys and Humans using Surface-based Atlases. Vision Research 41: 1359-1378, 2001.

Wade, A., Augath, M., Logothetis, N., Wandell, B.A. (2008): fMRI measurements of color in macaque and human. Journal of Vision 8: 1-19, 2008.
Wandell, B.A., Dumoulin, S.O., Brewer, A.A. (2007): Visual Field Maps in Human Cortex. Neuron 56: 366-383, 2007.
Wang, G., Tanake, K., Tanifuji, M. (1996): Optical Imaging of Functional Organization in the Monkey Inferotemporal Cortex. Science 272: 1665-1668, 1996.
Wiesel, T.N., Hubel, D.H. (1966): Spatial and Chromatic Interactions in the Lateral Geniculate Body of the Rhesus Monkey. Journal of Neurophysiology 29: 1115-1156, 1966.
Young, M.P. (1992): Objective Analysis of the Topological Organization of the Primate Cortical Visual System. Nature 358: 152-155, 1992.
Zeki, S.M. (1973): Colour coding in rhesus monkey prestriate cortex. Brain Research 53: 422-427, 1973.
Zeki, S.M. (1978): Uniformity and diversity of structure and function in rhesus monkey prestriate visual cortex. Journal of Physiology 277: 273-290, 1978.
Zeki, S.M. (1980): The representation of colours in the cerebral cortex. Nature 284: 421-418, 1980.
Zeki, S.M. (1983): Colour coding in the cerebral cortex: the reaction of cells in monkey visual cortex to wavelengths and colours. Neuroscience 9: 741-765, 1983.